ESTIMATION OF STRESSED STATE OF THE WALL OF COILED VERTICAL CYLINDRICAL TANKS IN WELDING-IN OF INSERT PLATES

V.I. MAKHNENKO[1], **A.Yu. BARVINKO**[1], **Yu.P. BARVINKO**[1] and **P. TSIARKOVSKY**[2]
[1]The E.O. Paton Electric Welding Institute, NASU, Kyiv, Ukraine
[2]Company «Bikor», Kyiv, Ukraine

Given are the results of calculation of stressed state of the wall of a coiled tank with a capacity of 50,000 m^3 in welding-in of insert plates. Theoretical estimation of the possibility of loss of stability of the wall due to the effect of residual welding stresses is presented. It is shown that the welding technology recommended by standards fails to provide retention of the designed geometrical shape of the wall in the case of replacement of its vertical assembly welded joints arranged in line by joints with the welds separated in chords.

Key words: *overhaul, vertical cylindrical steel tanks, coiled billets, vertical assembly joints in wall, welding stresses, stability*

Recovery of performance of vertical assembly welded joints, arranged in line, in a wall of coiled cylindrical tanks of a high capacity (10,000 m^3 and more), intended for oil and oil products storage, during their overhaul is a topical problem [1].

As noted in [1], for a case of existing vertical assembly joints arranged in line, the optimal solution of this problem is to replace them by the joints with separated welds, according to the requirements of the standard of Ukraine [2]. Separated assembly joints are made by welding special insert plates into the tank wall over its entire height [1, 3].

The experience available in this area showed that one of the main obstacles to successful realisation of the method suggested for recovery of performance of the wall is formation in the repair locations of local deviations from the designed shape, much in excess of those specified by standards [2, 4].

To reveal causes of formation of inadmissible local deviations of the geometrical shape, the E.O. Paton Electric Welding Institute completed calculations of the stressed state of inserts and adjoining regions in welding of the insert plates into the high-strength 16G2AF steel wall of a coiled tank with a floating cover (Figure 1, *a*) and a rated capacity of 50,000 m^3 (diameter — 60 m and wall height — 18 m).

The probability of a local loss of stability of the wall under the effect of welding stresses was also estimated.

The calculations were made with allowance for the welding technology specified by standards [3]. Sequence of depositing the welds in this case is shown in Figure 1, *b*. The first to weld were the vertical

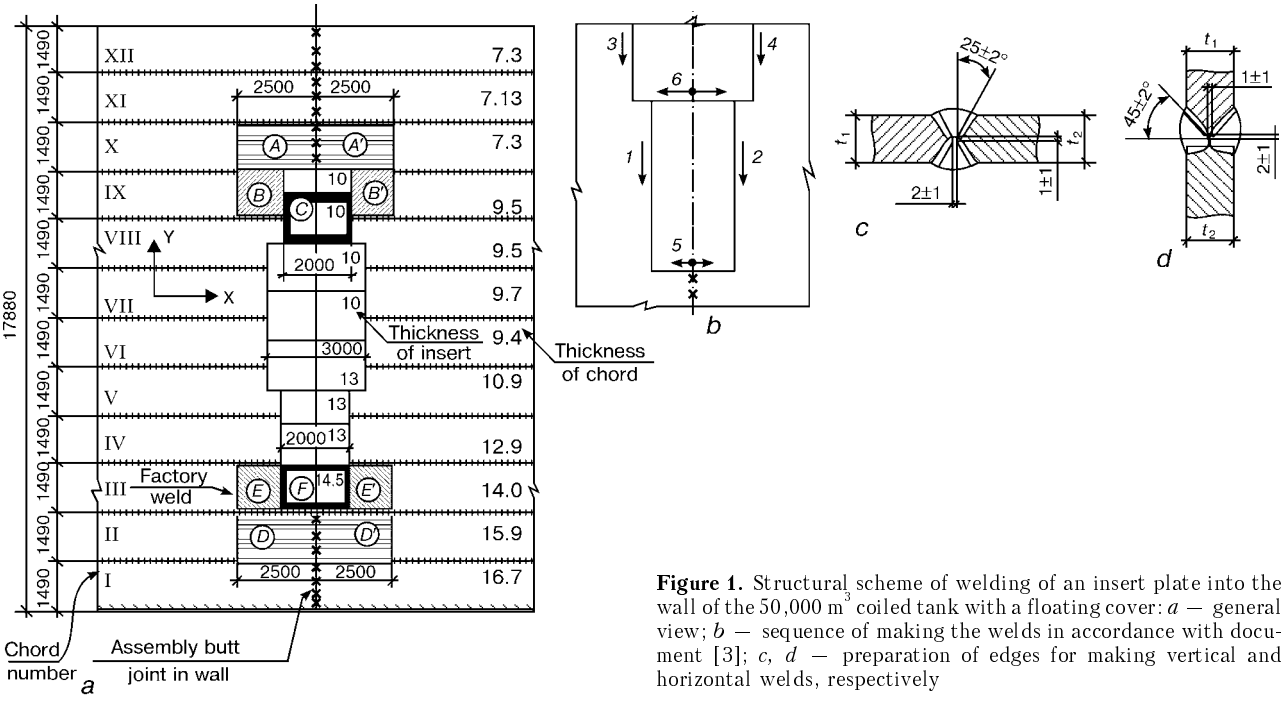

Figure 1. Structural scheme of welding of an insert plate into the wall of the 50,000 m^3 coiled tank with a floating cover: *a* — general view; *b* — sequence of making the welds in accordance with document [3]; *c*, *d* — preparation of edges for making vertical and horizontal welds, respectively

Table 1. Conditions of welding vertical and horizontal insert plates 7–17 mm thick

Electrode diameter, mm	*Deposition efficiency* α_d, *g/(A·h)*	*Weld layer*	*Welding current* I_w, *A*	*Arc voltage* U_a, *A*
3.0	9.0–10.0	Root	120–130 / 110–120	28–32 / 28–30
3.2	10.2	Filling	120–130 / 110–120	28–32 / 28–30

Notes. 1. Welding was performed at the direct current (reverse polarity). 2. Data for vertical welds are given in the numerator and those for horizontal welds are given in the denominator.

Table 2. Quantity of layers in the welds in the case of welding-in of insert plates

Weld type	*Thickness of plates joined* t_1–t_2 *(Figure 1), mm*	*Quantity of layers, pcs*
Vertical	14.5–14.0	6
	13.0–12.9	5
	13.0–(9.4–10.9)	5
	10.0–(9.4–9.7)	4
Horizontal	14.5–15.9	6
	13.0–13.0	5
	13.0–10.9	5
	10.0–10.0	4
	7.0–10.0	3

working welds in two neighbouring insert plates, then followed the horizontal weld between them. Inserts were welded in succession in the upward direction. Welding was carried out using covered electrodes 3 mm in diameter. Edge preparation, welding parameters and quantity of passes for filling the groove are given in Figure 1, *c*, *d* and in Tables 1 and 2. The insert plates were made from the 10G2FB steel plate. Strength properties of the weld metal, steels 16G2AF and 10G2FB are given in Tables 3 and 4.

Welding of insert plates into the tank wall is stipulated by the necessity of performing welding in a rigid contour, which is a peculiar feature of the said process. As seen from Figure 1, *b*, the effect of rigid fixation in making vertical welds shows up mostly in transverse shrinkage. Horizontal welds are made when fixation is rigid both for transverse and longitudinal shrinkages. Investigation of the stressed state of the tank wall in this case is of a practical interest in terms of prediction of variations in its geometrical shape during the welding process and development of measures for their elimination. As welding in a rigid contour has a restricted application, the literature analyses only few cases, e.g. welding up of a crack in a thin plate [5] and holes in thick-plate (t = 40 mm) structures [6].

Method for calculation of residual stresses in the tank wall. Cylindrical shell of the tank wall, taking into account its small curvature R = 30 m and thickness t (R/t = 1700–4300), was assumed to be a flexible plate for the calculation of stresses and estimation of the risk of loss of stability. The calculation method for investigation of the kinetics of welding stresses and strains was employed to determine the stressed state [5]. Assumptions of the simultaneity of making filling weld beads along the entire length of the plate and the plane stressed state (stresses $\sigma_{zz} = \sigma_{zx} = \sigma_{zy} \equiv 0$) were made to reduce the 3D problem to the plane one. The linearised problem was solved by the finite element method. This method involved rectangles with minimum sizes in the weld zone, gradually increasing with distance from the welds.

Heat input per pass, q, was determined from the following formula:

$$q = \eta_h U_a I_w \frac{1}{v_w} = \frac{U_a F_p}{\alpha_d} \gamma \eta_h \cdot 3600, \qquad (1)$$

where η_h is the net efficiency of heating equal to 0.7; U_a is the arc voltage; v_w is the mean welding speed for each pass, determined through the cross section area of a given pass, F_p (depending upon the number of layers deposited); α_d and I_w are the deposition efficiency and welding current, respectively; and γ is the density of the metal being deposited, equal to 7.8 g/cm^3 (see Table 2).

Thermal-physical properties of steels (thermal conductivity λ, heat capacity per unit volume $c\gamma$), elasticity modulus E, Poisson's ratio ν and temperature expansion α were taken from [7], and temperature dependence of the yield strength of steel and weld metal was taken from [5].

Method for estimation of the risk of loss of stability of the tank wall. At the initial stage of the investigations, where no experimental data were available, the shape of dents in the tank wall was described as rectangles $a \times b$ in size (regions A, A', B, B', C, D, D', E and F in Figure 1). This approach

Table 3. Mechanical properties of 16G2AF and 10G2FB steel plates (across the rolling direction)

Steel	*Plate thickness, mm*	*Location of cutting of specimens*	*Yield strength* σ_y, *MPa*	*Tensile strength* σ_t, *MPa*	*Elongation* δ, *%*
16G2AF (C – 0.16; Mn – 1.5; V – 0.1; Nb – 0.02 wt.%)	6.0–30.0	GOST 27772–88	≥ 440	≥ 590	≥ 20.0
	17.0	From the tank wall	565	724	14.7
			580	705	12.0
			547	706	16.0
10G2FB (C – 0.1; Mn – 1.5; V – 0.1; Nb – 0.1 wt.%)	10.0–20.0	TU 14-1-4083–88	≥ 450	590–690	≥ 22.0
	14.5	From insert plates	484	610	26.0
			469	598	22.0
			479	614	24.0

Table 4. Mechanical properties of metal of the weld made using the E60A (σ_t = 600 MPa) type electrodes (certificate data)

Yield strength σ_y, *MPa*	*Tensile strength* σ_t, *MPa*	*Elongation* δ, *%*
460*	620**	23*
550**	580–700	27**

*Minimum value.
**Maximum value.

allows investigation of the loss of stability of a thin plate with sides $a \times b$ in size. The plate, being part of the wall panel, was considered to be pivoted on the ends. Narrow zones of high tensile stresses in a region of the existing welds were chosen to serve as supports. The shape of the loss of stability between the conditional supports, according to the experimental results, was taken from a half-wave described by a sinusoid.

The presence of residual stresses due to the existing factory welds in the wall was neglected. Although they can have a certain effect on the loss of stability, it is difficult to estimate their level. This is attributable to the fact that the tank wall after welding was subjected to coiling and then loading during operation, which led to a certain relaxation and redistribution of the said stresses.

The approximated energy method was employed to solve the above problem on estimation of the risk of the loss of stability of a flexible plate. According to this method, the risk of the loss of stability in ranges of $0 < \bar{x} < a$ and $0 < \bar{y} < b$ is high, provided that the potential bending energy U for the given range and energy W of the membrane welding stresses σ_{xx}, σ_{yy} and σ_{xy}, associated with displacement from buckling and initial distortion of the median surface, meet the following condition [8]:

$$E = U + W < 0, \qquad (2)$$

where E is the overall energy of an elastic system;

$$U = \frac{1}{2}\int_0^a\int_0^b D_c \times \left\{\left[\left(\frac{\partial^2 f}{\partial x^2} + \frac{\partial^2 f}{\partial y^2}\right)^2 - 2(1-\nu)\left[\left(\frac{\partial^2 f}{\partial x^2}\frac{\partial^2 f}{\partial y^2}\right) - \left(\frac{\partial^2 f}{\partial x \partial y}\right)^2\right]\right\} d\bar{x}\,d\bar{y}, \qquad (3)$$

where $f = f(\bar{x}, \bar{y})$ are the normal displacements of the surface related to the loss of stability; D_c is the cylindrical rigidity equal to $\frac{E\delta^3}{12(1-\nu^2)}$; and δ is the plate thickness at points $\bar{x}$ and $\bar{y}$.

Energy W of the welding stresses is related to displacements $f = f(\bar{x}, \bar{y})$ and initial deviations in the form of $g = g(\bar{x}, \bar{y})$, which can be written as follows, according to [8]:

$$W = \frac{1}{2}\int_0^a\int_0^b \left[\sigma_{xx}\left(\frac{\partial \bar{\bar{f}}}{\partial x}\right)^2 + \sigma_{yy}\left(\frac{\partial \bar{\bar{f}}}{\partial y}\right)^2 + 2\sigma_{xy}\left(\frac{\partial \bar{\bar{f}}}{\partial x}\,\frac{\partial \bar{\bar{f}}}{\partial y}\right)\right] \delta\, d\bar{x}\,d\bar{y}, \qquad (4)$$

where $\bar{\bar{f}} = f(x, y) + g(\bar{x}, \bar{y})$; σ_{xx}, σ_{yy} and σ_{xy} are the welding stresses averaged through thickness δ.

At assigned σ_{xx}, σ_{yy} and σ_{xy}, the use of relationships (3) and (4) causes no difficulties, provided that the $f = f(\bar{x}, \bar{y})$ and $g = g(\bar{x}, \bar{y})$ function values are known. The following assumptions were made with a certain approximation (at a sufficient conservatism) [8]:

$$f(\bar{x}, \bar{y}) = f_0 \sin\frac{\pi\bar{x}}{a} \sin\frac{\pi\bar{y}}{b};$$
$$g(\bar{x}, \bar{y}) = g_0 \sin\frac{\pi\bar{x}}{a} \sin\frac{\pi\bar{y}}{b}, \qquad (5)$$

where f_0 and g_0 are the certain constants.

If $E < 0$, the probability of the loss of stability of the plate is sufficiently high.

Substitution of formula (5) in equations (3) and (4), and then (2), yields the final expression for the overall elastic energy of the system:

$$E = \frac{f_0^2\pi^4}{2}\int_0^a\int_0^b \times \left\{\left(\frac{1}{a^2} + \frac{1}{b^2}\right)^2 \sin^2\frac{\pi\bar{x}}{a}\sin^2\frac{\pi\bar{y}}{b} - \frac{2(1-\nu)}{a^2b^2}\left[\sin^2\frac{\pi\bar{x}}{a}\sin^2\frac{\pi\bar{y}}{b} - \cos^2\frac{\pi\bar{x}}{a}\cos^2\frac{\pi\bar{y}}{b}\right]\right\} \times D\,d\bar{x}\,d\bar{y} + f_0^2\left(1 + \frac{g_0}{f_0}\right)^2 \frac{\pi^2}{2}\int_0^a\int_0^b \times \left[\frac{\sigma_{xx}}{a^2}\sin^2\frac{\pi\bar{x}}{a}\sin^2\frac{\pi\bar{y}}{b} + \frac{\sigma_{yy}}{b^2}\sin^2\frac{\pi\bar{x}}{a}\sin^2\frac{\pi\bar{y}}{b} + \frac{2}{ab}\sigma_{xy}\cos\frac{\pi\bar{x}}{a}\cos\frac{\pi\bar{y}}{b}\right]\delta\, d\bar{x}\,d\bar{y}. \qquad (6)$$

In our case, where δ has a constant value within ranges $0 < \bar{y} < b$ and $0 < \bar{x}, < a$, it follows from equation (5) that

$$E = \frac{f_0^2\pi^2\delta}{2a}\frac{ab}{8}\left[\frac{\pi^2 E}{12(1-\nu^2)}\left(1 + \frac{a^2}{b^2}\right)^2\left(\frac{\delta}{a}\right)^2\right] + \left(1 + \frac{g_0}{f_0}\right)^2 \frac{8}{2ab}\int_0^a\int_0^b \times \left[\sigma_{xx}\sin^2\frac{\pi\bar{x}}{a}\sin^2\frac{\pi\bar{y}}{b} + \frac{a^2}{b^2}\sigma_{yy}\sin^2\frac{\pi\bar{x}}{a}\sin^2\frac{\pi\bar{y}}{b} + 2\frac{a}{b}\sigma_{xy}\cos\frac{\pi\bar{x}}{a}\cos\frac{\pi\bar{y}}{b}\right]\delta\, d\bar{x}\,d\bar{y}. \qquad (7)$$

Expression $K_i = (1 + g_0/f_0)^2 \geq 1$ is a correction for the initial curvature. If the share of the initial deflection in displacements of the stability loss is insignificant, i.e. $g_0/f_0 << 1$, $K_i \approx 1$. Further calculations were made mostly at a condition that $K_i \approx 1$. However, the authors understand that this is a sufficiently high idealisation, i.e. it is highly probable that in some cases the value of K_i may be higher than one.

Therefore, it is necessary to do the following to solve the problem under consideration for estimation of the probability of the loss of stability of the tank wall:

- determine welding stresses σ_{xx}, σ_{yy} and σ_{xy} induced by welding-in of the insert plates;
- select the shape of the surface of the stability loss in regions with a potential risk of formation of dents and calculate the U and W values for these regions;
- estimate the risk of the stability loss in accordance with inequality (2).

Results of calculation of welding stresses. Fields of residual welding stresses in the wall of a coiled tank with a rated capacity of 50,000 m^3 after making all the welds are shown in Figure 2 (see the inset). It can be seen from the data given that welding of the insert plates under the rigid contour conditions is characterised by the presence of extended zones

affected by rather high compressive ($\sigma_{ii} \geq 20$ MPa) and tangential ($\sigma_{ij} \geq 15$ MPa) residual welding stresses, this coinciding in general with the data of [5, 6]. However, extension of the zone affected by residual stresses is much in excess of that described in [5], which is attributable to a large length of the welds. In particular, this applies to tangential stresses σ_{xy}, the length of the zone of the effect of which in region A (Figure 3, see the inset), where the plates are about 7 mm thick, is approximately 50 cm, as well as to longitudinal stresses for the corresponding welds. Thus, longitudinal stresses σ_{xx} for horizontal welds and stresses σ_{yy} for vertical welds have the affected zone in region A equal to about 90 and 70 cm, respectively, from the end of the weld. In regions D, E and F, at lower thicker chords of the wall, the length of the zones of the above stresses is close to that in regions A, B and C, which is caused by approximately identical specific heat inputs per unit thickness of elements being welded in both cases.

The stressed state of the insert plates is characterised by compressive, σ_{xx}, and tensile, σ_{yy}, stresses present in their major part. These stresses are equal in absolute value to 5–10 MPa. In regions of the inserts adjoining the horizontal welds, compressive stresses σ_{xx} increase to 10–20 MPa. Stresses σ_{yy} remain constant. In the adjoining regions of the tank wall only compressive stresses σ_{xx} and σ_{yy} are effective.

Analysis of the stressed state of the tank wall at the level of horizontal welds shows that formation of dents in these locations occurs due to residual longitudinal tensile stresses, high in level and large in length, which are present in regions adjoining the weld ends.

Results of estimation of the risk of the loss of stability of the wall. Table 5 gives results of calculations of the values of U, W and $E = U + W$ using expressions (3) and (4) for regions under consideration, at $K_i = 1$. It can be seen from the data obtained that with the assumed idealisation, where initial deviations $g(\bar{x}, \bar{y})$ and residual stresses due to the existing factory welds are ignored, the risk of the loss of stability is the highest for region A, where the shell has minimum thickness, i.e. 7.3 mm. However, here the values of U and W are such that theoretically the loss of stability occurs only at $K_i = (1 + g_0/f_0)^2 \geq 2.22$, which corresponds to $g_0/f_0 = 0.50$, i.e. the initial camber should be about 50 % of the expected one in the case of the stability loss. The factor for region A' is also close to this value ($K_i = 2.24$). It is much higher for other regions. Thus, for region B, after making vertical welds, $K_i = 3.4$, while after final welding the tension in this region dominates the compression, which makes the probability of the stability loss very low.

Similar conclusion can be made also for regions D, D', E and F for the wall of a larger thickness. Here the higher values of K_i or g_0/f_0 are required for the loss of stability to occur. For region D, it is necessary that $K_i > 4.28$; for D' — $K_i > 4.0$; for E — $K_i > 3.6$ and for F — $K_i > 2.48$ (after making vertical welds).

Another additional factor, which was not allowed for in the above estimations, but which is capable of affecting the risk of the stability loss, is preheating of edges prior to welding to ≈ 150 °C. The absence of comprehensive data about parameters of this preheating prevented its direct allowance in the calculations of residual stresses. Therefore, this effect was conservatively estimated by increasing the welding heat input by 40 % (see Table 5).

As seen from the data obtained, in the case of preheating the risk of the stability loss in regions A and A' is approximately the same as without preheating. The effect of preheating is low.

Table 5. Calculation of the wall energy for different regions in welding of insert plates into the wall of the coiled tank with a capacity of 50,000 m^3, MPa

Wall region	*After making vertical welds*			*After making all welds*		
	$\frac{U}{f_0^2}$	$\frac{W}{f_0^2}$	$\frac{U+W}{f_0^2}$	$\frac{U}{f_0^2}$	$\frac{W}{f_0^2}$	$\frac{U+W}{f_0^2}$
			Without preheating			
A	91.88	−38.60	53.30	91.88	−41.40	50.50
A'	260.09	−104.00	156.10	260.09	−116.40	143.70
B	334.15	−51.20	283.00	334.15	−98.20	236.00
C	313.90	−126.10	187.80	313.90	5.80	319.70
D	235.30	−50.90	184.40	235.30	−55.50	179.90
D'	664.30	−141.80	522.50	664.30	−159.70	504.70
E	389.40	−54.30	335.20	389.40	−103.20	286.20
F	313.90	−126.70	187.30	313.90	5.80	319.70
$П_1$	7.84	−12.65	−4.81	7.84	−15.85	−8.01
$П_2$		N/D		8.28	−36.42	−28.14
			At heat input increased by 40 %			
A	91.88	−46.90	45.00	91.88	−41.90	50.00
A'	260.09	−107.80	152.20	260.09	−137.30	122.70
B	334.50	−82.80	251.80	334.50	−119.60	215.00
C	313.90	−149.40	164.50	313.90	−44.80	269.20
$П_1$	7.84	−12.03	−4.19	7.84	−13.55	−5.71

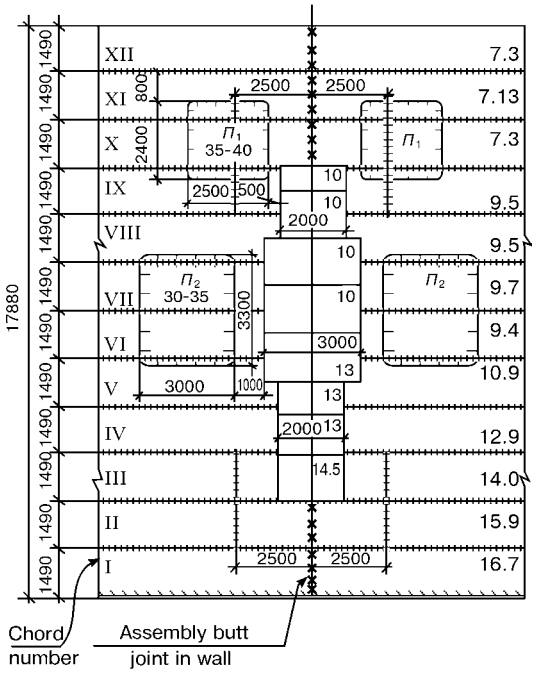

Figure 4. Location and sizes of experimentally found dents in the wall of a tank with a capacity of 50,000 m^3

Therefore, in welding of inserts into the wall of the tank with a capacity of 50,000 m^3, the probability of its loss of stability in regions *A, A′, B, D, D′, E* and *F*, confined by the factory butt joints, is low.

However, as proved by studies of the behaviour of the wall in welding-in of the insert plates, in practice the stability loss takes place even in the absence of an initial camber, especially with small thickness of the chords ($t \le 12$ mm). In this case the formation of dents in the tank wall occurs in regions Π_1 and Π_2 (Figure 4). In our case the Π_1 region was confined by a rigid disk of the upper stiffening ring and the circumferential weld between the upper and lower inserts, which is the zone of location of high tensile stresses. Boundaries of the Π_2 region are the said circumferential weld and thicker lower chord of the wall.

The above method (expressions (3), (4) and inequality (2)) was employed to make additional calculations for regions Π_1 and Π_2. Results of the calculations (see Table 5) showed that inequality (2) is met at $K_i = 1$, and in the regions under consideration one may expect the loss of stability of the wall in welding both without and with preheating. The calculation data proved occurrence of a local loss of stability of the wall in welding of insert plates in some chords or over its entire height by the technology recommended by standards [3].

Theoretical sizes of the affected zones and values of residual welding stresses formed in welding of horizontal and vertical inserts (Figure 5) served as the scientific base for development of the special technology for welding-in of the insert plates without any loss of stability of the wall.

CONCLUSIONS

1. The stressed state of the tank wall in the case of welding-in of insert plates under the rigid contour conditions is found to be characterised by a substantial length and high values of residual welding stresses. The presence of such stresses is the cause of the loss of stability of the wall.

2. The technology for welding-in of insert plates, recommended by standards [3], fails to provide the required geometrical shape in repair of assembly joints in the coiled tank wall.

3. Results of our investigations of the stressed state of the tank wall can be used for development of a special technology for welding-in of insert plates, ensuring geometrical shape of the wall within the tolerances specified by standards [2, 4].

Figure 5. General view of the assembly butt joint after repair made by welding of special inserts into tank of the oil-pumping station «Lisichansk». The tank has a capacity of 50,000 m^3 and is equipped with a floating cover («Pridneprovskie Magistralnye Nefteprovody»). Performer — «Bikor» Company

1. Barvinko, Yu.P., Golinko, V.M., Barvinko, A.Yu. et al. (2001) Improvement of performance of vertical erection welded joints in the wall of cylindrical tank made of coiled blancs. *The Paton Welding J.*, **7**, 27–32.
2. *VBN V.2.2-58.2–94*. Vertical steel tanks for oil and oil products storage under pressure of saturated vapours not higher than 93.3 kPa. Kyiv: Derzhkomnaftogaz.
3. (1988) *Safety regulations for tanks and instructions for their repair*. Moscow: Nedra.
4. (1995) *Instruction on engineering supervision, methods for inspection and rejection of pipe furnaces, tanks, vessels and units for oil refining and petrochemical industries*. Volgograd.
5. Makhnenko, V.I. (1976) *Computation methods for investigation of the kinetics of welding stresses and strains*. Kyiv: Naukova Dumka.
6. Karzov, G.P., Margolin, B.Z., Shvetsova, V.A. (1993) *Physico-mechanical modelling of fracture processes*. St.-Petersburg: Politekhnika.
7. (1967) *Physical properties of steels and alloys used in power engineering*. Refer. Book. Ed. by B.E. Nejmark. Moscow: Energiya.
8. Volmir, A.S. (1967) *Stability of deformable systems*. Moscow: Nauka.

PECULIARITIES OF COLD CRACKING IN WELDING OF HIGH-STRENGTH LOW-ALLOY STEELS*

V.I. SHVACHKO and **S.N. STEPANYUK**
The E.O. Paton Electric Welding Institute, NASU, Kyiv, Ukraine

Peculiarities of cold cracking of high-strength low-alloy steels are considered using a physical model. It is shown that their structure becomes highly sensitive to the embrittling effect of hydrogen under the influence of high temperature, losing the positive effect of thermomechanical treatment, and thus, becomes more susceptible to cold cracking.

Key words: *high-strength low-alloy steels, thermomechanical treatment, cold cracks, reversible hydrogen brittleness, microcleavage stress, toughness coefficient, high-temperature heating, HAZ of a welded joint*

High-strength low-alloy (HSLA) steels are the advanced high-quality materials used for the fabrication of critical structures. They are characterised by increased strength and retain high ductility [1]. However, welding these steels results in cold cracks (CC) which are formed in their welded joints. The existing methods for elimination of CC provide for the use of preheating of a welded joint or employment of austenitic welding consumables, this leading to a substantial increase in costs and labour consumption of welded fabrication [2].

Development of more suitable methods for elimination of cracking requires in-depth studies of the mechanism of cold cracking. Such studies should allow for the specific peculiarities resulting from the technology of manufacture of HSLA steels. Steels of this grade were developed on the base of improved low-carbon steels, in which the level of strength is achieved by special alloying, combined with the use of strengthening mechanisms during the γ–α transformation process and tempering [1].

The main factors affecting cold cracking, which have been established so far [3, 4], include metal structure, solute hydrogen, total stresses, strain rate and metal temperature. Cold cracking may take place only under the simultaneous effect of all these factors. Exclusion of at least one (any) of them will prevent this type of degradation.

Investigation of the mechanism of cold cracking under conditions of the actual welding process is hampered by continuous variations in temperature, structure, stresses, hydrogen mass transfer and a number of other parameters, which are interrelated to add to. In this connection, the study described in this article was carried out using physical modelling [5].

Cold cracking of welded joints is a manifestation of the general physical effect, i.e. embrittlement of iron and its alloys under the impact of hydrogen dissolved in metal, under specific conditions of the welding thermal cycle [3]. According to the classification of hydrogen embrittlement [6], cold cracking belongs to type six of the second kind, i.e. reversible hydrogen brittleness (RHB), induced by diffusible hydrogen [5, 7]. Therefore, the appropriate physical model developed by the E.O. Paton Electric Welding Institute from the concept of microcleavage for steels with the bcc lattice was used as the basis of the mechanism of CC formation [3, 5, 8].

Submicrocracks are formed in the bulk of metal under plastic deformation by the dislocation mechanism or as a result of microcleavage of particles of the second phase, carbide precipitates or non-metallic inclusions. Macrofracture is caused by that of the submicrocracks which loses stability at the moment of its formation in the total field generated by a dislocation cluster or external stresses. In this case, the moving dislocations carry with them part of hydrogen dissolved in metal. Thus, during the submicrocrack initiation process, hydrogen is carried by dislocations directly into the bulk of the formed cavity, where it is chemosorbed on the juvenile surfaces in the form of negative ions [3]. This leads to decrease in the surface energy of the submicrocrack. Thus, hydrogen decreases a critical fracture stress, upon achieving of which the crack, by overcoming the potential barrier, propagates in the force field by the self-catalysed reaction.

It follows from analysis of the accepted model of cold cracking that sensitivity of steel to the embrittling effect by hydrogen, which determines the degree of the risk of CC formation, depends primarily upon the type of the metal lattice. This is associated with the fact that the fracture mechanisms realised in the fcc lattice differ from those realised in the bcc lattice, and they have hydrogen diffusivity which differs by several orders of magnitude, this affecting the hydrogen transportation mechanism. The fact that HSLA steels have the bcc lattice causes their susceptibility to RHB. The impact on the sensitivity to hydrogen cracking by structural characteristics of this grade of steels was studied by mechanical uniaxial-tension tests of specimens subjected to high-temperature heating.

* The study was performed under the supervision of Prof. I.K. Pokhodnya.

Table 1. Chemical composition of steels under investigation, %

Steel	*C*	*Mn*	*Si*	*Ni*	*Cr*	*Mo*	*Al*	*Co*	*Ti*
AB-2Sh	0.100	0.75	0.23	2.80	1.00	0.21	0.008	0.005	0.019
MA	0.009	0.10	0.60	18.50	0.05	5.00	0.500	8.500	1.200

The indicator of the ability of a material to resist microcleavage, i.e. toughness coefficient K_t, was used as a criterion for quantitative estimation of the embrittling effect of hydrogen [9]:

$$K_t = R_{mce}/\sigma_y, \quad (1)$$

where σ_y is the yield strength of metal and R_{mce} is the fracture stress of metal deformed to degree e. Numerical values of R_{mce} are determined from the following formula [10]:

$$R_{mce} \approx S_k(1 + b)/(b(1 + 2/\eta)), \quad (2)$$

where S_k is the mean fracture stress in the neck; $b = \ln(1 + \eta/2)$; $\eta = 0.92(e - 0.1)$; $e = \ln(1/(1 - \psi))$; and ψ is the reduction in area. The S_k and ψ values are determined by uniaxial tension tests of standard smooth cylindrical specimens.

HSLA steel of the AB-2Sh grade was used for the investigations, and maraging (MA) steel was used for comparison (Table 1). To determine the effect of the level of heating on the sensitivity of these steels to the embrittling impact of hydrogen, the billets were preliminarily heated for the same period of time in a furnace preheated to a certain temperature and then cooled in air. The metal structure was checked after each heat treatment. The specimens were simultaneous by hydrogenated electrolytically in the 5 % solution of sulphuric acid with an addition of 0.05 % sodium thiosulfate. The current density being not in excess of 10 mA/cm^2, which prevented the probability of formation of irreversible defects. The standard smooth cylindrical specimens were tested at room temperature at a strain rate of 5 mm/min.

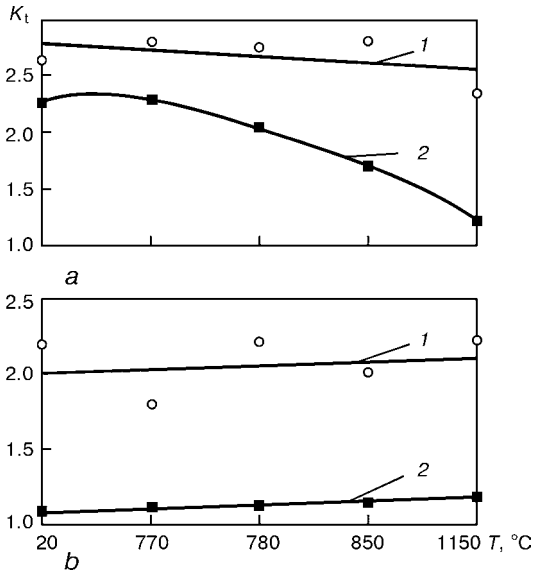

Figure 1. Dependence of toughness coefficient K_t upon the heat treatment temperature for steel AB-2Sh (*a*) and MA (*b*): *1* — non-hydrogenated; *2* — hydrogenated

The mechanical test results are shown in Figure 1 in the form of dependence of toughness coefficient K_t upon the heat treatment temperature. As seen from the plots presented, both steels in the hydrogenated state have a high level of toughness ($K_t \geq 2$). However, the specimens of MA steel exhibit catastrophic embrittlement in the presence of hydrogen, i.e. K_t becomes close to one (Figure 1, *b*), which is indicative of a decrease in brittle strength of metal to the yield strength level. It should be emphasised that it is the presence of hydrogen that causes the ultimately brittle state of the martensitic structure, which initially has a sufficient toughness.

In contrast to MA steel, steel AB-2Sh in the initial (untreated) state exhibits insignificant embrittlement in the presence of hydrogen (Figure 1, *a*). However, after heat treatment, toughness of this steel substantially decreases under the effect of hydrogen. It also starts being catastrophically embrittled, like MA steel. As shown by metallography, this decrease in K_t of steel AB-2Sh is not caused by formation of the martensitic structure characteristic of MA steel. With all the types of the heat treatment used, steel AB-2Sh retains the bainitic type of the structure. The only difference is that the degree of dispersion of the precipitates decreases, and their distribution in matrix becomes more uniform, as well as some changes in the grain size and microhardness take place (Table 2).

It follows from the above data that the sensitivity of steel to RHB depends upon the phase composition of metal and its crystalline structure. This is of a particular importance for HSLA steels. They are strengthened during manufacture due to special thermomechanical treatment which provides a high dislocation density in the initial structure. After that, formation of the pre-precipitation zones in the dislo-

Table 2. Metallography data

Steel	*Heat treatment temperature, °C*	*Grain area*, 10^{-4} mm^2*	*Microhardness*, MPa*
AB-2Sh	20	2.20	2000
	780	3.30	2300
	850	4.25	2450
	1150	5.58	2690
MA	20	12	2350
	780	18	2950
	850	20	2320
	1150	29	2535

*Mean values.

cation grid nodes is achieved by the secondary hardening method, which is followed by formation of coherent precipitates of special carbides [11]. Therefore, the special state of the microstructure leads to strengthening of steels and provides their very high resistance to RHB. However, heating to a high temperature decreases the effect of this treatment, which was found (see Figure 1, *a*) to be very favourable for hydrogen embrittlement. Therefore, during the fusion welding process, the structure of HSLA steel in the HAZ metal of the welded joint will become more susceptible to cold cracking (even without formation of quenching structures). In addition, this susceptibility will be different in different regions of the HAZ, as it depends upon the level of the achieved temperature.

It is extremely difficult to avoid this degradation of structure of HSLA steels in the HAZ metal in fusion welding, which is attributable to inevitability of high-temperature heating. Therefore, to reduce the risk of formation of CC in welding HSLA steels, it is necessary to prevent ingress of hydrogen into the HAZ metal of the welded joint. For this, it is indicated to use the effect of fixation of hydrogen in the weld metal using energy traps with a high binding energy [11].

1. Gorynin, I.V., Rybin, V.V., Malyshevsky, V.A. et al. (1999) Main aspects of development and application of high-strength structural steel. *Voprosy Materialovedeniya*, **3**, 7–21.
2. Irving, B. (1992) Preheat: the main defense against hydrogen cracking. *Welding J.*, **7**, 25–31.
3. Pokhodnya, I.K., Shvachko, V.I. (1997) Physical nature of hydrogen-induced cold cracks in welded joints of structural steels. *Avtomatich. Svarka*, **5**, 3–12.
4. Pokhodnya, I.K., Stepanyuk, S.N., Shvachko, V.I. (2000) Role of temperature in hydrogen-induced cracking of structural steels and welded joints. *The Paton Welding J.*, **2**, 2–7.
5. Shvachko, V.I. (1999) Reversible hydrogen embrittlement of steels as a physical phenomenon. *Fiziko-Khimich. Mekhanika Materialov*, **4**, 3–15.
6. Kolachev, B.A. (1985) *Hydrogen embrittlement of metals*. Moscow: Metallurgiya.
7. Shvachko, V.I. (2000) Cold cracking of structural steel weldments as the reversible hydrogen embrittlement effect. *Int. J. Hydrogen Energy*, Vol. 25, 473–480.
8. Pokhodnya, I.K., Shvachko, V.I. (1996) Cold cracks in welded joints of structural steels. *Fiziko-Khimich. Mekhanika Materialov*, **1**, 53–66.
9. Meshkov, Yu.Ya., Pakharenko, G.A. (1985) *Structure of metal and embrittlement of steel joints*. Kyiv: Naukova Dumka.
10. Pokhodnya, I.K., Shvachko, V.I., Kotrechko, S.A. et al. (1998) New method for quantitative estimation of susceptibility of steels to hydrogen embrittlement. *Fiziko-Khimich. Mekhanika Materialov*, **4**, 79–84.
11. Pokhodnya, I.K., Shvachko, V.I., Stepanyuk, S.N. (2001) Hydrogen traps in welded joints. In: *Transact. of Int. Conf. on Hydrogen Treatment of Materials*. Donetsk.

PECULIARITIES OF PLASTIC DEFORMATION OF DISSIMILAR MATERIALS IN PRESSURE JOINING

L.I. MARKASHOVA, V.V. ARSENYUK and **G.M. GRIGORENKO**
The E.O. Paton Electric Welding Institute, NASU, Kyiv, Ukraine

Considered are regularities occurring in physical-chemical processes of plastic deformation, mass transfer and phase formation, which accompany formation of joints in dissimilar materials (copper, titanium, aluminium and their alloys, and different grades of steels) characterised by a limited mutual solubility under conditions of pressure joining for a wide range of external loading rates, i.e. from $1 \cdot 10^{-4}$ to $1 \cdot 10^{4}$–$1 \cdot 10^{5}$ s^{-1}.

Key words: *plastic deformation, pressure joining, dissimilar materials, loading rate, localisation of deformation, sliding system, shear band, dislocation, twinning, rotation*

Plastic deformation is known to be one of the main parameters of pressure joining of metals and metals to non-metals [1–6]. It is the plastic deformation that is usually related to formation of a physical contact [1, 7], cleaning of surfaces from oxide films (especially under cold deformation conditions) [1, 3], activation of the mating surfaces which shows up as formation of active centres [4, 8], and, finally, development of volumetric interaction associated with activation of diffusion, recrystallisation, etc. In this case the contact zone acquires a more or less homogeneous structure, while mechanical, service and other properties of the joints become close to those of the base metal [1, 2, 8–13].

It should be noted that the plastic deformation process is one of the types of relaxation (relief) of internal stresses which grow during external loading of joining, or, to be more exact, the type of plastic relaxation which occurs by different mechanisms, such as sliding of individual dislocations, contribution of collective movement of the crystalline lattice defects, turns of microvolumes, including twinning, etc. In a case where the plastic deformation is locked for some reasons, relaxation of internal stresses in the deformed zone occurs by the cracking mechanism.

Therefore, considering a many-aspect character of the effect of deformation on formation of the joint and its properties, it is very important to have the most comprehensive idea of this significant process. In this respect it is of interest to have information on the character of distribution of the deformation within the joining zone, localisation of the deformation in depth of a material joined and its degree, and mechanisms of this process taking place under different conditions of pressure joining.

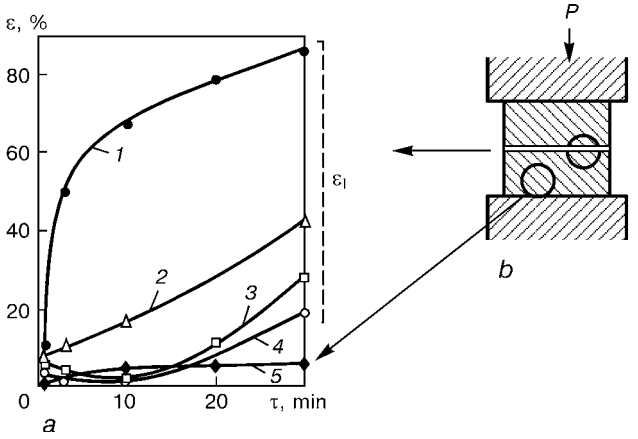

Figure 1. Distribution of strain ε in nickel joints produced by DB: *a* — ratio of total volumetric macrostrain to localised strain at different depth δ within the bonding zone; *b* — schematic of the bonding loading process at δ = 35 (*1*), 200 (*2*), 300 (*3*), 400 (*4*) μm and total macrostrain (*5*) (ε_l — localised strain; *P* — bonding pressure; τ — bonding time)

This article gives some of the results of the investigations concerning the above issues.

Experimental procedure and materials. Investigations were conducted on samples made from model materials, such as nickel NP-2 and alloys on its base of the KhN77TYu (C — < 0.15; Cr — 20.0; Ni — 77.0; Ti — 0.8; Al — 0.8 wt.%) type, joints in dissimilar metals and their alloys, such as commercially pure aluminium AD-1 and strengthened aluminium of the 1201 (Al–Cu) type, commercial titanium VT1-0, copper M-0 and M-1, steel St.3 (C — 0.14–0.22; Mn — 0.3–0.6 wt.%) and stainless steel. The joints were made at different rates of the joining deformation, $\dot{\varepsilon}$ (from $1 \cdot 10^{-4}$ to $1 \cdot 10^{4}$–$1 \cdot 10^{5}$ s^{-1}), which are used with such joining processes as diffusion bonding (DB), percussion welding (PW), magnetic-pulse welding (MPW), explosion welding (EW) and others. The general character of distribution of the plastic deformation and the degree of its localisation within the contact zone of a joint were studied by optical methods using coordinate grids with a base of 10–20 μm. This enabled estimation of not only the strain which is localised in the contact zone, but also its distribution in longitudinal and transverse directions (compressive and tensile strains). In addition, the degree of the deformation and its propagation depth were evaluated on the basis of variations in configuration of preliminarily varied structural elements used as references. The plastic deformation mechanisms, which are usually related to the type of structures formed within the deformation zone, were determined by the results of electron microscopy of the fine structure of metals joined. A series of such studies was carried out using the JEOL transmission electron microscope JEM- 200CX at an accelerating voltage of 200 kV. Foils for transmission studies of the contact zone in dissimilar joints were prepared by a specially developed integrated procedure of ion thinning in the ionising argon beam. This procedure provided data on the character of plastic deformation, degree and depth of its localisation and micromechanisms of this process.

Experimental results. As shown by the results of investigation into peculiarities of plastic deformation of metals joined at different loading rates within a range of $\dot{\varepsilon} \cong 1 \cdot 10^{-4}$–$1 \cdot 10^{5}$ s^{-1}, covering the DB and EW ranges, the plastic deformation had a clearly defined heterogeneous character under all thermal-deformation conditions, which was proved by the layer-by-layer measurement of its values within the joining zone in longitudinal and transverse directions with respect to the joining deformation direction. This regularity is characteristic of all the types of materials joined, i.e. model materials, such as nickel, and others characterised by different degrees of deformability and phase compositions.

An example of distribution of strain in nickel joints made by the joining process with low deformation rates is shown in Figure 1. As it can be seen from Figure 1, *a*, the values of strain are substantially different at different depths of the metal deformed. A detailed distribution of compressive and tensile strains can be seen in estimation of variations in coordinate grids in longitudinal and transverse directions of the samples. The distribution of strain in depth of the bonding zone at a bonding temperature of T_b = 1000 °C for 1 min is shown in Figure 2. As seen from the Figure, under the DB conditions, in joining nickel to nickel at a deformation rate of $\dot{\varepsilon} \cong 1 \cdot 10^{-3}$–$1 \cdot 10^{-4}$ s^{-1} the strain is localised within the welding zone at a depth of δ = 35–50 μm. As the process time increases, it amounts to 40–60 %, which is approximately by an order of magnitude higher than the total strain of the samples joined, equal to 4–5 %. Judging from the ratio of the localised com-

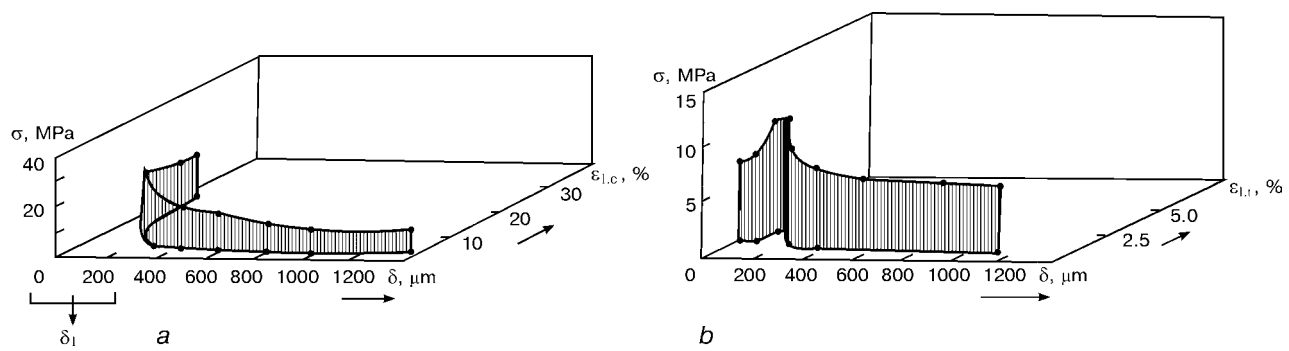

Figure 2. Distribution of stresses σ and localised strains, i.e. compressive $\varepsilon_{l.c}$ (*a*) and tensile $\varepsilon_{l.t}$ (*b*), respectively, at different depths δ from the interface between the metals joined (δ_l — localisation depth)

Distribution of localised strain in depth of the joining zone at $\dot{\varepsilon} = 1 \cdot 10^{-4} - 1 \cdot 10^{5}$ s^{-1}

Joining method	ε_l, %	δ_l, μm	$\varepsilon_{l.c}/\varepsilon_{l.t}$
DB	40–60	≤35–50	$\frac{8-10}{1}$
PW	90–95	≤50	N/D
EW	1000	150–200	$\frac{1}{15-20}$

pressive strain $\varepsilon_{l.c}$ to tensile strain $\varepsilon_{l.t}$ ($\varepsilon_{l.c} \cong 8-10\ \varepsilon_{l.t}$), the compressive strain is dominant. Corresponding diagrams were plotted for the nickel + Ni–Cr alloy joints made by the DB method at T_b = 800, 900 and 1000 °C and τ = 1–30 min for each temperature.

It should be noted that the range of localisation of strain shows up very clearly under all the conditions investigated. However, it increased in width to some extent with an increase in the process temperature and time. Similar patterns of distribution of the strain under the DB conditions were obtained also for the samples of other metal pairs studied.

Increase in the external loading rate in transition to high-speed joining processes (PW and EW) leads to increase in the degree of localisation of strain within the contact zone, as well as its propagation depth.

The Table gives the main parameters of plastic strain in the joining zone, i.e. values of the localised strain ε_l and localisation depth δ_l, which were experimentally found for different metals (nickel, aluminium and their alloys) at the investigated joining deformation rates ε_l. As seen from the Table, the localised strain amounts to 90–95 % under conditions of the high-rate pulsed loading, e.g. in the case of PW, where the level of the total strain equal to 4–5 % is identical to that in DB. In the case of EW, the degree of localisation of plastic strain within the contact zone is equal to about 1000 %, which is characterised by occurrence of a substantial increase in shear strains ($\varepsilon_{l.t} \cong 15-20\ \varepsilon_{l.c}$). The depth of the localised strain zone also changes with increase in the joining deformation rate, and amounts to 40–60, ≤50 and 150–200 μm at DB, PW and EW, respectively.

The next task was to reveal the mechanisms of realisation of plastic deformation localised along the length of the joining zone. Given that the types of the resulting structures are indicative of a plastic deformation mechanism, transmission electron microscopy of the fine structure and dynamics of variations in the types of structures formed directly along the contact surface in depth of the joining zone was carried out to determine the character of occurrence of plastic deformation in the joining zone. Peculiarities of structure formation within the contact zone at different rates of the joining deformation are shown in Figure 3. The Figure also shows the general character of structures of the contact zone in joints made under the DB, MPW and EW conditions. Figure 4 shows the most characteristic types of structural elements formed in the zone of localisation of strain under conditions of the above joining processes and the corresponding diagrams.

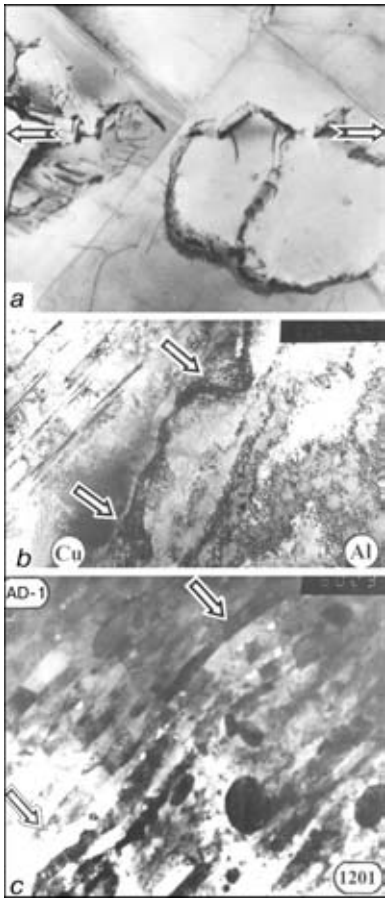

Figure 3. Structural changes in the contact zone, taking place in different joints depending upon thermal-deformation conditions of the joining process: *a* — nickel alloy of the KhN77TYu type in DB; *b* — aluminium + copper in MPW; *c* — AD-1 + 1201 in EW (×20000)

Thus, Figure 3, *a* and Figure 4, *a* illustrate formation of the characteristic structural elements (chaotic distribution of dislocations, ball-shaped–cellular and sub-granular structures near the contact surface) typical for the structure of the nickel alloy joints made under the low-rate DB conditions. In the case of increase in the deformation rate, e.g. in MPW (Figure 3, *b*) and EW (Figures 3, *c* and 4, *b, c*), the turbulent character of metal flow is dominant in the contact zone, turns of structural elements (in the form of fragmentation and twinning of grains), as well as the clearly defined orientation of structures are seen. This is proved by elongation of cells in a direction of effective stresses and formation of banded structures. In addition, turns of microvolumes covering regions of the sub-grain and even grain sizes also take place. Structure of some zones with non-destroyed individual dislocations acquires characteristic speckled contrast, the formation of which is usually related to alternation of crystalline and non-crystalline (amorphous) phases [14], which is proved, as a rule, by the appearance of halo on the microdiffraction reflections.

Statistical analysis of the types of structures performed on the basis of the investigation results showed that the process of the high-temperature deformation

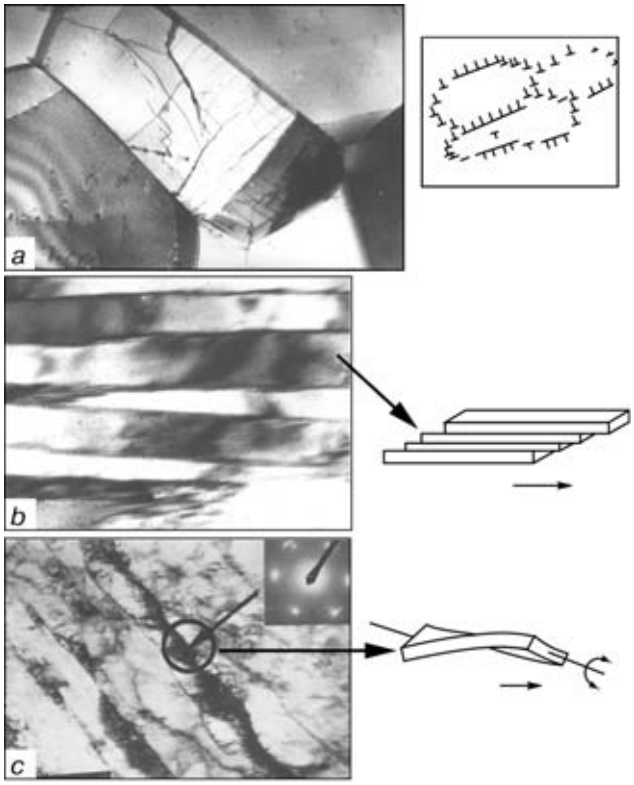

Figure 4. Types of structures in the localised strain zone at different external loading rates and their diagrams: *a* — cellular–sub-granular structure of the KhN77TYu type alloy in DB; *b* — shear bands in nickel in EW; *c* — reorientation turns and lines in nickel (see also Figure 3, *b*) (×30000)

leads, in addition to increase in the loading rate (i.e. in transition from DB to EW), also to formation of the following sequence of structures in the joining zone: flat dislocation clusters and chaotic distribution of dislocations; ball-shaped, block-like, cellular and sub-granular structures; fragments; twins; different types of banded structures (shear and reorientation bands). Changes of the types of structures in different metals within the joining zone, depending upon the joining deformation rates, are shown in Figure 5.

As seen from this Figure (left part), the similar types of structures and sub-structures (blocks, cells and sub-grains with clearly defined boundaries) are formed within the joining zone at the low joining deformation rates. The character of these structures does not depend upon the type of materials joined (their crystalline lattice, phase saturation and stacking fault energy). However, in transition to the higher joining deformation rates (in the case of PW, MPW and EW) the character of structures formed in the joining zone dramatically changes (see curves in the right part of Figure 5). This is associated with growth of the share of the collective forms of movement of the crystalline lattice defects, which show up as the intensive shear and reorientation bands, as well as structures the formation of which is caused by turns of structural elements. In this case, in metals characterised by lower values of the stacking fault energy (SFE), such as copper, Ni–Cr alloy and stainless steels, against the total amount of all the types of the formed structures there occurs an increase in the shear of structures whose formation is related to the turns of microvolumes in the deformed regions, i.e. twins, fragments with the clearly defined knife-like boundaries, etc. (Figure 5, *b*). In the case of joining materials with a complex phase composition, e.g. strengthened aluminium of the 1201 type, phase precipitates of the intermetallic type with a different character of band formation are seen: dominant in the structures are the reorientation bands, which are more discrete than the shear bands whose orientation drastically changes in the region of deceleration of the bands by the phase precipitates (Figure 5, *b*).

Statistical analysis of the results of direct studies of the fine structure and types of structures formed in the joining zone in dissimilar metals allows the following conclusion. Depending upon the conditions and rate of loading in the joining process, the plastic deformation (within its localisation zone) is realised involving different micromechanisms. At minimum deformation rates, i.e. $\dot{\varepsilon} \cong 1 \cdot 10^{-4}$–$1 \cdot 10^{1}$ s^{-1}, independently of the type of metals joined, the plastic deformation localised along the surface of contact of

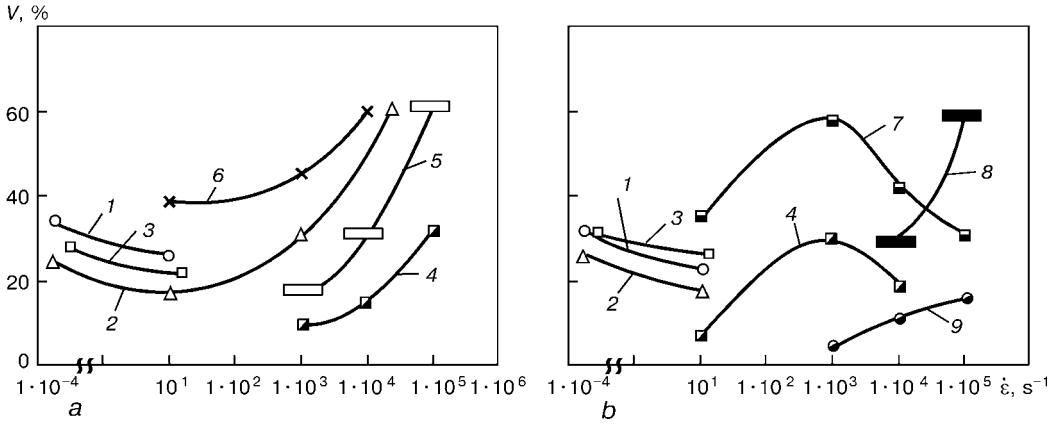

Figure 5. Dependence of the deformation mechanism upon the deformation rate in pressure joining of metals, which are similar in composition and have high SFE values (aluminium AD-1, nickel and Ni-base alloys) (*a*), metals with phase precipitates and metals characterised by lower SFE values (strengthened aluminium 1201, copper and stainless steel) (*b*): *1* — chaotic distribution of dislocations; *2* — ball-shaped–cellular structures; *3* — sub-granular structures; *4* — fragmented structures; *5* — shear bands; *6* — collective forms of movement of the crystalline lattice defects; *7* — twinning; *8* — reorientation bands; *9* — turns of grains and several grains (*V* — volume fraction of the types of structures)

the metals occurs mostly by the dislocation mechanism, which is realised through dislocation sliding along the crystallographic systems. This is accompanied by successive crystallographic turns of the deformed volumes. However, increase in the deformation rate, i.e. $\dot{\varepsilon} \cong 1 \cdot 10^4 - 1 \cdot 10^5$ s^{-1}, leads to a change in the mechanism of the plastic deformation, which now is realised by the mechanisms related to the intensive collective forms of movement of the crystalline lattice defects (translation in the form of shear and reorientation bands), as well as to involvement of the more radical (rotation) plastic deformation micromechanisms. The high-energy high-rate joining processes are also characterised by formation of the special mechanism of plastic flow of metal in the local contact region, similar to the hydrodynamic flow. Under such conditions the structure of metal is of the characteristic amorphous-crystalline type, which is interpreted as the atom-vacant and heavily non-equilibrium one [14].

Results of investigations of the dynamics of structural, including orientational, changes in the region of localisation of deformation in the case of joining dissimilar metals at different joining deformation rates are considered in more details in a number of papers dedicated to studies of weldability of titanium to copper [15], heat-resistant brittle alloys of the intermetallic type [16], high-strength aluminium alloys of the 1201 type [17, 18] and other hard-to-weld materials [19–22].

The data generated on peculiarities of plastic deformation, depth of its localisation and mechanisms of its occurrence make it possible to reveal factors which prevent the required flow of metal in depth of the joining zone, where the joining strain is localised, i.e. at a depth of about 50–200 μm, depending upon the joining process. This serves as the basis for selection of different technological approaches, which favour plastification of metal particularly in this joining zone. Some of such approaches were used for the development of a number of joining technologies.

For example, to make joints between aluminium AD-1 and high-strength aluminium of the 1201 type, the safety factor for ductility of the deformed layers of aluminium 1201 was increased due to special preparation of the mating surfaces, which allowed the latter to be cleaned from hardening intermetallic phases at a depth of about 200 μm. This resulted in minimisation of the collision parameters in reconditioning repair of thin-walled shell metal structures of the aircraft by explosion welding [18]. The phase instability effects appearing in a temperature range of α–β-phase transitions resulted in the activation of the deformation in DB of the Ti_3Al-based heat-resistant alloy [16]. Similar results were obtained in using special forming mandrels for joining titanium to copper in DB [15], Cu–Al transition pieces made by MPW [19] and other materials.

CONCLUSIONS

1. Integrated investigations were conducted to study peculiarities of plastic deformation within the contact zone in pressure joining of dissimilar metals in the case of variation in the joining deformation rate from $1 \cdot 10^{-4}$ to $1 \cdot 10^4 - 1 \cdot 10^5$ s^{-1}.

2. Plastic deformation has a heterogeneous character with a clearly defined localisation region over the entire range of external loading rates. Joints in dissimilar metals differ in the strain values ($\varepsilon_l \cong 40$–1000 %) and depth of their localisation zone ($\delta_l \cong$ $\cong$ 20–200 μm).

3. At $\dot{\varepsilon} \cong 1 \cdot 10^{-4}$ s^{-1} the plastic deformation is realised mostly by the dislocation mechanism; with an increase to $1 \cdot 10^4 - 1 \cdot 10^5$ s^{-1} it occurs mainly due to the collective forms of movement of the crystalline lattice defects and the rotation mechanisms.

1. Gline, C.Z. (1966) An analytical and experiment study of diffusion bonding. *Welding J.*, **11**, 481–489.
2. Putz, G., Starke, Z. (1967) Untersuchungen zur Weiterentwicklung des Kaltpreβschweiβens. *Schweiβtechnik*, **3**, 120–124.
3. Kazakov, N.F. (1976) *Diffusion bonding of materials*. Moscow: Mashinostroenie.
4. Gelman, A.S. (1970) *Fundamentals of pressure welding*. Moscow: Mashinostroenie.
5. Shron, R.Z., Zemzin, V.N. (1978) *Heat treatment and properties of welded joints*. Leningrad: Mashinostroenie.
6. Bakshi, O.A. (1977) *Theory and practice of welding manufacturing*. Sverdlovsk: UPI.
7. Einbinder, S.B., Glude, R.K., Loginova, A.Ya. et al. (1964) Fundamentals of pressure welding theory. *Avtomatich. Svarka*, **5**, 21–27.
8. Krasulin, Yu.P. (1983) *Interaction between metal and semiconductor in solid phase*. Moscow: Nauka.
9. Cunningham, C.W., Spetnak, I.W. (1962) Grain growth and sub-grain structure in pressure-bonded copper. *Transact. Metallurg. Soc. AIME*, **9**, 549–556.
10. Winslow, P.M., Horitz, D., Intyre, D.V. (1965) Adhesion and cohesion of metals in the space environment. *Pap. Amer. Soc. Mech. Eng.*, **16**, 9–11.
11. Wodara, J. (1965) Kaltpreβschweiβen. *Schweiβtechnik*, **9**, 411–415.
12. Yoshiyasu, I., Takahiko, S., Masahiro, S. et al. (1998) Characteristics of behaviour of diffusion in the transition zone of a copper-aluminium joint during friction welding. *Transact. Jap. Soc. Mech. Eng. AIME*, **618**, 494–499.
13. Kazuyuki, H., Takeshi, I., Takenobu, A. et al. (1993) Parameters of explosion welding and strength of joint in cladding stainless steel with different aluminium alloys using an intermediate stainless. *J. Jap. Welding Soc.*, **1**, 16–21.
14. Panin, V.E., Likhachev, V.A., Grinyaev, Yu.V. (1985) *Structural deformation levels of solids*. Novosibirsk: Nauka.
15. Markashova, L.I., Kireev, L.S., Zamkov, V.N. et al. (1997) Peculiarities of formation of an interfacial zone in pressure welding of dissimilar metals. In: *Welded structures*. Harwood A.P.
16. Zamkov, V.N., Markashova, L.I., Kireev, L.S. et al. (1992) Peculiarities of structural changes of refractory Ti_3Al-base alloy in vacuum pressure welding. *Avtomatich. Svarka*, **9**, 13–16.
17. Petushkov, V.G., Markashova, L.I., Zotov, M.I. et al. (1989) Micromechanisms and conditions of strain localisation in high energy loading. In: *Proc. of X Int. Conf. on High Energy Action on Metals*, Lyublena, Sept., 1989.
18. Petushkov, V.G., Markashova, L.I., Zotov, M.I. et al. (1989) Peculiarities of plastic deformation of aluminium in explosion welding. In: *Coll. pap. of Conf. on Special Methods of Welding*, Zagreb, March 30, 1989.
19. Markashova, L.I., Sergeeva, Yu.A., Statsenko, V.V. et al. (1990) Peculiarities of structure formation and mechanisms of plastic deformation in conditions of magnetic-pulse welding. In: *Welding of dissimilar, composite and multilayer materials*. Kyiv: PWI.
20. Markashova, L.I., Grigorenko, G.M., Arsenyuk, V.V. et al. (1998) On relationship between structure and properties of steel-aluminium joints made by friction welding. *Avtomatich. Svarka*, **8**, 7–14.
21. Zasimchuk, E.E., Markashova, L.I. (1990) Microbands in rolling-deformed nickel single crystals. *Materials Sci. and Eng. A.*, **127**, 33–39.
22. Ryabov, V.R., Markashova, L.I., Pavlenko, Yu.V. (1996) Study of weldability of the cordon-aluminium composite. In: *Proc. of I Int. SAMPE Symp. and Exhibition*, Anaheim, March 24–28, 1996.

TO THE QUESTION OF GMAW STABILITY

G.A. TSYBULKIN
The E.O. Paton Electric Welding Institute, NASU, Kyiv, Ukraine

The detailed analysis of transient and steady processes in welding circuit, as a result of which the region of stationary conditions and limits of their asymptotic stability were defined is presented.

Key words: *arc welding, stationary conditions, stability, transient and steady processes*

During developing new GMAW technologies and equipment, there is always a necessity of express-analysis in welding process conditions stability. The criterion according to which the process of arc welding is asymptotically stable, if steepness of the volt-ampere characteristics (VAC) of the welding arc is higher than steepness of the VAC of the power source feeding the arc is rather simple and efficient measure of stability.

Meanwhile it is well known that in certain conditions arc extinctions or short circuits of the welding gap that lead to violation of the welding conditions or to the full cessation may occur. It is this circumstance that seems to give reason to consider arc extinctions and short circuit as a result of instability of the welding process [5]. Though such interpretation of violation of the arc welding conditions causes objections of the conceptual character. The point is that violations of the conditions may occur as well while following the stability conditions.

In this connection this article gives the detailed analysis of the transient and steady processes of the welding circuit resulting in principal differentiation between the notions «violation of arc welding conditions» and «loss in stability» of these conditions.

Mathematical model. Consider the equations which within the frameworks of this task reflect the dynamic processes of interest occurring in the welding circuit during GMAW:

$$\begin{aligned} &L\frac{di}{dt} + (R + rh)i + u_a = u_s,\\ &u_a = u_0 + El + S_a i,\\ &u_s = u_* + S_s i,\\ &l = H - h \quad (0 < l < l_{cr}),\\ &\frac{dh}{dt} = v_e - v_m,\\ &v_m = Mi. \end{aligned} \tag{1}$$

In these equations L is the circuit inductance; R is the total resistance of the conducting wires and sliding contact in the welding nozzle; $r = 4\rho/\pi d^2$ is the coefficient that characterises electric resistance of electrode stickout h per unit length; ρ and d are the specific resistance and the electrode diameter, respectively; $u_a = u_a(i, l)$ is the arc voltage which is the function of welding current i and arc length interval l; $u_s = u_s(i)$ is the welding power source voltage; u_0 is the sum of near-electrode voltage drops; u_* is the open-circuit voltage; $E \equiv \partial u_a/\partial l$ is the electric field intensity in the arc column; $S_a \equiv \partial u_a/\partial i$ and $S_a \equiv \partial u_s/\partial i$ is the steepness of VAC of the arc and power source with a nominal current value i_0, respectively; H is the distance between the edge of the nozzle and free surface of the weld pool; l_{cr} is the critical value of the arc length, when the arc extinction occurs; v_e is the melting electrode feed speed relative to the torch nozzle; v_m is the electrode melting rate; $M = \partial v_m/\partial i$ is the steepness of characteristic of electrode melting at a nominal value of current i_0 and preset electrode stickout h_0; t is the current time.

The system of equations (1) does not include minor parameters, which characterise mostly the electrode metal transfer through the arc gap, movement of the free surface of the weld pool towards the axis of the electrode stickout and heat inertia of the arc itself. The effect of these and other minor parameters on the arc welding process is negligibly low.

Solving equations (1), with the respect to l at H = = const yelds one compact equation:

$$T_e T_s \frac{d^2 l}{dt^2} + T_s \frac{dl}{dt} + l = g, \quad 0 < l < l_{cr}, \tag{2}$$

where

$$g = \frac{u_* - u_0}{E} - v_e T_s \tag{3}$$

is the fixed control effect; T_e and T_s are the constants of time determined by relationships

$$T_e = \frac{L}{R_*}; \quad T_s = \frac{R_*}{EM}, \tag{4}$$

where

$$R_* = R\left[1 + \frac{r(H - l)}{R}\right] + S_a - S_s. \tag{5}$$

Equations (2) and (3) present the mathematical model of the controlled process of the arc length variations, $l = l(t)$, during GMAW. The attention should be paid to the fact that this model considers the actual physical limitations of the arc length $0 < l < l_{cr}$. It means that differential equation (2) at $l \le l_{cr}$ and $l \le 0$

has no sense, i.e. it describes processes occurring in welding circuit only during the arcing time.

Stationary conditions. Consider first the stable arc length component, $l_\infty = \lim_{t \to \infty} l(t)$ which according to the equations (2), (3), at $d^2l/dt^2 = 0$, $dl/dt = 0$ is determined by the following relationships:

$$l_\infty = g = \frac{u_* - u_0}{E} - v_e T_s; \quad 0 < l_\infty < l_{cr}. \tag{6}$$

It can be seen from (6) we can see that increasing the open-circuit voltage u_* or decreasing the electrode feed speed v_e leads to elongation of the arc l_∞. With some critical value $\frac{u_* - u_0}{E} - v_e T_s = l_{cr}$ the arc extinction occurs and the arc fades out. Increasing v_e or decreasing u_* according to (6), leads to the reduction of l_∞ and at $v_e = \frac{u_* - u_0}{E T_s}$ arc length l_∞ becomes zero.

Consequently there is a special range of steady conditions where the natural limitations on the arc length $0 < l_\infty < l_{cr}$ are not violated. Moreover by tuning the parameters u_* and v_e we can always define their ratio $\frac{u_* - u_0}{E} - v_e T_s = g_*$, when the welding process is conducted in the desirable way. This is the case used in practice.

The limitations of the noted range of the steady conditions are the relationships:

$$u_* - u_0 > E T_s v_e; \quad u_* - u_0 < E T_s v_e + E l_{cr}, \tag{7}$$

which are derived on the basis of (6).

The range of the steady arc welding conditions determined from formulae (7) is shown in Figure 1. Conditions included in this range according to [6] can be called stationary, as they do not vary in time at g = const, that is they are optimized without natural interruptions during arcing caused by the arc extinctions or short circuits of the arc gap. The higher range corresponds to non-stationary conditions which are characterized by the periodic arc extinctions. According to [4] they cannot be recommended for practical usage. Conditions of the range located below range *2* are physically non-realizable, as here $l < 0$.

But we should not miss the fact that within the limits of model (2) and (3) it is correct to consider only stationary conditions, i.e. those which are included in the said range, as outside this range equation (2), firstly, has no sense. Secondly, it is clear that steady conditions are possible only in case where transient conditions in the welding circuit attenuate asymptotically which means that the asymptotic stability of the welding process is guaranteed. Consider this issue in more detail.

Stability limits. Returning to relationship (5) it can be easily seen that $R_* = R_*(l)$, that is why equation (2) is linear. At the same time as coefficient r which belongs to (5) is low the relationship

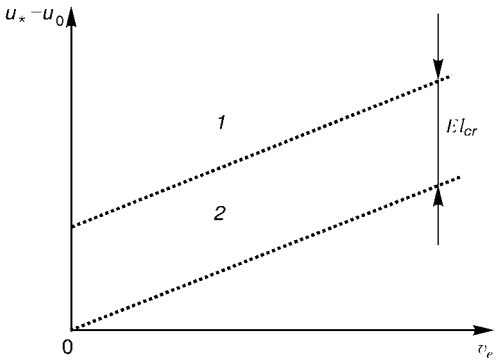

Figure 1. Limits of the conditional ranges: *1* — non-stationary; *2* — stationary

$\max_l \left\{\frac{r(H-l)}{R}\right\} = \frac{rH}{R} << 1$ is valid. Consequently for the estimation of stability we can use a simpler equation

$$R_* = R + S_a - S_s, \tag{8}$$

which does not depend upon l.

Introducing a new variable

$$\lambda = l - g, \tag{9}$$

we will obtain no load equation with fixed g

$$T_e T_s \frac{d^2\lambda}{dt^2} + T_s \frac{d\lambda}{dt} + \lambda = 0, \tag{10}$$

which describes the transient process in the welding circuit.

According to Stodola's algebraic criterion the transient process $\lambda(t)$ will certainly attenuate ($\lim_{t\to\infty} \lambda(t) = 0$) if the coefficients of equation (10) are positive, i. e. if $T_e > 0$ and $T_s > 0$. As L, E and M are positive, the above inequalities will be met according to the expression (4), only if $R_* < 0$. Then the sufficient and necessary algebraic condition of asymptotic stability of the processes in the welding circuit will ensue from the relationship (8) which can be written down in a usual form

$$S_a - S_s > -R. \tag{11}$$

As follows from inequality (11), the range of stability is actually wider than the range, which is de-

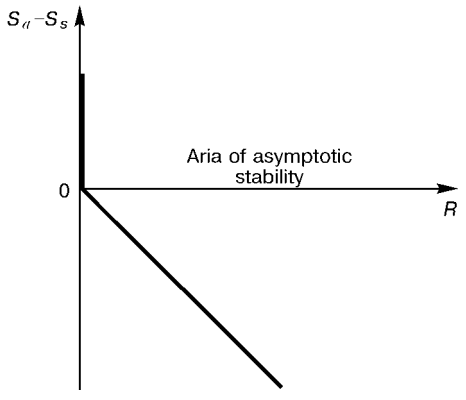

Figure 2. Limits of the range of asymptotic stability $R = 0$, $S_a - S_s > -R$

termined by the criterion $S_a - S_s > 0$ [1–4], and the higher the R value, the wider the range (Figure 2). It is sometime useful considering this fact.

Mind that here we consider the linearized model of equations (2) and (3) of the process under investigation. Therefore the point is just stability «in the small» [7–9], i. e. with such deviations of the arc length l from its stable value l_∞ where as a result of possible deviations of parameters S_a, S_s and R no violation of the condition (11) occurs. Consider one more point. In a real welding circuit $T_s >> 4T_e$, and this means that attenuation of the transient process $\lambda(t)$ is of an aperiodic character. Therefore, with any variations in the control effect of g in $[0, l_{cr}]$ interval, for example during tuning the conditions, the arc length l is always smaller than l_{cr}.

So in realisation of inequality (11) stationary conditions, i.e. conditions limited by the relationships (7), are asymptotically stable. However the limits of the stationary conditions (7) cannot be considered as the stability limits, i.e. without meeting inequality (11) conditions within these limits become transient. This is an essential point which should not be neglected in investigation of stability of the GMAW processes.

CONCLUSIONS

1. The limits of the range of stationary conditions are not the limits of stability of the arc welding process. They just single out those conditions in which the arcing goes without arc extinctions and short circuits in the arc gap. If the operation conditions go outside this range, this leads to violation of stability of the welding process.

2. The loss of stability in the arc welding process occurs only at violation of condition (11).

1. Nikitin, V.P. (1934) *Electric machines and transformers for arc welding*. Moscow-Leningrad: Energoizdat.
2. Paton, B.E., Lebedev, V.K. (1966) *Electric equipment for arc and electroslag welding*. Moscow: Mashinostroenie.
3. Leskov, G.I. (1970) *Welding arc*. Moscow: Mashinostroenie.
4. Lenivkin, V.A., Dyurgerov, N.G., Sagirov, Kh.N. (1989) *Technological properties of shielded welding arc*. Moscow: Mashinostroenie.
5. Sudnik, V.A., Erofeev, V.A., Logvinov, R.V. (1999) Study of stability of shielded arc welding process. In: *Transact. of Tula Univer. on Computer Technologies in Joining of Materials*. Tula.
6. Buki, A.A. (1991) *Modelling of physical-chemical processes of arc welding*. Moscow: Mashinostroenie.
7. Barbashin, E.A. (1967) *Introduction to stability theory*. Moscow: Nauka.
8. Voronov, A.A. (1979) *Stability, controllability, observability*. Moscow: Nauka.
9. Tsybulkin, G.A. (1986) On one algebraic condition of stability of linear dynamic systems. In: *Cybernetics and computer engineering*, Issue 69.

ENERGY DOSING IN ULTRASONIC WELDING OF RIGID POLYMERS

Z.P. LUGOVOJ and **N.P. NESTERENKO**
The E.O. Paton Electric Welding Institute, NASU, Kyiv, Ukraine

Specific features of technology of ultrasonic welding of rigid polymers on the example of products made from polymethylmethacrylate are described. Mathematical model of thermomechanical processes realized in the zone of welding was suggested and the main stages of polymer vibroheating were analyzed. Criterion of automatic dosing of applied energy, based on the dependence of deformation and temperature of weld zone on the amplitude of wave guide oscillations has been developed.

Key words: *polymers, ultrasonic welding, welding condition parameters, thermomechanical processes, dosing of energy, welding cycle*

Owing to their unique physical-mechanical properties and comparatively low cost the plastics find more and more wide application in many branches of industry, medicine, agriculture, etc. In this connection the problem of their joining is actual. At present the polymeric parts and structures are joined using bolts, rivets or other mechanical means, and also by their adhesion and welding [1]. The latter has a number of advantages as compared to other methods, as the joints produced are close by their mechanical, dielectric and other properties to the initial material.

Among the existing types of welding it is impossible to distinguish one type which could satisfy economic, technological and service requirements. Each method has advantages and drawbacks and, depending on physical-mechanical properties of polymer, purpose of product, production quantity, the definite type of welding can be preferred. It is shown in works [1–3] that to join the products of rigid polymers (polystyrene, polymethylmethacrylate, etc.) it is most rational to use the ultrasonic welding (USW). However, the implementation of USW in the production encounters a number of technological, materials science and design problems.

In the present article the regularities of the process of formation of welded joints in USW on the example of polymethylmethacrylate (PMMA) are shown, ge-

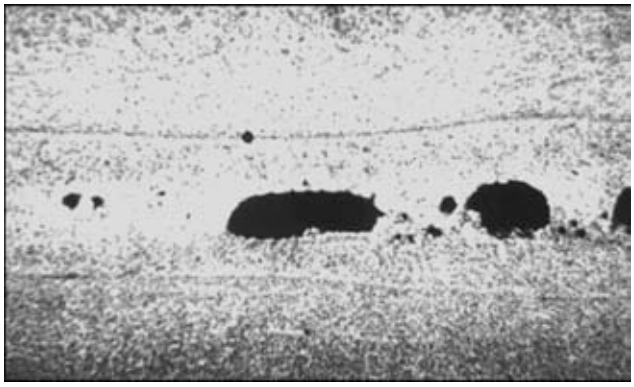

Figure 1. Macrostructure of PMMA welding zone (×60)

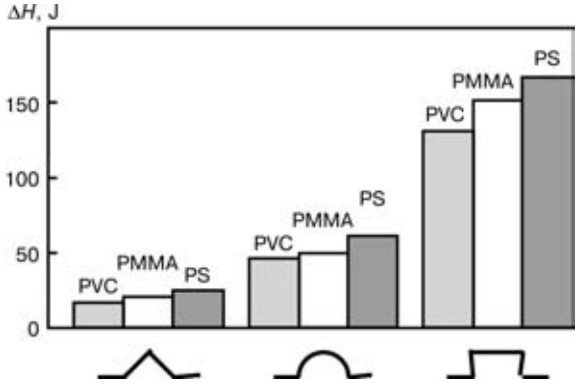

Figure 2. Dependence of heat amount ΔH on the type of polymer and shape of grooving

neral approaches to the selection of optimum condition parameters of welding rigid polymers are formulated and criteria of automatic dosing of mechanical energy, applied to the welding zone are suggested.

The main difficulty of welding of PMMA consists in the fact that temperature of melting the joint zone can exceed 580 K during the process of applying ultrasonic oscillations, which is higher than the temperature of material decomposition [1, 4]. Due to this the defects in the form of voids or products of polymer thermal destruction are observed in the welded joint when the intensive conditions are used (Figure 1). Varying the main welding condition parameters it is possible to reduce the amount of pores, but in this case the significant thinning of parts being welded is occurred. To increase the quality of welded joint is possible by artificial edge grooving [2, 3]. For this purpose the relation between the shape of stress raiser and with power and deformational processes in the joint zone at different USW conditions was studied.

Projections of three types were made on the welded samples (75×20×4 mm) from polyvinylchloride (PVC), PMMA and polystyrene (PS): flat, semicircular and V-shaped. Projections had equal height and similar volume (V = 225 mm^3). Welding was performed in installation of Branson 8600 type using a step wave guide. To define the boundaries of varying main parameters of USW conditions and to reduce the expenses for experiment a mathematical model of thermomechanical processes, realized in the joint zone, was developed.

Mathematical description of thermomechanical processes in USW in the system of coordinate (x_1, x_2) is given in the scope of a binding problem of thermoviscoelasticity, whose statement includes equations of oscillations

$$\tilde{\sigma}_{ij,\,j} + \rho\omega^2\tilde{u}_i = 0,$$

of energy

$$c_v\dot{T} = (kT_{,\,i})_{,\,i} + \overline{D}', \quad i, j, k \leftrightarrow x_1, x_2$$

physical equations for stresses and rate of dissipation of mechanical energy

$$\tilde{\sigma}_{ij} = 2\tilde{G}(\tilde{\varepsilon}_{ij} + \frac{\tilde{\nu}}{1 - 2\tilde{\nu}}\,\tilde{\varepsilon}_{kk}\,\delta_{ij});$$

$$\overline{D}' = \frac{\omega}{2}(\sigma_{ij}''\varepsilon_{ij}' + \sigma_{ij}'\varepsilon_{ij}''),$$

and also corresponding boundary and initial (for temperature) conditions.

Here, $\tilde{\sigma}_{ij}$, $\tilde{\varepsilon}_{ij}$ and $\tilde{u}_i$ are the amplitudes of components of stress tensors $\tilde{\sigma}_{ij} = \sigma_{ij}' + \sigma_{ij}''$, deformations and vector of displacements; ρ is the density; ω is the circular frequency; c_v is the heat capacity; k is the heat conductivity coefficient; T is the temperature in the weld zone; G, $\tilde{\nu}$ are the integrated shear modulus and Poisson's coefficient ($\tilde{G} = G' + iG''$, $\tilde{\nu} = \nu' - i\nu''$); δ_{ij} is the Kronecker's symbol.

The above-mentioned model is based on the following assumptions: body material is isotropic viscoelastic; all the mechanical variables (the components of vector of displacement) tensor of strains and stresses, are changed by a harmonic law at a circular frequency ω ($\omega = 2\pi f$), equal to frequency f of oscillations of the tool working edge; oscillating constituents of changing temperature during the period of oscillation are small as compared with a typical change of temperature during the welding cycle; inner losses are the main mechanism of dissipation of mechanical energy [4].

Problem in a two-dimensional statement was solved by using the numerical method of finite ele-

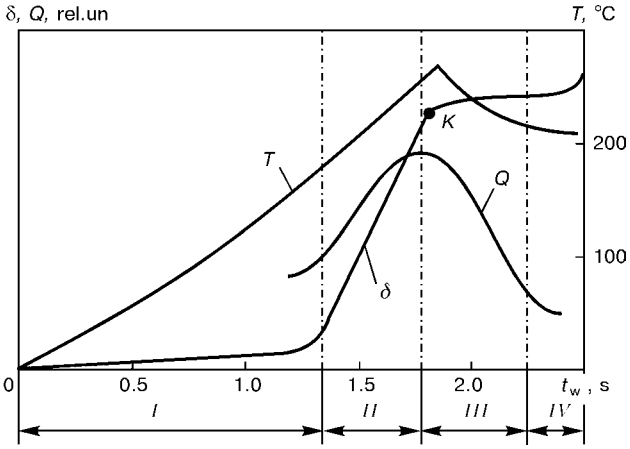

Figure 3. Dependence of temperature T, upsetting δ and joint strength Q on time of welding t_w

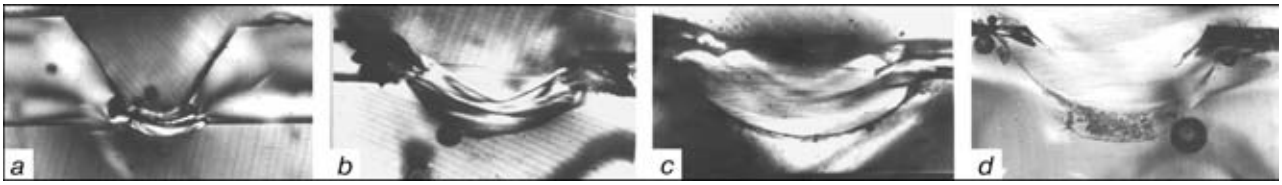

Figure 4. Macrostructure of welded joints of sample from PMMA: *a–d* — regions *I–IV* in Figure 3, respectively (×60)

ments [5]. To increase the effectiveness of calculations in the high-frequency zone of oscillations and to obtain the more detailed description of curvilinear boundaries of stress raiser, an eight-nodal isoparametric finite element was used. Within each of elements the displacements and temperature were approximated by quadratic functions of coordinates. Taking into account the short-time of welding cycles (0.1–5 s), the real scheme with time was used for integrating the energy equation. In addition, physical-mechanical characteristics of material were clarified and equations of movement were solved after a certain number of pitches. This process was interrupted when the temperature of polymer transition into a viscoyielding state was reached.

The calculations allowed us to determine the range of varying the amplitude of wave guide oscillations A = 10–45 μm and static compression force F = 100–1200 N.

The effect of parameters of USW conditions and physical-mechanical properties of polymer during welding time t_w is described by relation

$$t_w = \frac{2}{\omega} \int_{T_0}^{T_w} \frac{c_v(T)}{\beta \varepsilon^2 E''(T)} dT.$$

Here, t_w is the time of vibroheating of polymer from initial temperature T_0 to temperature T_w, that corresponds to its transition into viscoyielding state; $\varepsilon = A/h$ (h is the total thickness of parts welded); E'' is the modulus of Young's losses. Coefficient β characterizes the shape of surfaces welded and contact conditions at their interface.

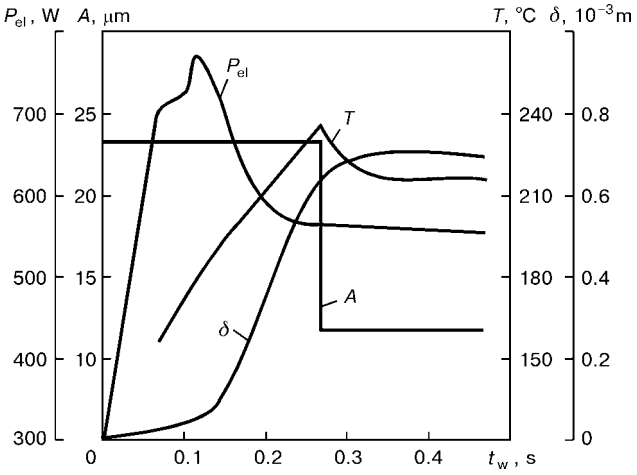

Figure 5. Dependence of electric power P_{el}, amplitude of wave guide oscillations A, temperature T in the weld zone and its upsetting δ on time of welding t_w

The investigations made it possible to establish the dependence of heat amount ΔH, required for polymer transition into the viscoyielding state, on the type of polymer and shape of grooves of edges being welded (Figure 2). It is seen from the Figure that energy ΔH depends not only on the type of polymer but also on the shape of grooving. Thus, V-shaped projection, in particular, is the lowest energy consuming. Mean values of energy activation for different shapes of projection are related approximately as 1:3:8. This ratio can be used as an approximate evaluation for determination of required power of the ultrasonic equipment.

To develop the criteria of mechanical energy dosing the thermomechanical cycles of PMMA USW were investigated more in detail. According to [1, 2], the artificial V-shaped stress raisers with an opening angle 60, 90 and 120° were made on the plate surfaces welded. During welding all the main parameters of technological condition, and also upsetting δ and welding zone temperature were recorded. Strength tests of welded joints were made on updated rupture machine of FP-10 type. Results of investigations are given in Figure 3. As is seen from the Figure, the dependence of upsetting value δ on the time of welding t_w has four typical regions.

In region *I* the heating of zone of contact of V-shaped projection with a lower part is occurred (Figure 4, *a*). Deformation of welding zone in this region is negligible. With increase in time of effect of ultrasonic oscillations the contact zone is heated to the temperature of a viscoyielding state of the polymer. The heated polymer begins to extrude intensively from this zone (region *II*) that is confirmed by visual observations of welds cuts under the microscope. At the end of region *II* of deformation curve (Figure 4, *b*) all the V-shaped projection is transformed into melt. The rate of deformation of the welding zone, which was maximum before, is decreased. In this case the melt temperature is close to the temperature of thermal destruction of polymer, and the welded joint strength Q is maximum.

The further increase in time of effect of ultrasonic oscillations leads to the fusion of parts under the wave guide, thinning of total thickness of parts welded (region *III*, Figure 4, *c*). In region *IV* of weld zone the voids and zones with products of thermal decay of polymer are formed and the strength of welded joints is abruptly decreased (Figure 4, *d*).

The carried out additional investigations on optimizing the USW conditions and search for new technological cycles enabled us to establish that temperature in the zone of welding can be stabilized by de-

crease in amplitude of oscillations of the wave guide by 40–50 % at the moment of time which corresponds to the beginning of region *III* of deformation curve (point *K* in Figure 3). The indicated fact has a good correlation with the results of [1, 2] in which, however, the principles of automatic control of welding process are not considered.

Figure 5 shows the developed cycle of USW of PMMA which makes it possible to dose the mechanical energy applied to the welding zone in the automatic conditions. The principle of criterion of dosing of applied energy consists in the fact that the decrease in amplitude of wave guide oscillation is realized at the moment of completion of the stage with a maximum rate of the welding zone deformation (see Figure 5). Technical realization of the mentioned method is attained using transducers of linear displacements, high-voltage watergate, appropriate block of signals being taken and microprocessor, which are built-in into the installation. The auxiliary control of the USW process proceeding is realized by indications of the wattmeter [6]. The developed method of control of USW of rigid polymers makes it possible to automate the technological process, to decrease the scattering of values of strength of joints by 10 %, and also to increase the weld quality due to absence of products of thermal destruction of the polymer in it.

1. Volkov, S.S., Chernyak, B.Ya. (1986) *Ultrasonic welding of plastics*. Moscow: Khimiya.
2. Mozgovoj, I.V. (1991) *Fundamentals of ultrasonic welding technology of polymers*. Krasnoyarsk: KGU.
3. Volkov, S.S. (1999) Optimisation of geometry of ultrasonic welded parts from rigid plastics. *Svarochn. Proizvodstvo*, **8**, 23–27.
4. Senchenkov, I.K., Chervinko, O.P., Nesterenko, N.P. (1991) Mathematical modelling of thermal vibration processes in technological systems for ultrasonic welding of plastics. In: *Abstr. of pap. of 3rd All-Union Conf. on Mechanics of Heterogeneous Structures*, Lvov.
5. Kozlov, V.I., Karnaukhov, V.G. (1983) Finite element method of study of thermomechanical behavior of viscoelastic bodies of revolution in cyclic loading. *Prikladnaya Mekhanika*, **11**, 40–45.
6. Nesterenko, N.P., Korab, G.N., Shkarlupa, P.I. (2000) Machine for ultrasonic welding of plastics. *Svarshchik*, **1**, 14–15.

METHODS OF DESIGN OF WELDING INDUCTORS (REVIEW)

R.V. YUKHIMENKO
The E.O. Paton Electric Welding Institute, NASU, Kyiv, Ukraine

The most widely used methods for design of welding inductors are considered. Advantages and drawbacks of the described methods and also the feasibility of their use in practice are outlined. Main relationships of parameters of experimental and claculated data of a linear inductor for heating flat surfaces and for seam induction welding are given.

Key words: *high-frequency welding, welding equipment, designs of inductors, methods of design, equivalent circuits*

The method of a high-frequency (HF) welding [1–3], providing a high rate of processes and a good quality of weld, has found a wide application in the manufacture of electrically-welded pipes, thus replacing other welding processes. In this connection, a problem arises in a valididity of results of designing induction heating units and in reduction of costs and terms of their experimental tests, because the existing heaters are complicated and expensive units.

Inductor is a basic element of the HF welding equipment. Therefore, its electromagnetic and technological characteristics define mainly the welding quality and process economical aspects. There are many designs of the inductors. Moreover, inductors of different types can be used even for heating one product. The following types of inductors can be conditionally distingished: for external cylindrical surfaces; for flat surfaces; for internal cylindrical surfaces; inductors for intricate bodies.

Any inductor contains an inductive wire, generating a magnetic field, current-carrying busbars, contact shoes for connection to a HF transformer, devices for water feeding for cooling inductor and heated surface (if necessary). Inductors for heating flat and internal cylindrical surfaces are often furnished with magnetic circuits which increase the efficiency factor and the device power factor. The magnetic circuits are also used for the formation of a magnetic field providing the required configuration of the metal layer being heated. In some cases the inductors are equipped with devices for arrangement of workpieces to be heated.

The main task of design of electromagnetic system for induction heating [4, 5] is the determination of input parameters of a loaded inductor: resistance and reactance, efficiency factor, power factor, current, voltage and number of turns by preset geometric parameters, current frequency, power and electrical properties of inductor and workpiece material. As the inductor and workpiece form a system with distributed parameters, the conceptions of resistances are not adequately defined, but refer obligatory to an equivalent circuit representing an electrical circuit,

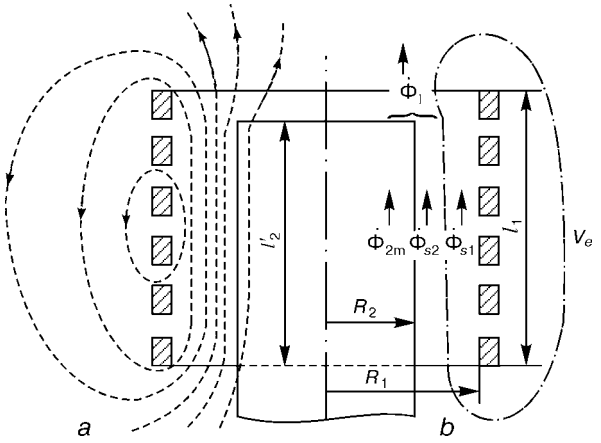

Figure 1. Pattern of magnetic field of inductor with a non-magnetic load (*a*) and separation of fluxes in system (*b*)

which is used for a mathematical modelling of a loaded inductor.

In spite of the wide use of numerical and analytic methods of calculation the approximated methods are mainly used in practice of designing of induction heaters, making it possible to find the integral parameters of systems (resistance, power factor, efficiency factor) with a satisfactory accuracy. Among them a method of a magnetically-coupled circuits [6] and a method based on compiling magnetic equivalent circuits of inductors are widely used [7–9].

Method of magnetically-coupled circuits, which uses the replacement of winding of inductor and workpiece by two inductively-coupled coils, gives good results for simple cylindrical or oval inductors in heating non-magnetic bodies with a clearly expressed surface effect. For complex induction systems, including several windings and bodies heated, the calculation is abruptly complicated, therefore, it is possible only in use of the computer [10]. The calculation is especially difficult using this method for systems containing ferromagnetic bodies and magnetic core heated.

Method based on compiling magnetic, and then dual electrical equivalent circuits was first suggested for crucible furnaces and cylindrical heating inductors with a loading being equal in length to the inductor winding. The comprehensive testing and development of the method for cases of non-equal lengths of inductor and workpiece [11] promoted its wide use for design of inductors of different types under the name of *method of a general flow* [7]. Calculations using this method are applicable both for non-magnetic and the ferromagnetic bodies.

Design of induction devices on the basis of ***magnetic equivalent circuits*** found a wide application [7–9] and at present it is one of main engineering methods in the design of inductors. The principle of this method consists in the fact that all the space in which a magnetic flux is passing is divided into sections; then their magnetic resistances are found using analytic or other methods.

We assume that the magnetic field is homogeneous in the entire length of body or its calculated region being heated l_2', locating inside the inductor (Figure 1) that makes it possible to find magnetic Z_{m2} and corresponding electrical resistance of loading as a length of a finitely long system. At known Z_{m2} the magnetic equivalent circuit can be considered as a four-terminal network, transforming Z_{m2} into input magnetic resistance of the inductor.

The total flow of inducror $\dot{\Phi}_i$ (Figure 2), created by winding, is divided into flow $\dot{\Phi}_{s1}$, not depending on loading, and flow $\dot{\Phi}_1 = \dot{\Phi}_{s2} + \dot{\Phi}_{2m}$ passing along the body heated $\dot{\Phi}_{2m}$ and along the part of gap adjacent to it $\dot{\Phi}_{s2}$ and then closing through region V_e (see Figure 1) with magnetic resistance R_{me}.

Magnetic circuits R_{ms1} and R_{ms2} refer to the gap regions through which flows $\dot{\Phi}_{s1}$ and $\dot{\Phi}_{s2}$ are passing.

Electrical circuit (Figure 3) corresponds to magnetic equivalent circuit. Resistance of loading $Z = r_2 + jx_{2m}$, gaps x_s and path of return closing x_e are reduced to the number of inductor turns w_1 and are coupled with magnetic resistances by relation

$$Z_i = j\omega w_1^2 / Z_{mi}. \qquad (1)$$

Additional resistance Z_{ad}, not associated with an equivalent circuit, takes into account a resistance of winding r_1 and resistance of elements (busbars, series capacitors) which can be connected into circuit at the region to power source with known $\dot{U}_i$. To calculate the internal reactance of winding x_{1m} is simpler and more accurare not separately but as a part of a gap resistance.

Direct use of the circuit (Figure 3) for design of inductors is difficult due to impossible practical determination of a point of branching magnetic fluxes and, respectively, electric currents using this method, therefore, we take auumption that all the flow in the gap together with $\dot{\Phi}_{2m}$ is closed in the form of a com-

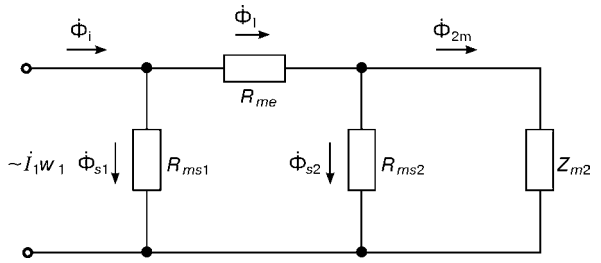

Figure 2. Magnetic equivalent circuit of inductor

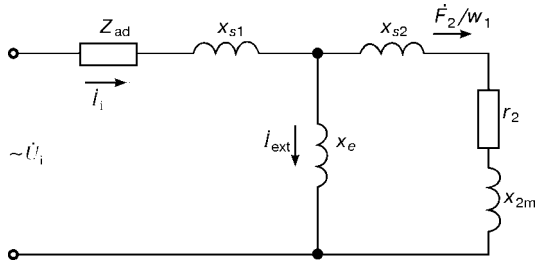

Figure 3. Electrical equivalent circuit of inductor

mon flow through the space V_e. Circuit (see Figure 3) at $x_{s2} = x_s$ and $x_{s1} = 0$ corresponds to this method of calculation, named *calculation by a common flow*.

Resistance of inductor will be equal to

$$Z_i = Z_{ad} + r_2 + jx_i = Z_{ad} + r_2 c + jc\left(x_i + \frac{x_i^2 + r_2^2}{x_e}\right), \quad (2)$$

where $x_e = x_{2m} + x_s$ is the reactance of gap and loading; x_e is the resistance of return closing ; c is the coefficient of reducing loading parameters to inducror, equal to

$$c = \frac{x_e^2}{r_2^2 + (x_e + x_l)^2}. \quad (3)$$

Using this method of calclation it is most difficult to determine the resistance x_e which gives a minimum error in calculation and depends on the nature of distribution of electrical current in loading. Here, an artificial procedure is used [8]. Let us assume that all the current in loading is concentrated in the band of width a, equal to a slot width a_{sl} (Figure 4). In addition, we consider that resistance x_e is little changed, if to make allowance for the effect of real loading on it using an additional gap Δh beyond which the magnetic field is not spread. A number of calculations showed that Δh should be so that additional inductive resistance Δx_h was equal to loading resistance x_{2m}:

$$\Delta h = \frac{x_{2m} a_{sl}}{\omega\mu_0} = \frac{x_0}{\omega\mu_0}, \quad (4)$$

where μ_0 is the magnetic permeability of vacuum; ω is the angular frequency of current.

The taken assumption makes it possible to determine x_e. Moreover, when x_e is calculated the loading is changed by a superconducting plane being at distance $h_{eq} = h + \Delta h$. This system can be considered as a half of the busbar with a distance $H = 2h_{eq}$ between busbars having an external magnetic circuit. The second half of the busbar is obtained as a mirror reflection of inductor with respect to superconducting plane.

Applying the calculation by the method of a common flow to the busbar we shall obtain

$$x_e = \frac{\omega\mu_0 H}{2a_{sl}} \frac{K_L}{1 - K_L}, \quad (5)$$

where K_L is the correction factor of inductance of busbar.

This method is widely used because it gives the correct limiting transitions at change in length, diameter, properties of loading, and also frequency. Thus, at high increase in frequency ($f \to \infty$) the coefficient of reduction c is tended to a finite value $c_{limit} = x_e^2/(x_s + x_e)^2$ defined only by the system geometry.

The drawback of this method is a low accuracy for number of purposes, for example, for parametric optimizing of the inductor design. Method does not also take into account the effect of edge effects of loading and inductor on the distribution of power in loading. The position of loading with respect to a central plane of the inductor is not also taken into account (if $l_2 < l_1$).

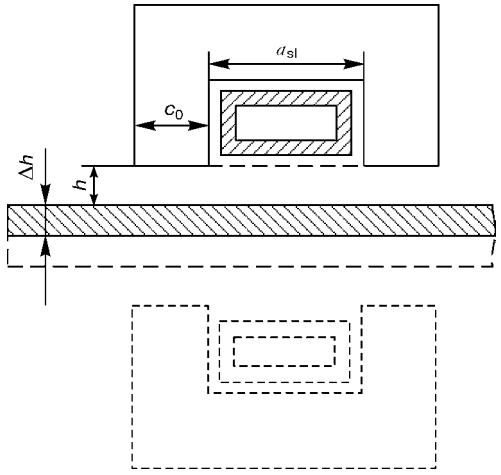

Figure 4. Design of a flat inductor with a magnetic core

In spite of these drawbacks the method of a common flow can be considered as one of main methods of approximated calculation of inductors which makes it possible to select the heater design at the initial stage of designing and to evaluate its parameters. Good results are obtained by the method of a common low in calculation of complex, including three-dimensional, induction systems.

If the inductive wire is furnished with a П-shaped magnetic circuit, then it is possible to use a *method of a working flow* [7, 12] based on referring all the inductive impedance x_e to the resistance x_{s1} in a nonbranched part of scheme (see Figure 3) and on determination of resistance x_e from the condition of unformity of flow $\dot{\Phi}_{2m}$ under the magnetic core pole. This method gives good results at a ferromagnetic loading, however, at large gaps its precision is quickly decreased. Limiting transitions are also not kept with increase in frequency ($f \to \infty$) or width of magnetic core pole ($c_0 \to \infty$), as the calculated coefficient of reduction c is tended in these cases to unity that does not reflect the reality.

To make allowance for the non-uniformity of magnetic field in an air gap of the inductor the calculation can be made using a *method of conformal representations* [13] at following assumptions: depth of current penetration into a metal heated is small as compared with a gap between the inductive wire and pipe, and the value of air gap is significantly smaller than a radius of a pipe curvature; electric characteristics of material heated are constant (μ = const, ρ = const); magnetic permeability of inductor iron is high; length of inductor is much larger than its cross-section; inductor current is changed by a harmonic law.

Results of calculation of magnetic field intensity at the surface of pipe heated in line $0x$ (see Figure 5) are presented in Figure 6 [13].

Analysis showed that at $\beta \to \infty$ and $a >> 1$ the calculated expression can be presented in a simplified form as

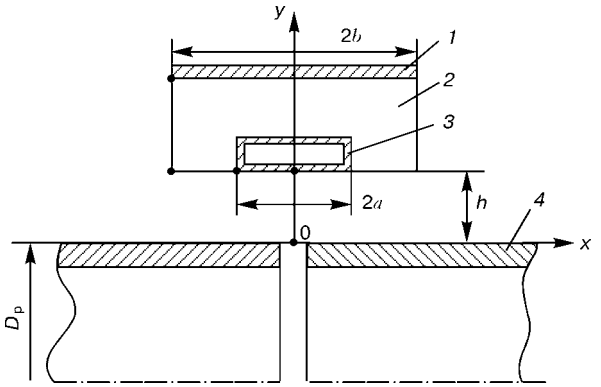

Figure 5. Scheme of heating pipe butts with a linear inductor in HF welding: *1* — part heated; *2* — induction wire; *3* — magnetic core; *4* — return wire

$$\frac{H_2}{H_{av}} = \frac{1}{1 + (0.44/a_0)} \approx 1, \qquad (6)$$

where $H_{av} = \omega I_0 / 2a$.

Consequently, magnetic field in inductor air gap is approximated with an accuracy up to 5 % only at $a_0 > 10$.

The inductive impedance of the linerar inductor–pipe system is determined from expression

$$x_s = \frac{\omega \mu_0 w^2 l_i}{2a_0} Q(a_0, b_0, c_0), \qquad (7)$$

where $Q(a_0, b_0, c_0)$ is the function taking into account the design sizes; l_i is the inductor length.

Resistance of pipe heated, reduced to the inductor current, is determined from equation

$$r_2' = \frac{w \rho_2 l_i}{2a\Delta_2} g_a(a_0, b_0, c_0), \qquad (8)$$

where ρ_2 is the specific electric resistance of material of pipe heated; Δ_2 is the depth of current penetration into a pipe metal; $g_a(a_0, b_0, c_0)$ is the function taking into account the non-uniformity of field at real sizes of inductor.

The comparative calculations showed that a satisfactory coincidence of results of calculations is observed at $a_0 > 2$, and with increase in a relative value

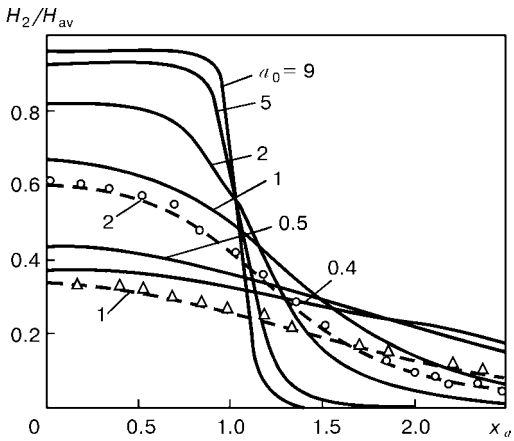

Figure 6. Distribution of magnetic field at the surface of part being heated along the axis $0x$ ($x_a = x/a$) at $b_0 = b/r \to \infty$, $c_0 = c/r \to \infty$ and different values $a_0 = a/r$

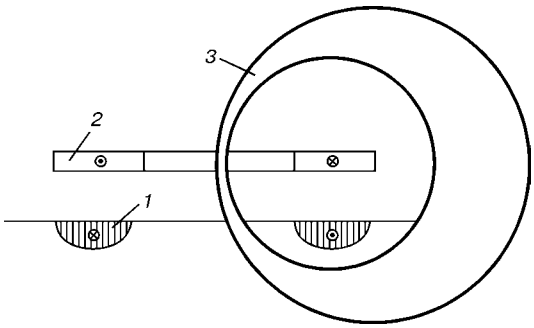

Figure 7. Induction system: *1* — load with currents; *2* — inductor; *3* — fictitious winding

of air gap the non-uniformity of inductor magnetic field is increased and the error in calculation is abruptly increased.

To specify the structure of an inductor–loading equivalent circuit a ***method of a fictitious winding*** has been developed (Figure 7) [9, 14]. When it is used, the electromagnetic field of n-circuit of an induction device is considered as a field of scattering of $(n + 1)$-circuit system, neutral in electric aspect, whose all the parameters are determined through $(n + 1)/2$ of short-circuit impedance of pairs of circuits including a fictitious winding. Moreover, an equivalent circuit of a preset region of the electromagnetic field is such a circuit for which voltages, currents and electric power are mathematically equivalent to intensities of electric, magnetic fields and flows of electromagnetic power (Poynting's vectors).

Among the magnetically-coupled circuits of the system two of them are distinguished having a minimum natural resistance (circuits of the system are reduced preliminary to a basic number of turns) and equivalent circuit is designed for them where parameters of the circuit are determined through natural resistances of circuits Z_{pp} and short-circuit resistances of pairs of circuits Z_{kqp} (Figure 8):

$$\begin{aligned} Z_1 &= 0.5(Z_{11} - Z_{22} + Z_{k12}); \\ Z_2 &= 0.5(-Z_{11} + Z_{22} + Z_{k12}); \\ Z_0 &= 0.5(Z_{11} + Z_{22} - Z_{k12}). \end{aligned} \qquad (9)$$

Selection of circuits with a minimum resistance defines at once the position of an exciting branch Z_0 in the equivalent circuit and can find a resulting magnetic flux, emf of device and exciting current in a simpler way. All the rest circuits and field areas at such selection of circuits are arranged along the Poynting's vector (in the direction of energy spreading from sources of the field to users) and are, to a certain degree, external as regards to selected circuits,

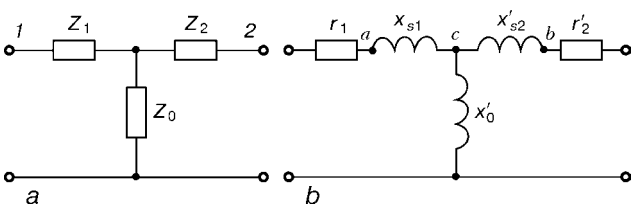

Figure 8. Equivalen circuits of two-circuit device: *a* — general form; *b* — inductor–load system

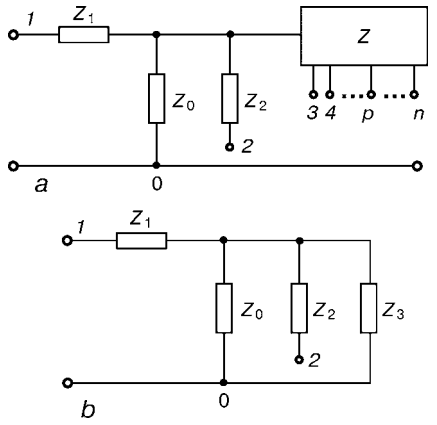

Figure 9. Generalized equivalent circuits of induction device with distinguished taps of circuits (*a*) and with equivalent two-terminal elements of external circuits (*b*)

that makes it possible to consider the volume of an induction device in the form of a laminar structure. In addition, the conditions of mating vectors of the electromagnetic field are preserved at the boundaries of layers that gives a feasibility of a cascade connection of equivalent circuits of layers, i.e. chains of circuits and equivalent circuits of fields regions in the preset direction.

In accordance with the above-mentioned, there is an opportunity to connect an equivalent circuit of external circuits and regions of field, in a general case multipolar, to the exciting branch Z_0 of the obtained circuit (Figure 9, *a*). Its internal structure is defined by a cascade of equivalent circuits of layers which can have different structures depending on nature of processes proceeding in them. For example, it may be inductance of circuits scattering, wave resistance of screen or impedance of massive body in a real form or in the form of an equivalent circuit. Similar equivalent circuits (Figure 9, *b*) are used effectively in investigation and calculation of processes in screened induction devices, transformers with magnetic shunts, tanks and others.

Let us consider now an equivalent circuit, having a practical importance, of a multi-circuit induction device [9, 15] with large air gaps between current-carrying circuits and in the magnetic system. As non-adequacy of solution is typical of problems of synthesis then it is necessary to use conditions of conformity

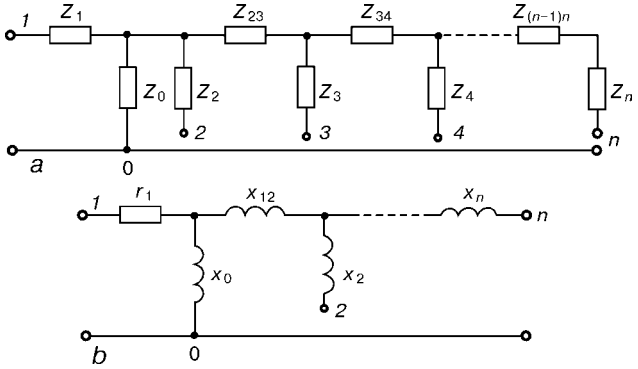

Figure 10. Equivalent circuit of multi-circuit device with a high scattering of magnetic field (*a*) and coaxial system of circuits (*b*)

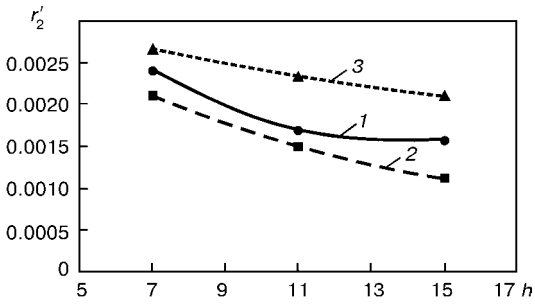

Figure 11. Dependence of resistance of layer heated on gap: *1* — experimental data; *2, 3* — calculated data using method of a common and working flow, respectively

of circuit to modelling device or its element when designing equivalent circuits [16].

An equivalent circuit, adequate to the induction device, should have a number of independent branches (not being reduced by identical transformations to the least number of branches) equal to number of independent magnetic links between the current-carrying circuits of the device. Number of these links in *n*-circuit device is equal to the number of combinations by 2 from $(n + 1)$, that is not less than

$$N = \frac{n(n+1)}{2}. \qquad (10)$$

Secondly, the parameters of short-circuiting of pairs of circuits should be equal to the resistance between corresponding points of its equivalent circuit (at other open windings). Some circuits of different configuration satisfy this condition. When selecting circuit it is necessary to provide a minimum number of closed circuits and to have a simplest structure, for example, a ladder structure.

Taking into account the above-mentioned, the structure of external circuits can be presented in the form of a chain of four-terminal networks of Γ-shaped links formed from longitudinal $Z_{(p-1)p}$ and transverse Z_p parameters, cascade connected in the sequence of increment of natural resistances of the circuits (Figure 10, *a*).

Figure 10, *b* presents an equivalent circuit for design of multi-circuit induction devices with a co-axial system of windings. These circuits were used successfully in calculation and designing systems of double-sided induction current conductor for HF welding of pipes [16].

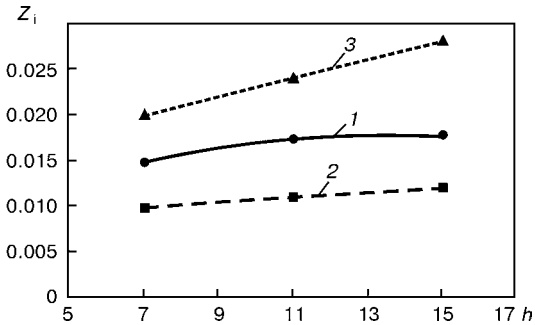

Figure 12. Dependence of impedance of inductor on gap: *1–3* — the same as in Figure 11

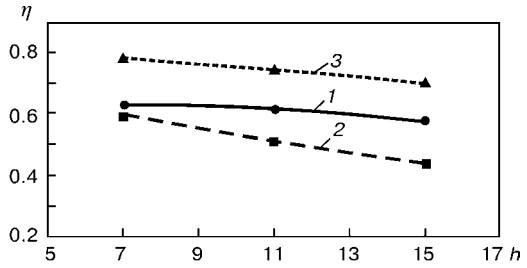

Figure 13. Dependence of effeciency factor of linear inductor on gap: *1–3* — the same as in Figure 11

Design of the device using a full equivalent circuit in the condition of operation of all the circuits is made by simple efficient algorithms, taking into account the features of topological structure of the ladder circuits [17].

Here, sources of voltage or current and elements of the external circuit can be connected in the equivalent circuit to terminals of network or the terminal can be connected to a common busbar of the circuit in case of absence of other sources or consumers of energy. Thus, the use of rational methods of synthesis of equivalent circuits makes it possible to develop effective efficient algorithms for design of induction devices.

The method of a fictitious winding allows making equivalent circuits for any inductively-coupled circuits. Moreover, it is possible to indicate precisely the point of connection of a branch of magnetizing and to define the reactance of primary and secondary circuits. Design of induction devices using equialent circuit compiled by the method of a fictitious winding provides a quite sufficient precision for practical use.

At the same time it is known that this method was not used for design of linear welding inductors.

To confirm the above-described information an experiment on a linear inductor with a length l_i = = 19.5 cm, width of a magnetic core slot a_{sl} = 1.2 cm was performed. Value of gap between inductor and part heated was as follows: h = 0.7, 1.1 and 1.5 cm. Inductor was supplied with a current of 8000 Hz frequency.

Figures 11–14 give relationships of main parameters of a linear inductor obtained experimentally and by calculations. The experimental data and calculations show that the methods of design of the linear inductors have an approximated nature.

Thus, the method of a working flow has a satisfactory precision within the limited range of parameters of the inductor–workpiece system. The accuracy of calculation is decreased with a gap increase. In addition, this method gives some higher values r_2' as it does not ensure the correct limiting transitions with increase in frequency $(f \to \infty)$ or relation $(c/h \to \infty)$. The method of a common flow gives valid limiting transitions providing the wider region of satisfactory accuracy of calculations. Thus, the error in calculations using the method of a commom flow is 10–25 % as compred with experimental data, and 20–45 % as compared with method of a working flow.

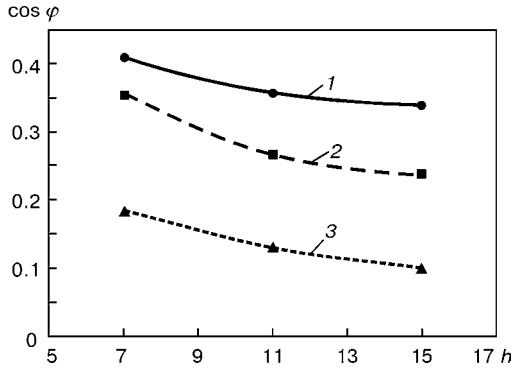

Figure 14. Dependence of power factor of inductor on gap: *1–3* — the same as in Figure 11

Thus, it can be concluded that the existing methods of design of welding inductors cannot provide sufficient accuracy for practical application, as they do not fully reflect the real picture of proceeding processes. In particular, it concerns the distribution of current inducting in loading which is taken into account in calculations using correction coefficients. However, the use of some assumptions results in errors during determination of parameters of inductors that influences to a certain extent both technical and economical characteristics of the HF welding equipment.

In conclusion the actuality of the further improvement of design of welding inductors, especially linear inductors, used for heating flat surfaces and for seam induction welding of products, pipes in particular, should be noted.

1. Shamov, A.N., Bodazhkov, V.A. (1963) *Design and service of high-frequency units*. Moscow-Leningrad: Mashgiz.
2. Glukhanov, N.P., Bogdanov, V.N. (1962) *Welding of metals in high-frequency heating*. Moscow-Leningrad: Mashgiz.
3. Ivanov, V.N., Lunin, I.V., Kulzhinsky, V.L. (1979) *High-frequency welding of metals*. Leningrad: Mashinostroenie.
4. Nemkov, V.S., Demidovich, B.V. (1988) *Theory and design of induction heating device*. Leningrad: Energoatomizdat.
5. Pismenny, A.S. (1997) Electromagnetic field and natural resistance of inductors for heating flat surfaces of items. *Avtomatich. Svarka*, **11**, 28–31.
6. (1967) *Thermal-electric equipment*. Refer. Book. Moscow: Energiya.
7. Slukhotsky, A.E., Ryskin, S.E. (1974) *Inductors for induction heating*. Leningrad: Energiya.
8. Nemkov, S.S. (1984) Design of plane inductors with magnetic cores on the base of magnetic equivalent circuits. In: *Thermal-electric processes and units*. Cheboksary: I.N. Ulianov ChGU.
9. Pismenny, A.S. (1994) Equivalent circuits and methods of design of induction welding and thermal-electric units. *Avtomatich. Svarka*, **4**, 20–23.
10. Demidovich, V.B., Nemkov, V.S. (1975) Computer-aided design of cylindrical inductor with non-magnetic loading. In: *Transact. of VNIITVCh*, Issue 15.
11. Nemkov, V.S., Slukhotsky, A.E. (1970) Calculation of parameters of short-spacing inductors using equivalent circuits. *Ibid*., Issue 11.
12. Slukhotsky, A.E., Nemkov, V.S., Pavlov, N.A. et al. (1981) *Induction heating units*. Leningrad: Energoizdat.
13. Pejsakhovich, V.A., Paradnya, P.A. (1978) Method of design of linear inductor. *Elektrotermiya*, **3**, 12–13.
14. Lebedev, V.K., Pismenny, A.S., Yavorsky, Yu.D. (1976) Design of inductor for high-frequency welding. *Avtomatich. Svarka*, **3**, 50–54.
15. Cherry, E.C. (1949) The duality between interlinked electric and magnetic circuits and the formation of transformer equivalent circuits. *Proc. of Phys. Soc. B*, **350**, 101–111.
16. Pismenny, A.S. (1981) Electric design of devices of double-sided inductive core for welding of tubes. *Avtomatich. Svarka*, **3**, 44–47.
17. Aleksandrova, M.G., Belyanin, A.N., Bryukner, V. et al. (1983) *Computer-aided design of electric circuits and electromagnetic fields*. Moscow: Radio i Svyaz.

SYSTEM OF IN-PROCESS QUALITY CONTROL OF WELDING EQUIPMENT DURING ITS MANUFACTURING

B.E. PATON[1], **A.E. KOROTYNSKY**[1], **M.I. SKOPYUK**[1], **V.I. YUMATOVA**[1], **E.A. KOPILENKO**[2], **G.V. PAVLENKO**[2], **G.L. PAVLENKO**[2] and **N.V. CHMYKHOV**[2]
[1]The E.O. Paton Electric Welding Institute, NASU, Kyiv, Ukraine
[2]Company «SELMA», Simferopol, Ukraine

In view of the increasing number and diversity of the types of welding equipment and higher requirements to its quality, practical implementation of the requirements of GOST 25616–83 in production testing involves a considerable material consumption and time. A variant of forecasting the technological properties of welding equipment is proposed, which is based on the results of electric testing, using a variable resistive load. Various variants of applying the hardware, program and algorithmic elements of the systems of in-process control of welding equipment parameters are considered.

Key words: *welding, welding equipment, system testing, fuzzy logic, simulation mode, linguistic variables*

It is known [1] that the methods of testing the arc welding equipment, as well as the criteria of their quality assessment are specified in GOST 25616–83. Practical implementation of this standard requires two highly qualified welders (of not lower than 5th category), availability of a large volume of metal for making the samples, as well as a considerable consumption of welding consumables. Another important factor lowering the cost characteristics of this type of control is the considerable time required, which is related to processing the test results. As the full cycle of testing of one unit of welding equipment turns out to be quite long, it is also necessary to take the power consumption into account.

In view of the tendency to increasing the volume of production and range of welding equipment, which became obvious at the end of 1990s in the leading enterprises of Ukraine, as well as ever growing requirements to its quality, the tasks of organizing in-process control and certification of finished products acquire foremost importance.

It may be stated with confidence that if the above standard is taken as the basis for testing, the task of automation of control of welding equipment parameters becomes unsolvable, as it is impossible to perform the scope of full-scale testing, envisaged by this document. In this connection, it is necessary to look for such conceptual approaches, which would allow replacing the load applied during welding by its simulator during testing. In this case the welding-technological properties of the controlled equipment are predicted by models developed on the basis of the results of testing electric parameters using, for instance, a ballast resistor (BR). Devices of an electronic simulator of a welding arc would be preferable [2, 3], but they are quite complex and expensive.

Authors of [4] suggest using the actual welding arc as the load. As is noted in this article, in this case it is practically impossible to have an accurate estimate of the condition of welding equipment, as it will depend on the quality of the used welding consumables, shielding gases, etc.

From [5] it is known that the problem of testing complicated technical systems, to which welding equipment belongs, is difficult to describe, using traditional analytical approaches. Up-to-date approaches of simulation of such systems are based on set-theoretical method with a developed system of inference. Algorithms for solving this class of problems are, as a rule, based on the use of neural networks [6] and theory of fuzzy sets [7]. This paper deals with the issues of construction of an automated work place of a controller (AWPC), which should primarily be mounted in the factories-manufacturers of welding equipment.

Structure and main components of the AWPC engineering complex. The complex includes (Figure 1) the following components: subsystem of acquisition and preliminary processing of information on the parameters of the studied process; block of technological interface (BTI) including a set of sensors and an interface unit (IU) designed for program control of the tested source of welding current and controlled ballast resistor (CBR); switching unit (SU) allowing fast connection of input and output channels of welding equipment to the testing system; system interface, which is a MacLab Device of AD Instruments Company; set of computing means — Machintosh PB 180c personal computer, printer and modem of the computing local network (LN). The

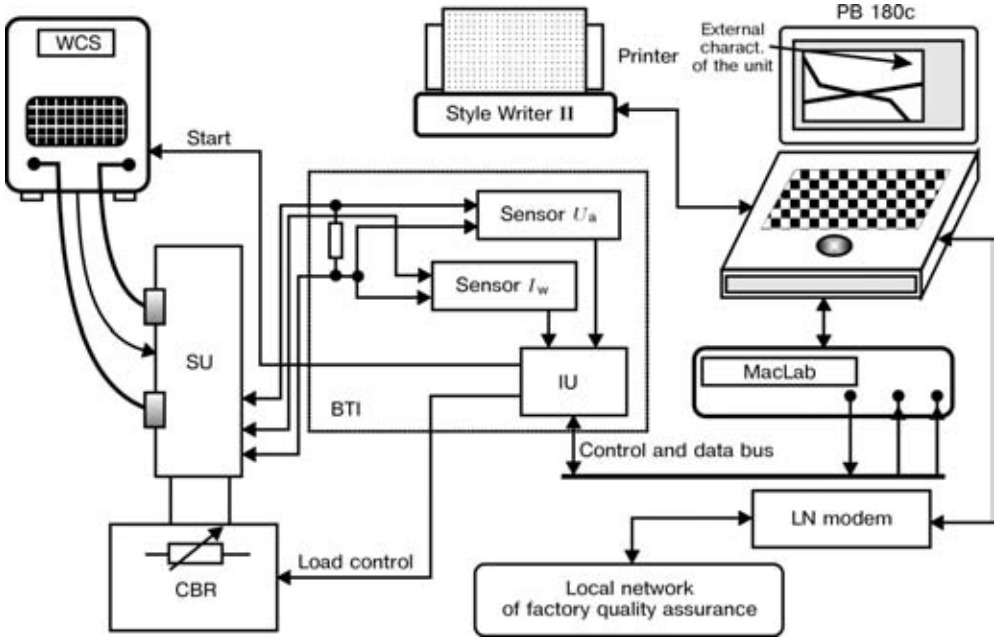

Figure 1. Schematic of an automated work place of a controller: WCS — welding current source (for other explanations see the text)

latter is designed for organizing a common factory network of control and management of the quality of welding equipment manufacture.*

Let us dwell in more detail on the adjustable equivalent of the load, which is a program–controlled BR, the schematic of which is given in Figure 2. The device is based on eight resistors *R1–R8*, the weight of which is selected in keeping with coefficients of binary-decimal code 1, 2, 4, 2. Such a tetrad-decade method of CBR construction allows setting any value of testing current in the range of 0–990 A with the step of 10 A.

Both *K1–K8* contactors and contactless switching elements may be used in the device. The second variant makes its design more complicated (this is particularly true for turning on the switching mode in AC welding sources). It, however, offers reliability and good dynamic properties, which is highly important in testing an inverter power source.

Controlled parameters of the welding process

Parameter	*Designations*	*Parameter evaluation*
Initial arc ignition (arc process start)	a_1	Poor
	a_2	Satisfactory
	a_3	Good
Arc elasticity	b_1	Poor
	b_2	Satisfactory
	b_3	Good
Stability of the steady state mode of the welding process	c_1	Poor
	c_2	Satisfactory
	c_3	Good
Metal spatter (determined by the coefficient of spatter)	d_1	Strong
	d_2	Medium
	d_3	Small

Software of AWPC system includes an integrated LabView (or LabWindows/CVI) environment to develop systems of input, analysis and presentation of the data with an applied program generator; integrated TILShell environment for development of expert systems based on fuzzy logic and neural networks; applied software to assess the quality of welding equipment, oriented towards the solution of the problems of welding equipment quality control.

Evaluation of welding equipment parameters. Criteria of evaluation of the parameters of welding-technological properties of welding equipment are completely taken from GOST 25616–83 (Table). There are, however, differences in the testing methods. As was mentioned above, full-scale experiment is not used when control models are developed. Static and dynamic characteristics of the tested sources are obtained in the simulation mode. When they are constructed in the dialogue mode and appropriate decisions are taken, languages are used which are capable of describing fuzzy categories, close to human notions and concepts. In this case linguistic variables and verbal categories of the type of «small», «medium», «large», «strong», «bad», «satisfactory», «good» are used. Technical condition of the welding unit is determined by comparing the parameters characterizing it in the normal and faulty conditions. If analogs of any faults of the welding unit are available, then knowledge of its technical condition in terms of fuzzy approaches takes the following form:

if a_1 (b_1, c_1, d_1) or a_2 (b_2, c_2, d_2) or ... or a_n (b_n, c_n, d_n) are satisfied, then the condition of the welding unit is an analog;

* The above AWPC complex is Machintosh based. Its conversion to IBM base does not present any particular difficulties in terms of engineering support and software.

if not a_1 (b_1, c_1, d_1) *or* a_2 (b_2, c_2, d_2) *or ... or* a_n (b_n, c_n, d_n) *are satisfied, then the condition of the welding unit is not an analog.*

Here n is a set of reference situations, which are determined and established by the results of full-scale tests.

To evaluate the dynamic parameters required for forecasting the welding-technological properties of the tested equipment, it is necessary to measure the additional derivatives by current dI/dt and voltage dU/dt.

Work and functional capabilities of AWPC system. The testing program is started after connection of the unit being tested to the SU. The unit is successively loaded using CBR in the specified current range. The load step is set by the operator from the system panel and is executed by the «Load control» command. Analog signals generated by the current and voltage sensors are measured in each cycle of new load. The sensors are based on Hall transducers to increase the noise stability. The measurement frequency is determined and set by the operator, in keeping with the instructions developed for each kind of the tested products. Measurement results are entered into the computer external memory.

After completion of the cycle of acquisition of the obtained data the programs of its initial processing and evaluation of the quality of the tested equipment are run. The latter program is made using a base of fuzzy rules incorporated into its expert system. It is created by formalizing the qualitative data obtained by the results of polling the specialists (highly qualified welding technologists) and analysis of experimental data derived in full-scale testing.

It should be noted that the above system of in-process control of welding equipment parameters may be used by enterprises, which apply welding technologies on a large scale for periodical checking and certification of their welding equipment stock (for instance, in ship-building, power engineering, etc.). In this case just its metrological certification is required. With some upgrading and appropriate software AWPC system may function in the mode of a welding training facility.

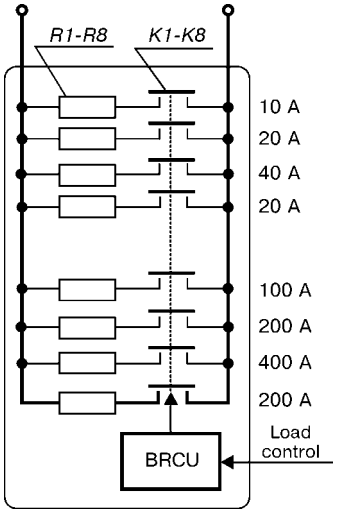

Figure 2. Program-controlled ballast resistor: BRCU — ballast resistor control unit

1. *GOST 25616–83*. Arc welding power sources. Procedure of welding properties testing. Introd. 28.01.83.
2. Pentegov, I.V., Sidorets, V.N., Genis, I.A. (1984) Welding arc modelling as an element of electric circuit and construction of equivalent circuits. *Avtomatich. Svarka*, **12**, 26–30.
3. Sidorets, V.N., Pentegov, I.V. (1991) Simulator of welding arc to evaluate current sources applied in arc welding. *Ibid.*, **7**, 15–18.
4. Melton, G. (2001) Validation of arc welding equipment — revision of BS 7570. *Welding&Metal Fabric.*, **5**, 10–12.
5. Bogatyrev, L.L. (1995) Methods of diagnostics of technical systems under the conditions of fuzzy initial information. *Izv. Vuzov, Elektromekhanika*, **2**, 130–131.
6. Gladkov, E.A. (1996) Problems of prediction of quality and control of weld formation during welding with application of neural network models. *Svarochn. Proizvodstvo*, **10**, 36–41.
7. Orlovsky, S.A. (1981) *Problem-solving with fuzzy initial information*. Moscow: Nauka.

CLASSIFICATION OF ARC WELDING FLUXES BY THE METHOD OF THEIR APPLICATION, MANUFACTURE, COMPOSITION AND TYPE OF METAL BEING WELDED

V.S. SIDORUK and **V.I. GALINICH**
The E.O. Paton Electric Welding Institute, NASU, Kyiv, Ukraine

A classification of welding fluxes by various features is proposed. It is suggested that the number of classification parameters is increased, compared to the existing ones, namely from 1 to 12 by the application method, from 3 to 7 by the manufacturing method, from 10 to 18 by composition, and up to 26 taking into account the forecast slag compositions, etc.

Key words: *classification of fluxes, designation, submerged-arc welding, open-arc welding, welding with backing flux, fused, agglomerated, ceramic, synthetic, regenerated fluxes, mechanical mixture, slag mixture*

The tendency to globalisation of world economy emerging over the recent years created the need to develop common technological approaches, in particular, in the field of welding [1]. Co-ordination of «unified» rules of international standards and codes began simultaneously [2]. Diversity of national standards (US, European, USSR, Japanese, etc.) for welding consumables led to the necessity of introducing a cross-reference and then to establishing common international standards through the International Institute of Welding (IIW), and later on through the International Standards Organization (ISO) [2].

So in [3] it is mentioned that in 1974 IIW proposed a draft of an International Classification and Coding of fluxes for automatic SAW of low-carbon and low-alloyed steels. Then IIW published documents classifying electrode wires, fluxes and shielding gases for submerged-arc and gas-shielded welding of low-carbon and low-alloyed steels [4, 5]. In 1997 ISO produced drafts of International Standards ISO/DIS 14171 (classification of filler material and combinations of wire — flux for SAW of unalloyed steels identical to the common European standard EN 756) and ISO/DIS 14174 (classification of fluxes for SAW) [6].

Without giving a detailed description of the contents of the above documents, we will try to consider them proceeding from the local experience and results, as well as completeness and effectiveness of classification and coding of welding fluxes.

Classification by the method of application (purpose). By the method of application of fluxes both the classification systems of IIW and ISO cover only SAW for unalloyed, low- and high-alloyed steels. Without disputing the need for such a comparatively «narrow» standard, we believe it is rational to widen the classification of welding fluxes, so that it covers all the aspects of their application, as well as all the metals and alloys welded by the submerged-arc process. For instance, in what category should the flux be classified, which is used for mechanized welding of aluminium by a semi-submerged arc process [7]? Or what flux may be used as backing material in SAW?

When fluxes are classified by their purpose, we proceed from the definition of the concept of «welding flux» given in [8]: «Flux (for welding and brazing) is a material added to the welding or brazing zone to ensure shielding, oxide reduction, liquefying the slag and lowering the slag temperature, as well as to fulfill a number of other metallurgical functions... In addition to fulfilling the basic functions, the flux in welding usually promotes a stable arcing and improved weld formation».

There exist not only arc welding processes, when the arc is kept under a layer of flux, but also open arc welding processes. Let us name some of them:

- semi-SAW with additional gas shielding [9];
- combined use of shielding gas and flux fed into the welding zone in the form of a fine powder mixture [10];
- using fluxes-pastes for welding aluminium [11];
- using activating fluxes for welding various metals and alloys [12], including those in the form of aerosols [13];
- finally such a combination of shielding gas and flux is possible, when the flux is used in the form of a fibrous material (flux felt, flux cardboard, flux paper), placed along the weld [14].

Actually SAW proper cannot be regarded as finally developed.

Let us name some of the areas of search:

- SAW with continuous covering of the electrode wire by metal powder fed from the hopper [15];
- SAW with additional protection, for instance, by argon [16];
- multi-electrode welding into separate pools with combined protection of the front arc by carbon dioxide gas, and of the next arcs by flux [17];
- SAW with feeding metal powder into the arc zone with the flux-cored wire [18];

• SAW with additional feed of alternative flux components (fluorides, mechanical mixtures of components, similar to the flux-cored wire charge, etc.) to the arc zone [19–22];

• process of SAW with minimal, down to zero, penetration of the base metal, for which special activating fluxes are used [23].

The latter process developed at the PWI may be particularly effective in surfacing dissimilar metals, narrow-gap welding and irreplaceable in welding steels and alloys, where surface melting is inadmissible, because of the loss of properties, for instance, in chromium-nitrogen steels, containing up to 1 % nitrogen [24];

• use of fluxes containing iron powder, for instance, ceramic [25];

• use of exothermal fluxes [26].

In view of the above, the list and designations of fluxes, classified by the method of application (purpose) may be as follows.

For SAW (covered or buried arc):

1. S — conventional SAW;
2. SG — gas-shielded SAW;
3. S + G — consumable multielectrode welding with combined shielding of the arcs: of the front arc (one or several) by gas, of the next arcs by flux;
4. SMP — SAW with additional feeding of metal powder into the arc zone: in a mixture with flux or from a separate hopper co-axially with the electrode or with preliminary pouring of grit into the gap between the edges, etc.;
5. ES — exothermic SAW;
6. SCW — SAW with flux-cored wire containing metallic powder, exothermal mixture or substances replacing the flux components, for instance, fluorides, nitrides, boron-containing substances, etc.;
7. SAF — SAW with activating flux.

For open-arc welding:

8. VFA (visible flux-air arc welding) — consumable electrode semi-SAW in air
9. SGF - gas-shielded semi-SAW;
10. SGCW — welding with flux-cored wire, containing flux components with gas shielding of the arc;
11. A-TIG — nonconsumable-electrode argon-arc welding with application of activating flux.

Backing fluxes:

12. BF — backing flux.

Classification by the method of manufacture. By the method of manufacture the classification of fluxes according to the draft of ISO/DIS standard envisages only three types of fluxes: F — fused, A — agglomerated and M — mixtures prepared by the manufacturer of two or more fluxes (standard, existing). It is a step back compared to IIW classification, as bonded, or according to the local terminology, ceramic fluxes and mechanical mixtures of various initial components, for instance, recycled, as in [27], are not taken into account. We believe that this list of flux manufacturing methods cannot be regarded as complete, either. In our opinion, it is necessary to add to it the method of making synthetic fluxes developed at the PWI [28].

Manufacture of such fluxes involves single-phase synthesis of complex compounds of the type of natural minerals: wollastonite, nepheline, dioside, enstatite, etc. Component selection and synthetic flux manufacturing technology are the same as for the agglomerated fluxes, with the difference, however, that first of all, components are ground simultaneously, and, secondly, sintering temperature is significantly higher at about 1050 °C. In addition to the basic components, an intensifier of the process of mineral formation is added in the form of Si-containing components, for instance, broken glass, mineraliser (fluorite or fluorspar) and water. By their technological properties synthetic fluxes are close to the ceramic fluxes, being superior to them in some respects. They have higher mechanical strength of grains, being closer to fused fluxes by this property. Their other advantage is the low hygroscopicity, they ensure an extremely low content of diffusible hydrogen in the weld metal of up to 1 ml/100 g at the flux basicity of up to 2.5 [28].

In view of the above, the following list of fluxes by the manufacturing method and appropriate designations are proposed:

1. F — fused;
2. AS — agglomerated or sintered;
3. AB or (alternatively) B — agglomerated with a binder or bonded;
4. CM — mechanical mixture of initial components;
5. FM — mechanical mixtures of ready fluxes, for instance, fused;
6. S — synthetic;
7. R — recycled.

Classification by composition. In IIW document of 1974 [3] the welding fluxes designed solely for SAW (under a layer of flux), were divided into six groups, depending on the condition of slag-forming components:

1. CS — calcium-silicate;
2. MS — manganese-silicate;
3. AR — alumina-rutile;
4. AB — alumina-basic;
5. FB — fluoride-basic;
6. ST — alloying fluxes, without indicating the slag base.

Since the classification of ISO fluxes [6] is the most complete now, it is worthy of a more detailed consideration. Compared to IIW classification, the number of flux types classified by composition is increased up to 11. Fluxes of the systems of ZS (zirconium-silicate), RS (rutile-silicate), AS (alumina-silicate) and AF (alumina-fluoride) are added. Fluxes of ST system were removed from the Classification Table, while fluxes of Z system (of any other composition) were introduced.

Let us note right away that the last line in the Classification Table [6] may be considered as an indication of the fact that the Table is not yet complete,

and the work on development of new flux compositions still goes on. We, however, believe it is incorrect to designate by Z symbol an indefinite number of fluxes with an unspecified composition. Instead of Z symbol it is rational to use a dash or dots. For our part we suggest adding to the above Table the fluxes not yet shown in it. They include primarily halide fluxes, which we suggest denoting by symbol H, and rutile-basic fluxes — RB. ANF-5 developed at the PWI can be named as an example of H system flux [29]. RB slag system corresponds to the European standard EN 499-1995.

A common drawback of the above IIW and ISO classification systems is the fact that the fluxes are classified only by two main components, their total content in some cases being just 45 %, as the lower limit (for instance, fluxes of AB system). Today already there exist fluxes, where the slag system is based on three main components. Among them are, for instance, the following fluxes:

- on alumina-fluoride base, which may be designated AFB (see AHF-17 flux) [29];
- on rutile-alumina-silicate base RAS (see EN 499-1995);
- on fluoride-calcium-boride base, which we suggest designating FCBo (ANF-22) [29];
- on fluoride-alumina-calcium base FAC (ANF-29) [29].

Actually, IIW and ISO/DIS Classification Tables already contain information sufficient to call some «two-component» fluxes the three or even four-component fluxes. For instance, MS flux contains up to 15 % CaO and, in addition, it may contain MgO. Therefore, it is better to designate it as SMB (in the Table this designation is given in the brackets). It is better to designate flux AB as SFAB, FB — FBM, ZS — ZSM, AF — AFB. AS system flux is given in [6] as a multicomponent flux ASFBZ as in addition to Al_2O_3, SiO_2, also the content of CaF_2, MgO and ZrO_2 is specified in it.

Analyzing the compositions of certain fluxes, we can see that the specific content of a particular flux does not always coincide with the sequence of symbols in their designation. For instance, in UM20 flux [29] SiO_2 content is 50–53 %, and that of CaO — 30–31 %. Therefore, a more informative designation for the above flux would be SC. AN-348A flux has the greatest amount of SiO_2 (41–44 %), then — MnO (34–38 %), then CaO (6.5 %) and MgO (5.0–7.5 %). A more accurate designation of this flux would be SMB. AN-26S flux contains 29–33 % SiO_2, up to 22 % CaF_2, 19–23 % Al_2O_3, 15–18 % MgO and 4–8 % CaO, therefore it is better to designate it as SFAB, and not AB, etc.

In view of the above-said, we suggest for discussion an expanded classification table of welding fluxes by composition, which reflects the flux systems to ISO and IIW classifications, and fluxes developed at the PWI and not mentioned in the above standards, as well as the forecast slag compositions.

Classification of fluxes by the type of metals and alloys, which are welded and surfaced using these fluxes. In [6] it is proposed to classify the fluxes for welding and surfacing some steels and wear-resistant alloy cladding. All the fluxes are subdivided into three classes:

class 1 — for welding and surfacing low-carbon and low-alloyed steels;

class 2 — for welding and surfacing stainless and high-temperature resistant steels alloyed with chromium and Cr–Ni steels and/or nickel and its alloys;

class 3 — mostly for surfacing wear-resistant alloys. These are alloying fluxes with transfer of carbon, chromium or molybdenum from the flux into the weld metal.

The above standard does not include a class of medium-alloyed steels, which by the national classification (GOST 5200–50) contain alloying elements of manganese, silicon, chromium, nickel, molybdenum in the total amount of 2.5 to 10 %. In addition, it is known that some fluxes designed for steel welding, are suitable for welding other metals and alloys. For instance, AN-348A, OSTs-45, AN-20, AN-26 fluxes are used for welding not only steels, but also copper [29]; ANF-5, ANF-7, ANF-8, 48-OF-6, AN-29, AN-292 fluxes are used for welding both alloyed steels (Tables 7.38 and 7.39 in [29]) and nickel and its alloys (Table 3.18 in [29]). Therefore, the classification should include information on application of fluxes for welding and surfacing various metal and alloys, and not only steels and wear-resistant alloys.

In our opinion, such a classification may have the following form and respective codes:

1. F-St (u, l) — fluxes for welding and surfacing low-carbon and low-alloyed steels;
2. F-St (m) — fluxes for welding and surfacing medium-alloyed steels;
3. F-St (h) — fluxes for welding and surfacing high-alloyed steels;
4. F-Cu — fluxes for welding and surfacing copper and its alloys;
5. F-Ni — fluxes for welding and surfacing nickel and its alloys;
6. F-Al — fluxes for welding and surfacing aluminium and its alloys;
7. F-Ti — fluxes for welding and surfacing titanium and its alloys;
8. F-S — (WR) — fluxes for welding wear-resistant alloys, etc.

In this case letters u, l, m and h in items 1–3, respectively, denote: low-carbon (unalloyed), low-, medium- and high-alloyed steels; WR in item 8 — wear-resistant alloys.

If the flux is applied in welding several types of metals and alloys, it should be designated by a symbol of two, three or more characters. For instance, AN-348A flux should be classified as F-St (m, l)-Cu; ANF-5 flux as F-St (h)-Ni, etc. As regards alloying of the deposited metal through the flux, it is a separate classification feature and a separate section of the

Common classification of welding fluxes by composition

Accepted designation of the flux and designation recommended by us (in brackets)	*Local ordinal No. (in the classification system)*	*Basic components, wt.%*	*Slag base of the flux*	*Flux grade, reference*
		IIW classification		[5]
CS (SC)	1	$CaO + MgO + SiO_2 > 50$; $CaO + MgO > 15$	Calcium-Silicate	UM20, Linde20 (Blau) [29]
MS (SMB)	2	$MnO + SiO_2 > 50$; $CaO < 15$	Marganese-Silicate	AN-348 [29]
AR	3	$Al_2O_3 + TiO_2 > 45$	Aluminate-Rutile	AN-67A (the PWI catalogue)
AB (SFAB)	4	$Al_2O_3 + CaO + MgO > 40$; $SiO_2 > 22$; $CaF_2 < 15$	Aluminate-Basic	AN-26S [29]
FB (FBM)	5	$CaO + MgO + CaF_2 + MgO > 50$; $SiO_2 < 20$; $CaF_2 > 15$	Fluoride-Basic	AN-22 [29]
ST	6	Composition not indicated	Alloying	
		ISO/DIS classification (addition to IIW classification)		[5]
ZS (ZSM)	1	$ZrO_2 + SiO_2 + MnO > 45$; $ZrO_2 < 15$	Zirconium-Silicate	[6]
RS	2	$TiO_2 + SiO_2 > 50$; $TiO_2 < 20$	Rutile-Silicate	[6]
AS (ASFBZ)	3	$Al_2O_3 + SiO_2 + ZrO_2 > 40$; $CaF_2 + MgO > 30$; $ZrO_2 > 5$	Aluminate-Silicate	[6]
AF (AFB)	4	$Al_2O_3 + CaF_2 > 70$	Aluminate-Fluoride	ANF-17 [29]
Z	5	Any composition		
		Existing fluxes are not taken into account in IIW and ISO classifications		
H	1	CaF_2, NaF, $BaCl_2$, BaF_2, Na_3AlF_6, etc.	Halogenide	ANF-5 [29]
RB	2	$TiO_2 + CaO + MgO > 45$	Rutile-Basic	EN 499–1995
ABFN	3	$Al_2O_3 + CaO + MgO + CaF_2 + NaF_2 > 80$; $CaF_2 > 22$	Aluminate-Basic-Fluoride	ANF-16 [29]
RAS	4	$TiO_2 + Al_2O_3 + SiO_2 > 50$	Rutile-Aluminate-Silicate	EN 499–1995
ASF	5	$Al_2O_3 + SiO_2 + CaF_2 > 50$; $CaF_2 > 22$	Aluminate-Silicate-Fluoride	ANF-14 [29]
FCBo	6	$CaF_2 + CaO + B_2O_3 > 50$	Fluoride-Calcium-Boride	ANF-22 [29]
FAC	7	$CaF_2 + Al_2O_3 + CaO > 50$	Fluoride-Aluminate-Calcium	ANF-29 [29]
		Forecast		
CR	1	$CaO + TiO_2 > 45$	Basic-Rutile	
CM	2	$CaO + MgO > 45$	Basic-Manganese	
AC	3	$Al_2O_3 + CaO > 45$	Aluminate-Calcium	
CF	4	$CaO + CaF_2 > 45$	Calcium-Fluoride	
HBo	5	CaF_2, NaF, $CaCl_2$, etc. + B_2O_3	Halogenide-Boride	
MA	6	$MnO + Al_2O_3 > 45$	Manganese-Aluminate	
MR	7	$MnO + TiO_2 > 45$	Manganese-Rutile	
MF	8	$MnO + CaF_2 > 45$	Manganese-Fluoride	

classification, related to metallurgical behaviour of flux.

CONCLUSIONS

1. It is rational to widen the classification of fluxes by the method of application (purpose) by introducing «for open-arc welding» and «backing» sections in addition to the «sumberged-arc» section.

2. In the classification of fluxes by the method of manufacture it is rational to:

- present agglomerated fluxes as two variants AS (agglomerated by sintering) and AB or alternatively B (agglomerated with a binder or bonded);
- present mechanical mixtures M as two varieties: MC (mixed components) — mechanical mixtures of initial components, and MF (mixed fluxes) — mechanical mixtures of ready fluxes;
- synthetic S and recyclable R fluxes should further be added.

3. From the classification of fluxes by composition, presented in the draft of standard ISO/DIS 14174, it is rational to remove the flux composition designated as Z, as not having any specific meaning, and complement it with fluxes of H, RB, ABFN, RAS, ASF, FCBo, and FAC systems. It should further be noted that it is not rational to classify the fluxes by just the two main components, especially if their total content is not higher than 50 %. Some fluxes may be classified by three- or even five basic components, and then their designation becomes 3-, 4- and 5-symbol, respectively. The sequence of symbols of each flux component in the symbolic notation should follow the principle of «ponderability»: symbol of the component, the content of which is the greatest is in the first place, and that of the smallest is in the last place.

4. Add fluxes classification by the type of metals and alloys, which are welded using them.

5. We should note the contribution of the PWI to development of welding fluxes of chemical compositions of MS, AR, FB, AF, H, ABFN, ASF, FCBo, FAC; of the methods of their manufacture: F, AB, S, R; of the methods of their application: S, SMP, SCW, VFA, SCF, SGCW, A-TIG; SAF and BF were also proposed.

6. Development of welding processes and of fluxes and methods of their fabrication is carried on. Other effective solutions in the above fields may be also suggested in the future.

1. Thomas, S. (1999) Major players promote acceptance of global technology. *Welding Design & Fabrication*, August, 4.
2. David, R., Thomas, Jr. (1998) System for designation of welding filler metals. *Welding J.*, **2**, 29–32.
3. Podgaetsky, V.V., Lyuborets, I.I. (1984) *Welding fluxes*. Kyiv: Tekhnika.
4. *IIW Doc. XII-D-1–81*. Classification of wire electrodes, fluxes and shielding gases for submerged-arc and gas-shielded metal arc welding of mild- and low alloy steels.
5. *IIW Doc. XII-761–82*. Comment on Document IIW-XII-D-1–81.
6. (1997) *Draft international standard ISO/DIS 14174, ISO/TC44 Sc3*.
7. Gurevich, S.M. (1981) *Reference Book on welding of non-ferrous metals*. Kyiv: Naukova Dumka.
8. (1974) *Glossary on welding*. Ed. by K.K. Khrenov. Kyiv: Naukova Dumka.
9. Eichhorn, F., Dilthey, U., Wiertznion, H. et al. (1991) Elektrogasschweißen von Cr8Ni9 mit austenitischen Zusatzwerkstoffen. *Schweißen und Schneiden*, **3**, 163–166.
10. Nazarchuk, A.T., Kosyakov, V.P. *Process of arc welding*. USSR author's cert. 1547993, Int. Cl. B 23 K 9/16. Publ. 01.03.90.
11. Lukin, V.I., Karimova, S.A., Arzamasov, V.V. et al. (1999) Application of fluxes for argon-arc welding of aluminium alloys. *Svarochn. Proizvodstvo*, **6**, 29–31.
12. Lucas, W., Howse, D., Savitsky, M.M. et al. A-TIG flux for increasing the performance and productivity of welding process. *IIW Doc. XII-14448–96*.
13. Yushchenko, K.A., Kovalenko, D.V., Kovalenko, I.V. (1998) Aerosol activator PATIG S-A for A-TIG welding of steels. *Svarshchik*, **3**, 21–22.
14. (1993) Developing and application of flux-fibre welding consumables. In: *Sci.-techn. report on project 5.43.08/014–93*. Kyiv: PWI.
15. Blasig, K., Eichhorn, F., Kerkmann, M. (1983) Neue Einsatzgebiete des Unterpulverschweißens durch selbsttätigens kontinuierliches Ummanteln der Drahtelektrode mit Metallpulver und mit Hilfe von bandförmigen Schweißzusatz. *DVS-Ber.*, **83**, 9–14.
16. Shimizu, K., Iwamoto, N., Makino, Y. et al. (1987) Submerged-arc welding in the argon gas atmosphere. *Quart. J. of JWS*, **4**, 52–59.
17. Rybakov, A.A., Kravchenko, A.B., Bugatsky, G.P. et al. *Multi-arc welding process*. USSR author's cert. 1516269, Int. Cl. B 23 K 9/00. Publ. 23.10.89.
18. Dilthey, U., Dahl, W., de Lede, F. et al. (1993) Anwendung moderner Hochleistungsschweißverfahren bei der Verarbeitung hochfester Feinkornbaustähle. *DVS-Ber.*, **155**, 71–76.
19. Kurimoto, T., Yamauti, N., Inaba, I. et al. *Multi-electrode submerged-arc welding*. Pat. 63119983 Japan, Int. Cl. B 23 K 9/18. Publ. 24.05.88.
20. Paton, B.E., Voropaj, N.M., Slivinsky, A.M. et al. (1988) Set of environmentally clean welding consumables: fused flux–electrode wire. *Avtomatich. Svarka*, **5**, 43–48.
21. Kubenka, M., Prihal, A., Svedler, Z. et al. (1999) Submerged-arc flux-cored wire welding in production of CSPL a.s. Lodenice Kresice. *Zvaranie*, **1**, 5–6.
22. Lukkari, Y., Studholme, S. (1998) Unterpulverschweißen mit Fülldrähten. *Swei&Prüftechnik*, **4**, 54–56.
23. Sidoruk, V.S. (1998) On some tendencies of industrial application of flux. In: *Abstr. of pap. of Int. Sci.-Techn. Sem.*, Zaporozhie, Sept. 3–6, 1998.
24. Emelianenko, Yu.G., Ryabtsev, I.A. (1997) Second session of Scientific Council on new materials of International Association of Academies of Sci. *Avtomatich. Svarka*, **12**, 56–57.
25. Sakaguchi, S., Yamaguchi, T., Shida, C. One pass submerged-arc welding with flux containing iron powder for thick steel plates. *IIW Doc. XII-1159–90*.
26. Glushchenko, A.S., Leshchinsky, L.K. (1976) Increase of metal fusion rate in thermit submerged-arc welding. *Avtomatich. Svarka*, **10**, 68.
27. Leskov, G.I., Pismenny, A.S., Reznichenko, N.Ya. (1997) Automatic open arc welding in a jet of granular materials. *Avtomatich. Svarka*, **12**, 35–39.
28. Kasatkin, B.S., Tsaryuk, A.K., Vakhnin, Yu.N. et al. (1994) Synthetic welding fluxes: manufacturing and application. *Ibid.*, **3**, 62–66.
29. (1974) *Technology of fusion electric welding of metals and alloys*. Ed. by B.E. Paton. Moscow: Mashinostroenie.

WELDING THREE-PHASE TRANSFORMERS WITH IMPROVED TECHNICAL-ECONOMICAL CHARACTERISTICS

I.V. PENTEGOV, S.V. RYMAR, A.V. LAVRENYUK and **O.I. PETRIENKO**
The E.O. Paton Electric Welding Institute, NASU, Kyiv, Ukraine

New designs of three-phase welding transformers with tape multicore magnetic circuits are considered. As compared with traditional transformers, they have improved technical-economical characteristics and can be competitive at the market of welding equipment.

Key words: *power source, transformer, arc welding, welding equipment, CO_2, improved characteristics, competitiveness*

The basic element of the power source (PS) is a transformer which defines mainly its technological and technical-economical characteristics. Therefore one of the priority tasks in manufacture of PS is the development of new designs of welding transformers which should have the updated characteristics that is especially important in the conditions of competition.

In manufacture of portable PS for CO_2 welding used in autoservice workshops in repair works, the three-phase transformers of traditional designs with a laminated magnetic core are mainly used over long time [1]. Magnetic induction in the magnetic circuit of these transformers does not exceed 1.63 T that is due to saturation of steel of a magnetic core in the region of laminated butts. The mentioned transformers are difficult in manufacture, assembly and repair, have large dimensions and mass that complicates the PS transportation.

The use of tape core-type magnetic circuits [1, 2] makes it possible to increase the level of magnetic induction in them up to 1.75 T that can decrease the mass of active elements of the transformer, its dimensions and cost. Transformers with tape magnetic cores are characterized by a high adaptability to manufacture, assembly and repair.

There are three-phase transformers with tape wound multicore magnetic circuits of flat and three-dimensional designs [3]. Three-phase transformers with flat magnetic cores have small differencies in parameters of phases that is due to the asymmetry of designs. Most three-dimensional magnetic cores are completely symmetrical and, consequently, have similar parameters for all the phases. However, due to difficulties in manufacture and assembly, and also high cost they are used only in a special equipment. Therefore, the improvement of flat designs of magnetic-tape cores of three-phase transformers is actual.

Figure 1 shows the most widely-spread design of three-phase transformer with a tape magnetic core. There are small technological gaps between the tape core-type magnetic circuits *1* and *2* from which the multicore magnetic-tape circuit is composed. These gaps hinder the transition of magnetic fluxes of phases from one parts of the magnetic circuit into other parts. As a result, the magnetic flux in core-types magnetic circuits *1* and *2* is 57.7 % of the total magnetic flux passing in the phase [2]. Therefore, the need appears in increase of the cross-section of magnetic core by $2/\sqrt{3}$ times that leads to the increase in mass and cost of the transformer of the above-mentioned design, and also limits its application in welding PS.

The new designs of three-phase transformers with magnetic-tape cores (Figures 2 and 3), developed at the E.O. Paton Electric Welding Institute, have no above-mentioned drawbacks [4–6]. They do not require increase in cross-section of cores of magnetic circuits by $2/\sqrt{3}$ times, because the magnetic fluxes can transfer freely along the tape plane from one parts of the magnetic core to other parts. In designs presented in Figure 2, this is contributed by yoke cover plates *4* which are made from electrical steel and play a role of mixers of magnetic fluxes. In design, shown in Figure 3, the magnetic fluxes are passing from one parts of magnetic core to the other parts through the C-shaped core-type magnetic circuits *2*.

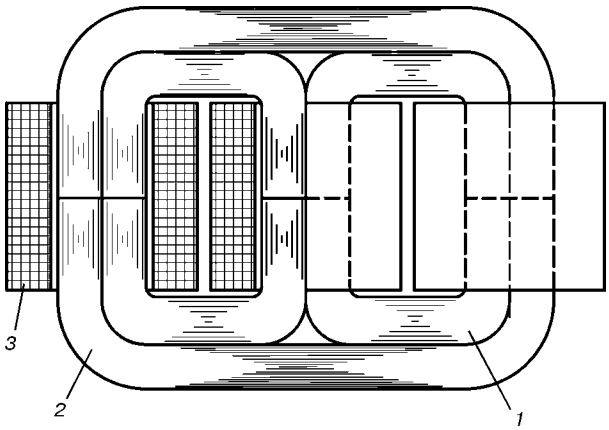

Figure 1. Traditional design of three-phase transformer with a tape multicore magnetic circuit: *1, 2* — tape core-type magnetic circuits; *3* — coil with windings

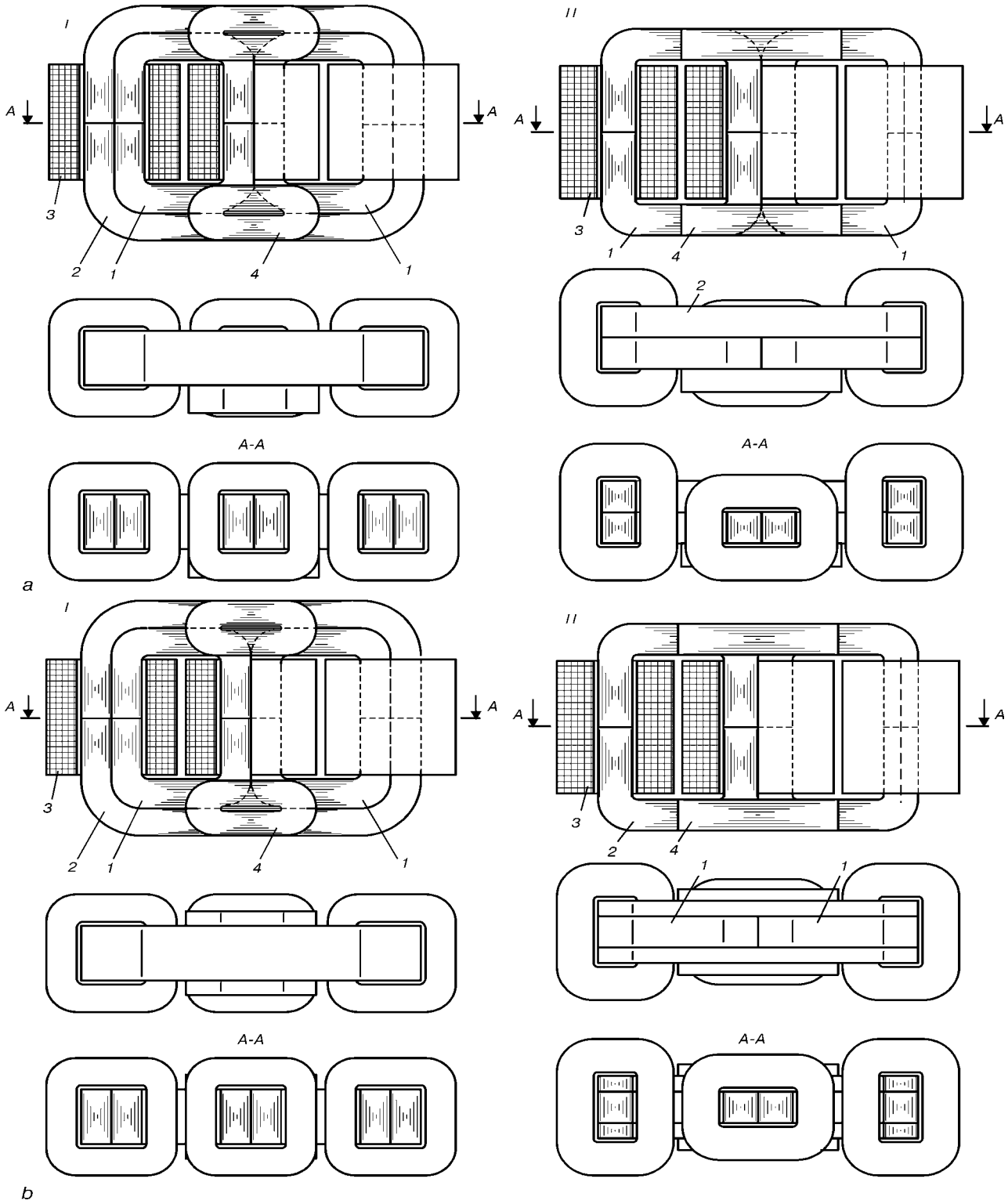

Figure 2. New non-symmetrical (*a*) and symmetrical (*b*) design (*I*, *II* — variants) of three-phase transformer with tape multicore magnetic circuit and yoke cover plates: *1*, *2* — tape core-type magnetic circuits; *3* — coils with windings; *4* — yoke cover plates

It should be noted that the use of designs shown in Figures 2, *II* and 3 in the three-phase transformers can provide better conditions of cooling the transformer, because the winding on a central core is turned by 90° with respect to windings at extreme cores. This increases the surface of their cooling and gives feasibility to increase the current density in conductors that also leads to the decrease in mass of the transformers.

Figure 2 shows the variants of tape multicore magnetic circuits of non-symmetrical (Figure 2, *a*) and symmetrical (Figure 2, *b*) design. When the latter are used the mass of yoke cover plates *4* is decreased due to increase in area of surface of transition of a

Parameter of transformer	In Figure 1	In Figure 2		In Figure 3
		Variant I, b	Variant II, b	
B_m	1.074	1.074	1.074	1.074
$J_{l.-t}$	1.000	1.000	1.096	1.096
a	1.015	0.918	0.965	0.940
b	1.460	0.958	0.916	0.892
l_{window}	0.995	1.078	1.000	1.055
h_{window}	1.018	0.982	0.960	0.960
w_1	1.012	1.058	1.053	1.110
M_s	1.051	0.964	0.893	0.903
M_{wind}	1.036	1.001	0.914	0.946
M_{tr}	1.044	0.982	0.903	0.923
C_s	1.036	1.001	0.914	0.945
C_{wind}	1.051	0.964	0.893	0.903
C_{tr}	1.041	0.990	0.908	0.933

Note. B_m — magnetic induction in transformer magnetic circuit; $J_{l.-t}$ — long-term current density in conductors of transformer windings; a, b — thickness and width of magnetic core, respectively; l_{window}, h_{window} — width and height of magnetic core window, respectively; w_1 — number of turns in primary windings of transformer; M_s, M_{wind} and M_{tr} — masses of steel of magnetic core, conductor of windings and active materials of transformer, respectively; C_s, C_{wind} and C_{tr} — cost of steel of magnetic core, conductor of windings and active materials of transformer, respectively.

magnetic flux from parts of magnetic core to the yoke cover plates.

At the PWI the optimized mathematical models of the above-mentioned designs of transformers were developed and optimized calculations of their main parameters were made (Table). Calculations were made for transformers of similar capacity (6 kV·A) with copper conductors of windings and close values of calculated temperatures of windings. Values of parameters of three-phase transformer with a laminated core were standardized for unity. Parameters of other types of designs of transformers are given in relative units and show the relation between the values of parameters of the transformer considered and corresponding values of parameters of three-phase transformer of a traditional design with a laminated core.

Analyzing the data of the Table it can be concluded that the transformer shown in Figure 2, *II*, *b* is best, following by transformer in Figures 3 and 2, *I*, *b*, then the transformer of a traditional design with a laminated core and, finally, the transformer shown in Figure 1.

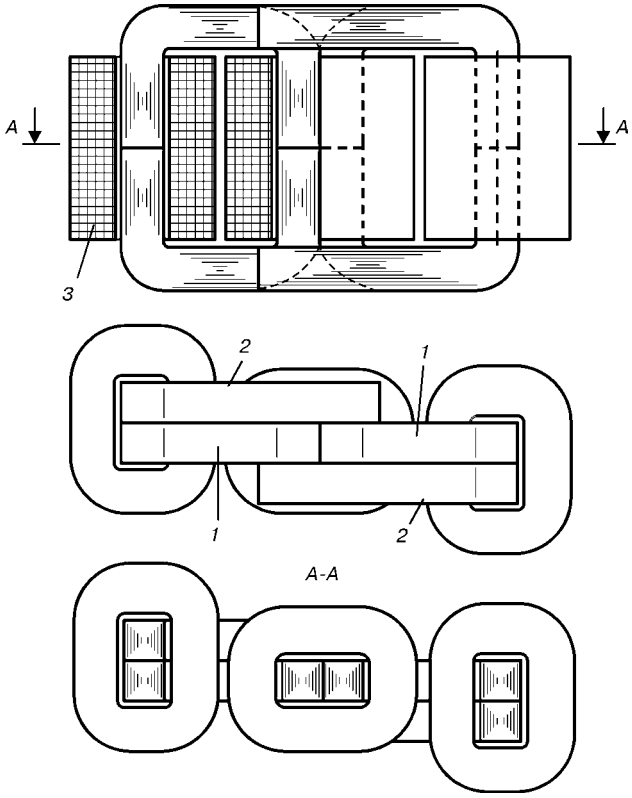

Figure 3. New design of three-phase transformer with tape multicore magnetic circuit (designations see in Figure 1)

Thus, the use of new designs of three-phase transformers with magnetic-tape cores in PS for CO_2 welding makes it possible to decrease mass, dimensions and cost of PS providing high welding and technological parameters of the power sources. This will give opportunity to develop the competitive portable PS for the CO_2 welding.

1. Tikhomirov, P.M. (1986) *Design of transformers*. Moscow: Energoatomizdat.
2. Flanagan, W.M. (1993) *Handbook of transformer design and applications*. Boston: McGraw Hill.
3. Erin, V.L. (1990) *Three-phase transformers with space magnetic cores from C-rods with reduced mass and no-load current and their computer-aided design*. Thesis for Cand. Tech. Sci. Degree. Kishinev.
4. Pentegov, I.V., Rymar, S.V., Petrienko, O.I. et al. *Tape multicore magnetic circuit of three-phase transformers and reactors*. Positive decision on appl. 2000127473, Ukraine, Int. Cl. M 01 F 27/24. Filed 25.12.00.
5. Pentegov, I.V., Rymar, S.V., Petrienko, O.I. et al. *Tape multicore magnetic circuit of three-phase transformers and reactors*. Positive decision on appl. 2000127474, Ukraine, Int. Cl. M 01 F 27/24. Filed 25.12.00.
6. Pentegov, I.V., Rymar, S.V., Petrienko, O.I. et al. *Tape multicore magnetic circuit of three-phase transformers and reactors*. Positive decision on appl. 20001010633, Ukraine, Int. Cl. M 01 F 27/24. Filed 29.01.01.

ON THE CAUSES FOR FORMATION OF DEFECTS IN WELDS OF E110 ALLOY MADE BY ELECTRON BEAM WELDING AND METHODS OF CONTROLLING THEM

V.I. VASILKOV[1], A.A. KISLITSKY[1], N.V. ONUCHIN[1], V.V. ROZHKOV[1], A.V. STRUKOV[1], V.B. CHIZHOV[2] and P.I. LAVRENYUK[3]

[1]Company «Novosibirsk Chemical Concentrate Works», Novosibirsk, Russia
[2]GNTs VNIINM, Moscow, Russia
[3]Company «TVEL», Moscow, Russia

The paper deals with the possible causes for initiation of outer and inner defects in EBW of fuel elements to fuel cladding of E110 alloy. It is shown that the sources of pores in welds are gaseous products of sublimation of organic and inorganic materials in microvolumes between the surfaces being welded. Recommendations are given on prevention of pores and undercuts in welds.

Key words: *electron beam welding, fuel element, microcontamination, pore, undercut, butt, beam control*

Difficulties of welding refractory metals, in particular, zirconium alloys, are associated with formation of pores in welds [1–4]. Study [1] indicates that their main cause in welds of a zirconium alloy with up to 2.5 wt.% niobium is hydrogen formed at dissociation of adsorbed moisture, which remains on the edge faces. Authors of [3, 4] are of a similar opinion. In [2] porosity is attributed to development of a reaction between C-containing contamination on the edges of the part being welded.

Two-component alloy E110 (based on zirconium with up to 1 wt.% niobium) is currently finding wide application in industry. It is mainly used in nuclear power engineering, in particular in manufacture of elements of nuclear reactor active zones, including manufacture of fuel elements and assemblies for nuclear power plants. Fuel elements designed for WWER type reactors, are shell structures filled with nuclear fuel and sealed by welds. Higher reactivity of the above alloy at high temperatures with respect to oxygen, hydrogen and nitrogen requires good protection of welded joints in fusion welding. Therefore, EBW became widely accepted for welding zirconium and its alloys.

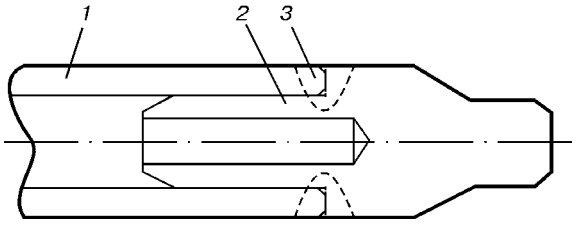

Figure 1. Schematic of a welded joint of a fuel element designed for WWER type reactors at EBW: *1* — cladding; *2* — plug; *3* — weld

The design of the fuel element weldment is shown in Figure 1. Considerable scope of production and high requirements to the quality of welded joints in elements of nuclear reactor active zones necessitate conducting the welding process in the automatic mode with provision of stable process parameters, eliminating the subjective factor of involvement of the operator of an electron beam unit.

Despite that, the main problem in mastering EBW of fuel elements with cladding of alloy E110 was porosity of welds revealed by X-ray inspection. During mastering and optimisation of the technology appearance of pores was found systematically, but periods of time with their maximal and minimal quantity were spontaneously observed, without any obvious connection to a specific technology or equipment. Simultaneously with the increase of the number of welds with pores, an increased number of welds with external defects of the type of undercuts were recorded, which, as a rule, were the consequence of the noted intensive splashing from the weld pool. Metallographic investigations of welded joint sections, rejected after X-ray inspection (presence of pores), showed that defects of this type, as a rule, are in that part of the weld, which corresponds to the location of welded edges of the plug and the cladding. The following was considered as the possible causes for weld porosity: base metal quality, tightness of fit in assembly of the cladding with the plug, possibility of microcontamination of organic and inorganic origin penetrating into the welding zone.

Tubes and plugs to make fuel elements are delivered as separate melts to the manufacturing plant, where they are divided into technological batches. Several technological batches of fuel elements can be made of one batch of components. To evaluate the influence of the quality of base material on pore formation statistical data on the melts of the supplied

Influence of the studied materials on pore formation in samples of welded joints

No.	*Studied material*	*Number of samples with pores, %*	*Note*
1	Water	0	Parts being welded were wetted with water
2	Deposit of a detergent solution	0	Parts being welded after the operation of degreasing with a detergent solution were not rinsed with pure water
3	Contamination from the process personnel gloves	0	Plug seats were rubbed with the gloves used during the shift
4	Uranium dioxide	0	Uranium dioxide dust was placed on 1/4 of butt perimeter
5	Cotton thread	0	4–5 mm long thread was put into the butt
6	Polyethylene film	10	A strip of 0.5×3.0×0.2 mm size was put into the butt
7	Vinyl ethereal	40	Vinyl ethereal chips 2–3 mm long scraped off a vinyl ethereal plate by the pipe end were placed into the butt
8	Rubber linoleum	100	Rubber linoleum chips 2–5 mm long were placed into the butt, which were scraped off the rubber linoleum sheet by the pipe end
9	Grease lubricant S1-13	0	Welding zone and half of the butt perimeter were rubbed with an oiled cotton napkin
10	VM-1 vacuum oil	0	Same
11	Lithol	94	»
12	Dust from plenum ventilation	70	Dust was placed around 1/4 of the butt perimeter

tubes and plugs was accumulated and analysed with its correlation with the technological batches of fuel elements and data of X-ray inspection of welds of these batches. Altogether the results of X-ray inspection of welds in fuel elements of 530 technological batches were analysed, which had been manufactured using tubes and plugs of 70 and 12 melts, respectively. Analysis results demonstrated that the presence of pores in the welds is related not to the specific melts of the components, but to technological batches of fuel elements, i.e. directly to the technological process of their fabrication, and the used material is not the cause for porosity in fuel element welds.

For a guaranteed fixing of the plugs in the cladding they are assembled with an interference. In this case the edge of the cladding enters the plug as far as it will go (see Figure 1), i.e. the gap in the butt between the surfaces being welded is practically absent. In order to determine the influence of the nature of the plug fit into the cladding on the possibility of porosity, a series of samples were made (20 pieces for each experiment). The plug was mounted in the cladding both with interference fit and with a gap, the size of which was varied from 0 up to 0.04 mm. Before welding the parts were subjected to degreasing by the technology accepted in fuel elements manufacture. Samples were welded during the period, when a low level of rejects because of porosity was observed in welding batch-produced items by the mode accepted for welding the fuel elements. Subsequent X-ray inspection of the welds of samples demonstrated a complete absence of pores in them, irrespective of the nature of plug fit into the tube. During the period, when an increased number of pores was observed in welding batch-produced items, investigations were further conducted to determine the size of interference between the plug and the shell. Measurement of internal diameter of the cladding and the seats of the plugs on batch-produced items showed that their assembly was achieved by providing interference within the above limits. Results of analysing the size of interference between the cladding and the plug in batch-produced items, when the selected welding modes were used, once more confirmed that the type of fit between the cladding and the plug does not have any noticeable influence on pore formation in the welds.

In keeping with the requirements of the technology of manufacture of fuel elements, before welding the cladding and the plugs are subjected to washing in a solution of special detergents, removing possible contamination from the surface. On the other hand, when the components are moving along the technological route during the operations of the fuel element assembly and charging, penetration of microparticles of organic and inorganic origin into the welding zone is quite possible, which under the impact of temperature under the conditions of a high vacuum in welding may form the gas phase and promote the formation of pores in welds. Presence of a tight butt impairs the conditions for its degassing. The sources of such mi-

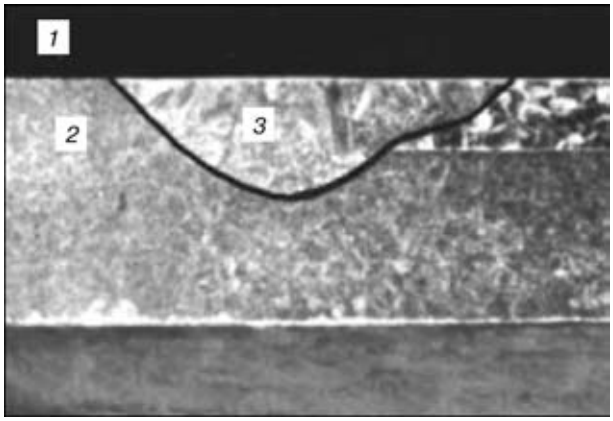

Figure 2. A weld of a fuel element sample made with a circular scan of the beam at the stage of current decrease (for designations see Figure 1)

crocontamination may be the surfaces of tables and transportation devices with coatings of organic materials (rubber linoleum, vinyl plastics, polyethylene), as well as random contacts of the surfaces being welded with various microparticles of different materials.

In order to verify this assumption, an experiment was conducted, which consisted in a purposeful introduction of various materials of organic and inorganic origin into the butts of welded joints and the adjacent plug seat zone. All the samples (20 for each experiment) had been first prepared by the technology used for batch-produced items. Presence of the studied material in the welded butt was controlled visually. Samples were welded by modes approved for batch production. All together the influence of 25 materials on pore formation was verified this way. After welding most of the samples had dips in the welds and undercuts formed because of splashing of the metal from the weld pool. All the samples of welded joints were subjected to X-ray inspection, the results of which are given in the Table.

It shows that there exist a number of materials, the presence of which in the welding zone does not lead to porosity, although metal splashes from the weld pool during welding are observed, which impair the appearance of welds. On the other hand, there exist a sufficient number of other materials, mainly of organic origin, which cause porosity.

The obtained data were the basis to make a number of organisational conclusions, aimed at achieving the required quality of production, which in this case may be regarded as intelligent performance (based on the achieved level of knowledge) by the technical and maintenance personnel in this production of the totality of the requirements, norms, rules of performance and organisation of work, providing a stable high quality of products. It was also recommended, when cutting the cladding to size, to bevel the edge at an angle of 14° through the entire thickness of the shell, instead of the earlier used 90°. The welding cycle included preheating of the welded joint by a lower power beam.

The welding mode was selected so that only surface melting of the butt edges occurred during preheating without the weld pool formation. Butt opening to the entire depth with formation of a guaranteed gap between the cladding edge and the plug was observed. Focusing current remained unchanged during welding and equal to 98–97 % of the current, providing a maximal focusing of the beam on the item surface. Deficit of material removed, when making the groove at the shell end face, was compensated by additional self-pressing passes.

The possibility of applying during welding special electron beam scans as a measure to avoid defects of undercut type was verified. Welded joints with undercuts were further treated by the electron beam with different scanning frequency and shape of the electron beam scan, using SU-229 type device, which was switched on at decrease of the beam current. The best results were obtained at beam scanning frequency of 60 Hz. Welds processed with a circular beam scan at such a frequency, had a smooth even surface and did not differ from those made by the approved technology. The width of the weld on the outer surface was increased by 0.5 mm (Figure 2), while the penetration depth in a section with a wider weld was smaller than the thickness of the cladding wall. Increase of scanning frequency led to a greater reinforcement along the weld edges and impaired its appearance. An additional positive moment of using a new geometry of the butt was increased stability of operation of the automatic system of guiding the electron beam to the butt of the welded joint. This also promoted making welds with an optimal reinforcement, and further on allowed eliminating the operation of their cleaning.

The results of this work were introduced into production, thus allowing a significant decrease of the number of welds with pores and stabilising the welding technology. Over a long period of service of fuel elements for WWER type reactors not a single claim was placed to the quality of electron beam welds.

CONCLUSIONS

1. The main cause for porosity in welds of fuel elements with cladding of alloy E110 made by EBW is microcontamination of the surfaces being welded by organic and inorganic materials.

2. The main method of elimination of porosity in such welds is taking integrated measures on maintenance of a high quality of production and maximal degassing of the weld during welding by optimising its technological modes and the design of the parts being welded in the joint zone. An effective means to remove the defects of the type of undercuts is application of welding modes with a circular scan of the beam in the current decrease stage at a frequency of 60 Hz.

1. Lebedev, N.V., Kosykh, M.A., Shchavelev, L.N. (1977) On causes of pore formation in electron beam welding of zirconium alloy with 2.5 % niobium. *Svarochn. Proizvodstvo*, **3**.
2. Ivannikova, A.D., Erokhin, A.L. (1968) Influence of surface contamination of titanium on pore formation in welding. *Ibid*., **2**.
3. Nikiforov, G.D., Redchits, V.V. (1971) On the mechanism of pore formation in welding of titanium alloys. *Ibid*., **3**.
4. Nikiforov, G.D., Makhortova, A.G. (1961) Sources of hydrogen dissolving in weld metal during welding. *Ibid*., **4**.

ELECTROHYDROPULSE PERMANENT JOINING OF HOLLOW PIECES USING EXPLODING ELEMENTS

A.I. BOROZNYAK
Company «Alchevsk Metallurgical Plant», Alchevsk, Russia

Investigations were conducted with electrohydropulse pressing of tubes into tube sheets with different configurations of channels. Dependencies of the degree of filling of die cavities upon the shape of cross sections of exploding elements were established. Device for pressing tubes into tube sheets was developed.

Key words: *electrohydropulse pressing-in, exploding elements, reduction of power consumption, exploding element profile factor*

The process of fixing of tubes in tube sheets of heat exchangers, using energy of the electric explosion of conductors, has found lately an increasing commercial application. The process involves different designs of cartridges [1] which are exploded using electrohydraulic units and current-conducting devices, supplying electric power to electrically exploded cartridges. Circular channels (Figure 1) are cut on the surface of each hole in a tube sheet more than 20 mm thick to increase strength and tightness of the pressed joint.

Available electrohydropulse (EHP) cartridges have a drawback which consists in a non-rational utilisation of the explosion energy. In this case it is utilised not for local deformation of the tube against the tube sheet channels, but for overall deformation along the entire length of the tube, which is equal to thickness of the tube sheet. It should be noted that a die-free forming is used as an estimation operation prior to actual pressing-in, as it allows the degree of filling of the tube sheet channels with a deformed billet to be approximately estimated by a workpiece configuration [1, 2].

Commercial cartridges use exploding elements (EE) of a round cross section. As proved by practice, the use of such cartridges results in semicircular protrusions formed on the workpiece surface. This is indicative of formation of a number of shock waves, the configuration of the fronts of which copies configuration of the EE cross section. In the case of pressing tubes into tube sheets with semicircular channels, this facilitates their filling up. It can be assumed that in the case of pressing into sheets with channels whose geometrical shape corresponds to the EE profile, filling of the tube sheets will be facilitated (compared with EE whose shape is inadequate to the channel profiles). In addition, in the commercial cartridges, instead of fixing the EE pitch, the following restriction should be met: a minimum pitch should be more than 5 mm to avoid break-down between the neighbouring turns [1]. As a result of misalignment of the EE pitches and channels the pressure diagram peaks do not correspond to cavities in the sheets.

The task was to investigate EHP pressing of tubes into tube sheets with channels of different configurations, using EE of different profiles, in order to decrease power consumption of the operation. Experiments were conducted to determine the effect of configuration of a cross section of EE on the degree of filling of the forming cavities in the split dies of different configurations, i.e. semicircular, triangular, square and trapezoidal. A nichrome wire 1 mm in diameter was used in devices with a round cross section of EE. To make triangular, tetrahedral and trapezoidal EE from the 2 mm dia. nichrome wire by rolling, channels of the corresponding profile were milled in rolls of the laboratory rolling mill. All the EE had the same cross section area equal to 0.79 mm^2. Forming channels of differing profiles, having the same height of H_d = 4 mm and cavity cross section area of F_d =

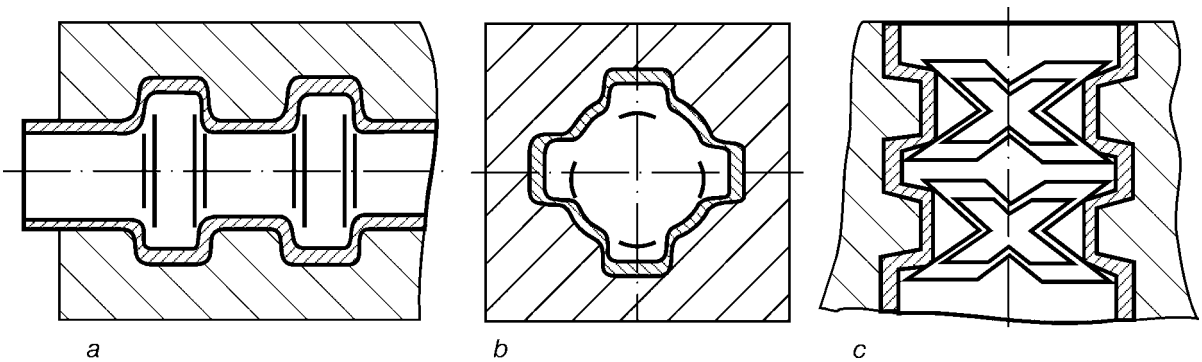

Figure 1. Possible variants of permanent joints in hollow pieces under axial loading (*a*), loaded by torque (*b*) and under the combined axial and torque loading conditions (*c*)

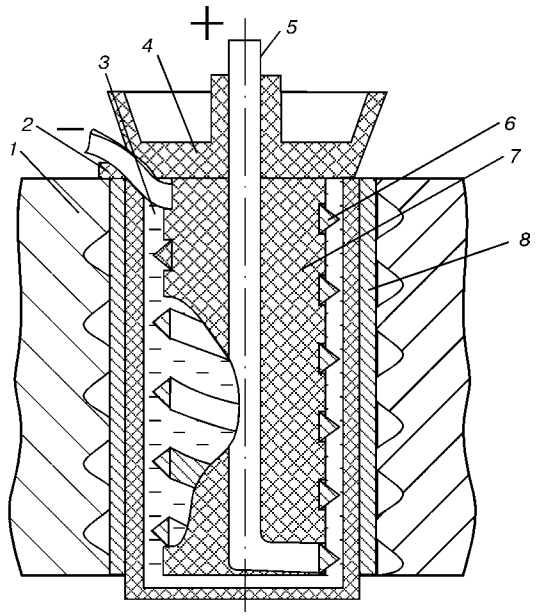

Figure 2. Device for expanding of tubular billets (see designations in the text)

= 6.28 mm^2, were milled on the internal surfaces of the split dies.

The steel tubes with an inside diameter of 20 mm and wall thickness of 0.5, 0.75 and 1.0 mm were subjected to expanding. Experimental studies were carried out using a laboratory unit with a maximum charging voltage of 60 kV and capacitance of the capacitor bank equal to 20 μF. A tubular billet was placed in the die with a certain configuration of the cavity. The device with EE which has one of the above cross section configurations was located inside the tubular billet. The EHP unit electrode was fed to the non-exploding current-conductor of the device, and the discharge was excited. The integrator energy was varied by increasing the charging voltage at a constant capacitance of 17 μF. Three samples were expanded under each of the conditions. Height of the formed rifts was measured after removing the workpiece from the split die. The profile factor of EE, K_{pr}, results from determining the ratio of the energy required for final filling of the forming cavity of the die in using the j-th EE to the energy required for final filling of the i-th cavity of the die in the case of coincidence of the EE profile and die channel configurations (i = = j). Analysis of its values showed that at the equal energy released in the discharge channel the filling of the die channels is of a higher quality in the case of coincidence of the EE profiles and die channels. Therefore, in pressing tubes into tube sheets with different configurations of the channels, the use of EE with an adequate profile configuration will provide quality joints at the reduced power consumption.

Investigations conducted resulted in the development of the device for expanding of tubular billets (Figure 2). It comprises die *1* with forming cavities, EHP expanding cartridge consisting of dielectric sleeve *2* filled with transmitting medium *3*, end plug *4*, current-conductor *5* with insulation, and EE *6* with a corresponding pitch and relative angular location on the surface of dielectric bushing *7*, as well as deformed tubular billet *8*.

The device functions as follows. The thermal explosion of EE is ignited under the effect of a high-voltage discharge created at EE *6*, through current-conductor *5* from the power unit (not shown in Figure 2). The pressure pulse thus formed propagates in a direction to the wall of the tubular billet. The shock wave, the configuration of the front of which repeats configuration of the cross section of EE, forms spiral protruding rifts on the tubular billet, thus favouring the quality filling of the channels in the tube sheet. This makes it possible to achieve high pressures within the zone of formation of the rifts.

CONCLUSIONS

1. Investigations were conducted to study EHP pressing of tubes into tube sheets with channels of different configurations, using EE of different profiles, in order to decrease power consumption of the operation.

2. It was established that the equal energy released in the discharge channel resulted in the higher-quality filling of the die channels, providing that their profiles coincide with the EE profiles.

3. Device for pressing tubes into tube sheets, ensuring power saving in EHP joining of hollow pieces, was developed.

1. Mazurovsky, B.Ya. (1980) *Electrohydropulse pressing of tubes into tube sheets of heat exchanging devices*. Kyiv: Naukova Dumka.
2. Weckerle, H.I. (1977) Der Einfluβ der geometrischen Gestalt des Werkstückes auf Energiübetragung beim elektrohydraulischen Umformen. *Blech-Rohre-Profile*, **6**, 267–270.

MAIN TENDENCIES OF DEVELOPMENT OF WELDING EQUIPMENT MANUFACTURE IN «SELMA-ITS» ASSOCIATION AND ITS APPLICATION IN RUSSIA AND CIS COUNTRIES

M.V. KARASEV, E.A. KOPILENKO, G.V. PAVLENKO, D.N. RABOTINSKY, V.L. SOROKA, V.V. SOLYANIK and **E.V. KARASEV**
SPA «SELMA-ITS», St.-Petersburg, Russia–Simferopol, Ukraine

Comparison of technical-economic characteristics of equipment applied in Russia and CIS is made, taking into account the world market of welding equipment. Characteristic directions of welding equipment improvement are outlined. Recommendations are given on its selection during performance of specific work.

Key words: *welding equipment, development tendencies, production structure, technical-economic characteristics, production refurbishment*

In 1999–2000 production started increasing in the majority of the Russian industrial enterprises, which was due to greater number of orders, resulting to an increase in the industrial production of CIS countries. Now these industrial enterprises face the task of a prompt improvement of the labour efficiency at a slight increase of the number of workplaces and number of workers. This problem is being solved under specific post-crisis conditions, characterised by:

- complicated economic and financial situation of the enterprises because of high taxes, customs dues, debts to the federal and local budget;
- high percentage of wear (up to 80–100 %) of the currently used machines, mechanisms, equipment and metal structures;
- availability of financial means for technical refurbishment of the fleet of mechanisms and equipment, and introduction of advanced technologies;
- lack of directed organisational and engineering work in the existing research institutes, capable of providing the modern technical documentation for the functioning industrial enterprises;
- lack of qualified experts, capable of developing and operating advanced equipment and technology (for instance, in Leningrad region there are approximately 20,000 vacancies in industrial enterprises and about 9,000 people listed in the labour exchange, but not required, while the number of students-metallurgists graduating from St.-Petersburg Technical University is reduced by approximately 10 times, compared to 1990);
- increase of the number of orders in the functioning enterprises and of production volumes, respectively;
- need to conduct stage-by-stage upgrading of production in the functioning enterprises to provide the ability of fulfilling these orders with the appropriate quality and price;
- desire of the majority of operating enterprises to quickly come back to the production level before the crisis period;
- availability of a large number of proposals for a complete (partial) upgrading or replacement of the fleet of currently used machines and equipment coming from foreign companies and much more seldom from local enterprises;
- need for a systemic (strategic) approach to the problem of technical refurbishment of enterprises, in order to increase the effectiveness of their operation.

This study is aimed at introducing a systemic approach and determination of the tendencies in the field of technical refurbishment of industrial enterprises, based on the most recent achievements of welding science, experience of manufacture and sale of welding equipment over the last ten years.

Analysis is based on operation of a group of enterprises of SPA «SELMA-ITS», which over the recent years has become a major manufacturer and supplier of welding equipment in Russia and CIS countries. Its production facilities are located in Simferopol and St.-Petersburg.

Structure of European and US markets of welding equipment, applied in metal structure fabrication. According to the data of [1], the world market of welding equipment and services was not less than $40–50 bln at the end of the XX century, of which 70 % were welding consumables and 30 % was welding equipment. Not less than half of the latter was the cost of equipment for manual arc and semi-automatic welding. Its share shows a stable tendency of increasing due to equipment for semi-automatic arc welding, with reduction of the share of equipment for coated-electrode manual arc welding.

Machines for flash-butt welding are not as widely applied, because of their specific features. However, their share in the welding equipment market is up to 31 %. The share of equipment for gas welding is reducing steadily and currently is not more than 17 %.

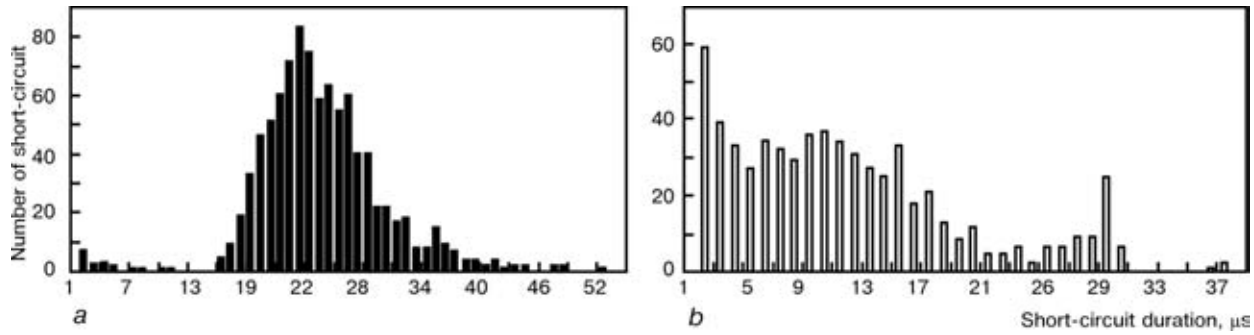

Figure 1. Histograms of distribution of short-circuit duration in VD-506DK (*a*) and VDU-506 (*b*) units in semi-automatic welding

The European market of welding equipment amounts to about 30 % of the world market.

As follows from [1], in advanced European companies, compared to those in the USA, the volume of application of equipment for gas-shielded welding is higher and that of equipment for coated-electrode welding is lower. Welding fabrication is based on fusion welding, the equipment and technology of which will develop through reduction of the share of coated-electrode manual arc welding and expansion of the mechanised processes of welding, especially with flux-cored wires.

There is every ground to believe that in the near future the share of manual arc welding in the world economy will stabilise on the level of 10 to 12 %, that of semi-automatic solid wire welding on the level of 40–50 %, that of semi-automatic flux-cored wire welding and SAW on the level of 30–40 and 5–6 %, respectively. The most promising is manufacture of specialised welding equipment for semiautomatic flux-cored wire welding, providing a simultaneous improvement of labour efficiency and welded joint quality.

Comparison of technico-economic characteristics of application of various kinds of welding equipment in metal structure fabrication in Russia and CIS countries. In 1993 Russia manufactured about 75,000 power sources for fusion welding, while their maximal output in FSU in 1989 was 330,000 pcs. In the first case the share of welding transformers was 49, that of welding rectifiers (for manual arc, semi-automatic and automatic welding) — 26, that of generators, converters and plants — 24, and that of specialised power sources — 1 %. Such a production structure cannot be regarded as satisfactory. For instance, in Japan with the overall output of 123,000 pcs in 1988, the share of transformers, rectifiers and rotary machines was 30, 40 and 30 %, respectively [2]. Development of circuit designs for welding equipment in Russia proceeds mainly along the traditional path laid down in 1970–1980 by VNIIESO (Russian Welding Institute), the PWI and other institutes. Theses directions of work performance were due to the availability of the respective components manufactured in the USSR at that time. The main difference in the circuit design of power sources developed in Russia from their foreign analogs consists in that a new class of sources was developed abroad on the basis of recent achievements in semiconductor field, namely rectifiers with an intermediate high-frequency unit (inverter). It allows a significant reduction of the weight and overall dimensions, improvement of dynamic properties of welding equipment, development of new control circuits and going over to a new class of sources with synergetic control. This provides an effective solution of the problem of mass transfer control and improvement of welded joint quality. As demonstrated by the Fair in Essen (Germany) in September 2001, the period of intensive development of the inverter-type welding equipment abroad is over, and the process of its improvement and upgrading is going on now. Manufacture of similar components is not planned in Russia in the next few years. Attempts at development of inverter-type welding units using the local components showed their low reliability, while development of similar local welding machines incorporating imported components demonstrated their low competitiveness.

Therefore, in «SELMA-ITS» Association developments in the field of thyristorized welding units were mostly based on the use of the local components, and were aimed chiefly at improvement of the control circuits. The power part of the sources, as a rule, did not undergo any basic changes.

In this connection, we should note development and manufacture of a new series of local rectifiers with DK index (VD-306DK, VD-506DK) designed for MMA, MIG and TIG welding. A new type of control circuits has been developed and verified in these rectifiers [3]. Rectifiers in the MIG and MMA modes are designed for short-arc welding with periodic short-circuiting, but are also successfully used for welding with a long arc. In them the combined external volt-ampere characteristics (VAC) were implemented on a production scale for the first time, namely MIG and MMA modes, where each VAC section characterises a certain stage of melting and transfer of electrode metal drop and allows implementing new approaches to controlling the welding process and mass transfer. In this case VAC is divided into compound sections, each of which is formed by its own self-sufficient source (first VAC section — high-voltage feed — provides an easy initial ignition of the arc, power part is formed by a semi-controlled rectifier, third section of VAC — low-voltage feed — rovides a controlled metal transfer into the weld

pool). The working point in arcing always is in the falling section of VAC. Rectifiers have the capability of adjustment of VAC slope, short-circuit current, hot start (custom features). It should be noted that the range of operating temperatures is from –40 to +40 °C, which is not provided by any inverter-type power source. By All-Union Research Institute of Pipeline Construction (VNIIST) estimate the welding characteristics of rectifiers are not inferior to the best models of the inverter sources, at least in manual arc welding. Figure 1 gives the histograms of distribution of short-circuiting times in welding in VD-506DK and VDU-506 units in the MIG mode.

As follows from Figure 1 the value of short-circuit duration in the sources with a combined characteristic is sufficiently stable, unlike the traditional VDU-506. This ensures high process properties of the welded joints, by providing a constant and stable size of the drops of the transferred metal (drop size is about 80 % of welding wire diameter at arc currents recommended for the given wire diameter). A complete cycle of investigations has been conducted to compare the mechanical properties of welded joints. It is found that the mechanical properties of welded joints, at least for MMA mode, are on the level of those provided by the inverter-type sources. Investigation results have been confirmed by the results of testing at VNIIST. A possibility was demonstrated of producing stable periodical short-circuiting of the arc gap at a constant frequency with application of combined VAC. Increase of arc current leads to a stable shortening of the short-circuit duration and shifting of the curve in Figure 1, *a* to the right. Size of the drops of the transferred metal is reduced, accordingly. Therefore, we have every right to call it a controllable transfer, achieved without applying any special pulses, as in the case of inverter sources in the «pulse» mode. Figure 2 gives the typical oscillograms of welding current and voltage in DK-type power sources in semi-automatic welding. Analysis of this Figure shows the high stability of the welding mode, unachievable before with the thyristorized sources. Oscillograms were recorded using a special PC-based measuring system and analog-digital converter.

Another new thyristorized power source is being introduced in parallel, which has a combined VAC based on VDU-506 for MIG and MMA modes, and which was called VDU-509. The need for its development and manufacture arises from the industrial enterprisers requiring a new power source for semi-automatic welding for up to 500 A currents with a fully-controlled rectifier. Its development incorporates all the positive experience gained in development and introducing into production the DK- type sources. Its difference consists in that the combined VAC is formed by the control board with preservation of an unchanged power components of the standard VDU-506. Short-circuiting sensor was applied for the first time, which allows lowering the power of the power circuit at short-circuiting, reducing the spatter. The working point in arcing may be switched from the VAC rigid section (applied in welding in the vertical and overhead positions at up to 280 A currents with

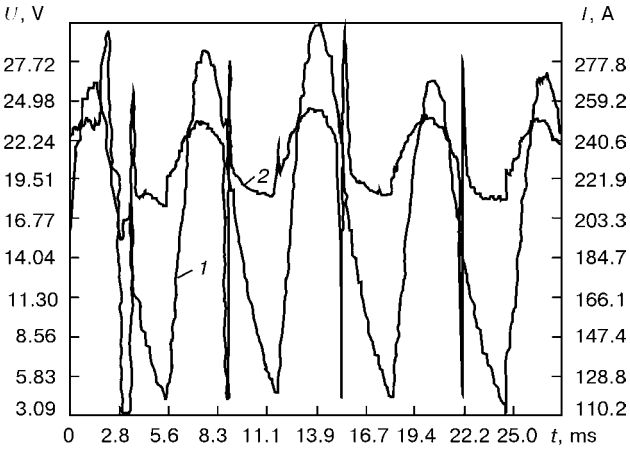

Figure 2. Oscillograms of welding current (*1*) and voltage (*2*) in semi-automatic welding in power sources of VD-506DK type with a combined VAC (shielding gas is argon, wire is Al-5Mg type)

up to 1.6 mm wire, as well as to form the weld with a concave surface in making fillet joints) to the VAC falling section (applied in welding in the downhand position and surfacing). Production testing of VDU-509 rectifier is being completed now in Company «Uralmash» (Ekaterinburg, Russia). From preliminary data electrode metal spatter decreased 5 to 8 times, process efficiency increased 15 %. Full-scale production of the power source is scheduled for the second quarter of 2002.

The next direction of welding equipment development in «SELMA-ITS» is designing choppers. All the world leaders in the field of arc welding are actively working on them. Lincoln Electric Company even set up a division on chopper technology. In the general form a chopper is a welding inverter for MMA, MIG/MAG and TIG welding, more exactly a welding converter, also with superposition of pulses on welding voltage, which has a much lower price and much higher reliability than the conventional inverter welding units. Any working frequency may be used, depending on the applied components. Power sources for choppers are mutlioperator power sources of VDM-1202, VDM-6303 types. The number of choppers, which may be powered from one multioperator rectifier, is determined by power characteristics, but considering that the chopper efficiency is not less than 95 %, a VMD-1202 rectifier supports not less than 6 choppers with the working current of 200 A or 4 choppers with the working current of 300 A. The first locally manufactured chopper will be displayed in «SELMA-ITS» booth in «Svarka-2002» Exhibition in St.-Petersburg.

In addition, another area of welding was pursued in our country, namely development of extremely simple, inexpensive and reliable welding units, using local components. They include welding rectifiers VD-309, VD-313, VD-2x313. They do not have such capabilities of welding, as those mentioned above, but are in demand constantly.

Calculations made for the basic technical-economic parameters of fusion welding equipment are highly significant. These data are interesting for all the enterprises, which have power saving programs.

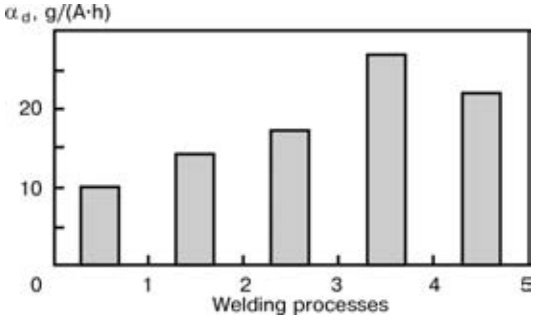

Figure 3. Dependence of the mean value of deposition factor α_d on welding processes: *1* — manual arc welding with coated electrodes in a modern VD-306DK power source; *2* — semi-automatic welding with solid wire in CO_2 in modern thyristorised power sources VD-306DK, VDU-506S; *3* — semi-automatic welding with solid wire in gas mixtures in modern thyristorised power sources VD-306DK, VDU-506S; *4* — semi-automatic welding with flux-cored wire in modern thyristorised power sources VD-306DK, VDU-506S; *5* — semi-automatic solid wire welding in gas mixtures in inverter-type synergetic power sources

Calculated values (Figure 3) are compared with the operating values in Company «Uralmash». A good correlation of the results is found within 5 % of the values. As follows from Figures 3–5, the most characteristic is the comparison of manual arc and semi-automatic welding. It should be noted that calculation was based on the data on a modern power source VD-306DK for manual arc, argon-arc and semi-automatic arc welding. If the parameters of a conventional rectifier source VD-306 (VD-306E analog) are used, the data become appalling. Power consumption will be 5.12 kW·h/kg with the time for making 1 m of weld equal to 0.084 h. If parameters of a multioperator welding rectifier VDM-1201 with ballast resistors are used, the situation becomes critical: power consumption will be 7.53 kW·h/kg with the same performance time.

Thus, if we proceed from average data, showing welder's activity, namely annual consumption of welding electrodes of 2 tons or of welding wire of 2.5 tons, the annual power consumption recalculated for one welder for different power sources will be, kW·h:

- modern welding rectifier VD-306DK — 7500;
- traditional welding rectifier VD-306D (VD-306E) — 10240;
- multioperator welding rectifier VD-1201 with ballast resistors — 15060;
- modern inverter-type power source or chopper for semi-automatic welding with solid wire — 2750;

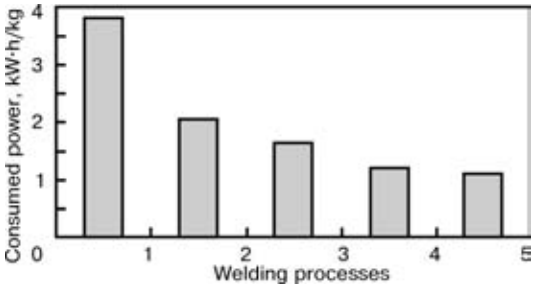

Figure 4. Dependence of average value of power consumption per 1 kg of the deposited metal on different welding processes (*1–5* — same as in Figure 3)

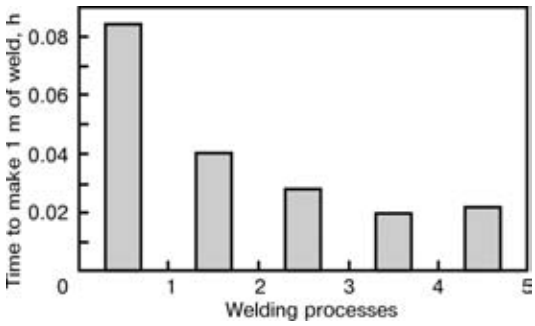

Figure 5. Dependence of mean value of time of making a weld on the welding process: *1* — without taking into account the time required to change the electrode; *2–5* — same as in Figure 3

- modern power source for semi-automatic welding (VD-306DK, VDU-506S) using flux-cored wire — 3000;
- modern power source for semi-automatic welding (VD-306DK, VDU-506S) when using solid wire and gas mixtures — 4000;
- modern power source for semi-automatic welding VD-306DK, VDU-506S when using solid wire and CO_2 — 5000.

Figure 6 shows power saving, when going over to modern welding equipment, depending on the number of welders.

On the other hand, it should be noted that application of modern welding processes provides not only a saving of company funds, but also an improved quality of the welded joint. Figure 7 shows the structure of the weld produced by semi-automatic welding with solid and flux-cored wire («Filark», Sweden).

A number of factors should be taken into account, when selecting the welding equipment:

- performance of a large scope of manual arc welding operations requires modern welding units (VD-306DK, VD-506DK), as they allow reducing spatter of electrode metal and power consumption and provide a high quality of the welded joint. When performing welding operations with multioperator power sources, it is rational to go over, as far as possible, to the use of across-the-line units (VD-2×313), which provide an almost two-times power saving;
- when going over to semi-automatic welding with solid wire in shielding gases, compared to CO_2 welding, electrode metal spatter decreases almost 1.5–3

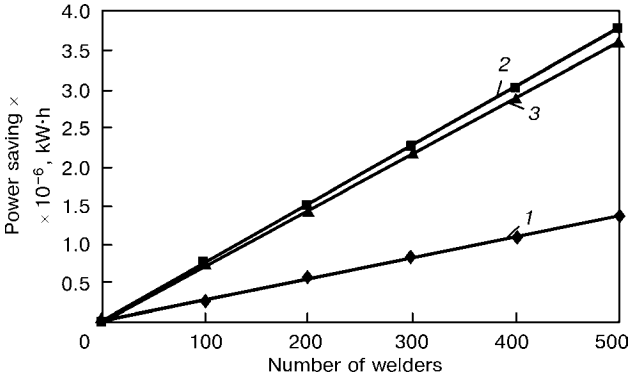

Figure 6. Power saving when going over to modern welding equipment, depending on the number of welders: *1* — from VD-306 (306E) type source to VD-306DK in manual arc welding; *2* — from a source of VDM-1201 type to VD-306DK in manual arc welding; *3* — from a source of VD-306 (306E) type (manual arc welding) to VD-306DK (semi-automatic flux-cored wire welding)

times, and electrode metal drop deposition on the weld and HAZ metal — almost 8–10 times, this determining subsequent labour consumption for spatter removal from the surface of parts being welded;

• welding sources of the type of VD-306DK, VDU-506S, VDU-506, VDG-303, VS-300BA, VDG-401 may be used. However, the optimal solution is using inverter-type synergetic sources like SINERMIG-401 or choppers. This allows further increasing the welding process efficiency at least by 25 %;

• when going over to semi-automatic flux-cored wire welding in CO_2 or gas mixtures, electrode wire spatter is practically absent, this actually eliminating subsequent labour consumption to remove spatter from the surface of items being welded. The possibility of employing welders with lower qualifications is notable. In this case use of welding sources of the type of VD-306DK, VDU-506S, VDG-303, VS-300BA, VDG-401 is optimal. Application of inverter power sources is not mandatory;

• in terms of mechanical properties the differences between the variants of semi-automatic welding consist in the change of relative elongation of the produced welded joint, which rises by ≈ 10 % and increase of impact toughness in the negative temperature region. Flux-cored wire welding provides the highest impact toughness (Charpy value down to –60 at T = = –40 °C). Solid wire welding in shielding gases gives a somewhat lower impact toughness of the welded joint KCU = 12.0–15.8 J/cm^2 at T = –40 °C.

Solid wire CO_2 welding provides an even lower impact toughness KCU = 8.4 J/cm^2 at T = –40 °C. Manual arc welding gives a still lower impact toughness KCU = 5–8 J/cm^2 at T = –40 °C.

Thus, proceeding from the above-said, it is possible to accurately enough outline the main directions of development, manufacture and application of welding equipment in Russia as follows:

1. Development and introduction into production of modern thyristorized power sources for all kinds of arc welding will be mainly pursued to improve the control circuits. This is due to the fact that CIS countries do not manufacture powerful transistors, required for a fundamental upgrading of the power circuit of the sources, whereas foreign-made products are rather expensive, this leading to non-competitive prices in the case of manufacturing an inverter-type power source. Work on improvement of the thyristor rectifier control circuits led to designing comparatively simple, but original control circuits, which allowed developing inexpensive high-quality power sources for all welding processes (MMA, MIG, TIG) incorporating local components. As to their welding properties, these sources are not inferior to the best samples of similar welding equipment of foreign companies and are superior to them as to operating conditions. Characteristic examples are welding rectifiers of the type of VD-306DK, VD-506DK, VDU-509 with a combined VAC.

The ratio of the quality and the price is selected from an optimal range. The industry has a demand for these rectifiers, as it becomes possible to make up the welding equipment fleet based on one source, this mark-

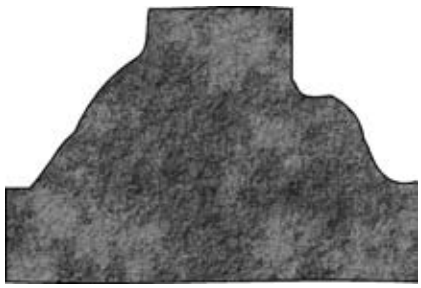

Figure 7. Appearance of a lack of penetration in solid wire welding (*right*), compared to flux-cored wire (*left*) at oscillation of the welder's hand

edly facilitating their service and allowing considerable funds to be saved, when purchasing the sources.

2. During refurbishment of welding production in welding enterprises special attention should be given to the problem of replacement of manual arc welding by semi-automatic welding or modern manual arc welding sources should be purchased. This allows the efficiency of welding operations to be increased several times with improved quality and a considerable amount of power to be saved (see Figures 2 and 4).

There exist two approximately equivalent methods for development of gas-shielded semi-automatic welding:

• the first method is related to improvement of expensive inverter-type sources or choppers, application of solid wire and use of gas mixtures in welding;

• the second method consists in further improvement of relatively inexpensive power sources of the type of VD-306DK, VDU-506S, VDG-303, VS-300BA, VDG-401, application of flux-cored wire and use of both gas mixtures and CO_2 in welding.

3. In the near future the main direction of development of thyristorized welding sources manufacture in Russia and CIS countries will be designing relatively inexpensive and competitive all-purpose rectifiers of local components. Their competitiveness will depend on the novelty of engineering solutions and manufacturing quality. Development of local components manufacture will determine further directions of power source improvement.

4. Manufacture of specialised inverter-type welding power sources (synergetic, orbital, etc., incorporating foreign components) will be the prerogative of foreign companies, until the local component manufacturing is in place.

5. The only possible direction of development of the local inverter-type welding systems, which may be competitive against foreign developments in the field and ensure commercial success, is as fast as possible mastering of local manufacture of choppers, which may be realised using local components and a minim number of foreign components. This will be seen from development of the situation in 2000–2003.

1. Bernadsky, V.N., Mazur, A.A. (2000) World and regional market of welding equipment. In: *Up-to-date problems and progress in the field of welding, allied technologies and equipment at the transition to XXI century*. St.-Petersburg.
2. Milyutin, V.S., Korotkov, V.A. (1999) *Welding power sources*. Manual. Chelyabinsk: Metallurgiya Urala.
3. Kopilenko, E.A., Pavlenko, G.V., Karasev, M.V. et al. *Method of arc welding with short-circuiting of the arc gap*. Declared pat. 42588A Ukraine. Publ. 15.10.01.

PHYSICAL-MECHANICAL CHARACTERISTICS OF STEEL–BRONZE COATINGS PRODUCED USING LASER SURFACING

A.P. SHATRAVA
Physico-Technological Institute of Metals and Alloys, NASU, Kyiv, Ukraine

Physical-mechanical characteristics of composite coatings produced using a laser surfacing were studied. Dependencies of service characteristics of working surfaces on structural-phase composition of deposited layers were established. Mechanism of improving wear-resistance of a friction pair was developed.

Key words: *composite coatings, laser surfacing, antifriction properties, physical-mechanical characteristics*

Development of new materials and technologies of their production to provide antifriction of friction pairs is one of the most important tasks of a general problem of friction, lubrication and wear in machines. Antifriction condition is characterized by a low and stable coefficient of friction at high wear-resistance and a good run-in [1]. The solution of this problem is most actual for machine parts operating under the conditions of limitation or full absence of lubricant in friction. Under these conditions its role can be played by a soft metal. Gold, silver, copper, lead, indium and barium are used as metallic lubricants [2].

Over the recent years composite materials are used effectively in the manufacture of machine parts including solid lubricants.

As an object of investigations the compositions of Fe–Cu system with different volume content of components in the filler material composition were selected. Coatings from above composite materials were produced from powders using a laser radiation [3]. Laser surfacing was performed in inert gas (Ar) which was used as transporting gas (gas consumption G_g = = 20–30 l/h) at feeding of powder of 50–100 μm dispersity and volume percent ratio 10–90 of one of components.

The filler powder (consumption was changed within G_{PV} = 2–5 cm^3/min or G_{PM} = 7.7–22.2 g/min) was fed under 45° angle to axis of laser radiation following the laser beam movement. Heat source with a power density $W_d = 1–5 \cdot 10^8$ W/m^2 was moved at a rate v = 4–20 mm/s providing deposited beads of 1.5–2.5 mm width and 1–1.5 mm height. Surfacing for wear tests was made on substrate of St.3 (C — 0.14–0.22; Mn — 0.3–0.6 wt.%; Fe — balance) in the form of rings of 1 cm^2 area.

As a result of laser gas-powder surfacing of composite material (steel–bronze) on surface of a steel sample different deposited coatings were formed which can be divided into three groups: *I* — steel + 10–30 % bronze; *II* — steel + 40–60 % bronze; *III* — steel + 70–90 % bronze (Figure 1).

A statistic analysis of structural phase constituents of electron images of microstructures obtained in electron microscope at X-ray microanalysis was made for all the above-mentioned compositions. Analysis was made using a unique procedure and software developed in Physico-Technological Institute of Metals and Alloys of the NAS of Ukraine [4]. The following structure parameters were studied: percentage, mean size and average area of inclusions, mean distance between them, their quantity, values of their maximum and minimum diameters, perimeters and coefficients of shape.

For coatings of compositions of *I* group the percentage of bronze inclusions was significantly lower than its content in the depositing powder (3–7 %). This is explained by the fact that not all the bronze enters the coating body, it can be evaporated partially or escape to the surface. Diameter of bronze inclusions for these compositions is 5–10 μm, the mean distance between them is 6–19 μm.

For coatings of compositions of *III* group the content of steel inclusions do not almost differ from the initial composition of powder, i.e. 6–24 %. Here, the mean diameter of steel inclusion is 18–36 μm, the mean distance between them is 8–22 μm.

The lowest scattering in sizes of steel and bronze inclusions in depth and most uniform distribution of inclusions in height and width of the deposited layer is observed for coatings with steel–bronze ratio 80:20 and 20:80.

In structure of coatings of other compositions (90 % St.:10 % Br. and 10 % St.:90 % Br.) the steel inclusions are concentrated near a base, while the bronze inclusions are concentrated near the surface of a deposited layer. Sizes of inclusions is of importance in places of their large concentration as they can coalesce between themselves.

The presence of large coalescent inclusions or entire layers is typical to some degree of coatings of compositions (30–70) % St.:(30–10) % Br. This prove the fact that even for a small time of heating and cooling these materials can laminate in coatings with approximately equal ratio.

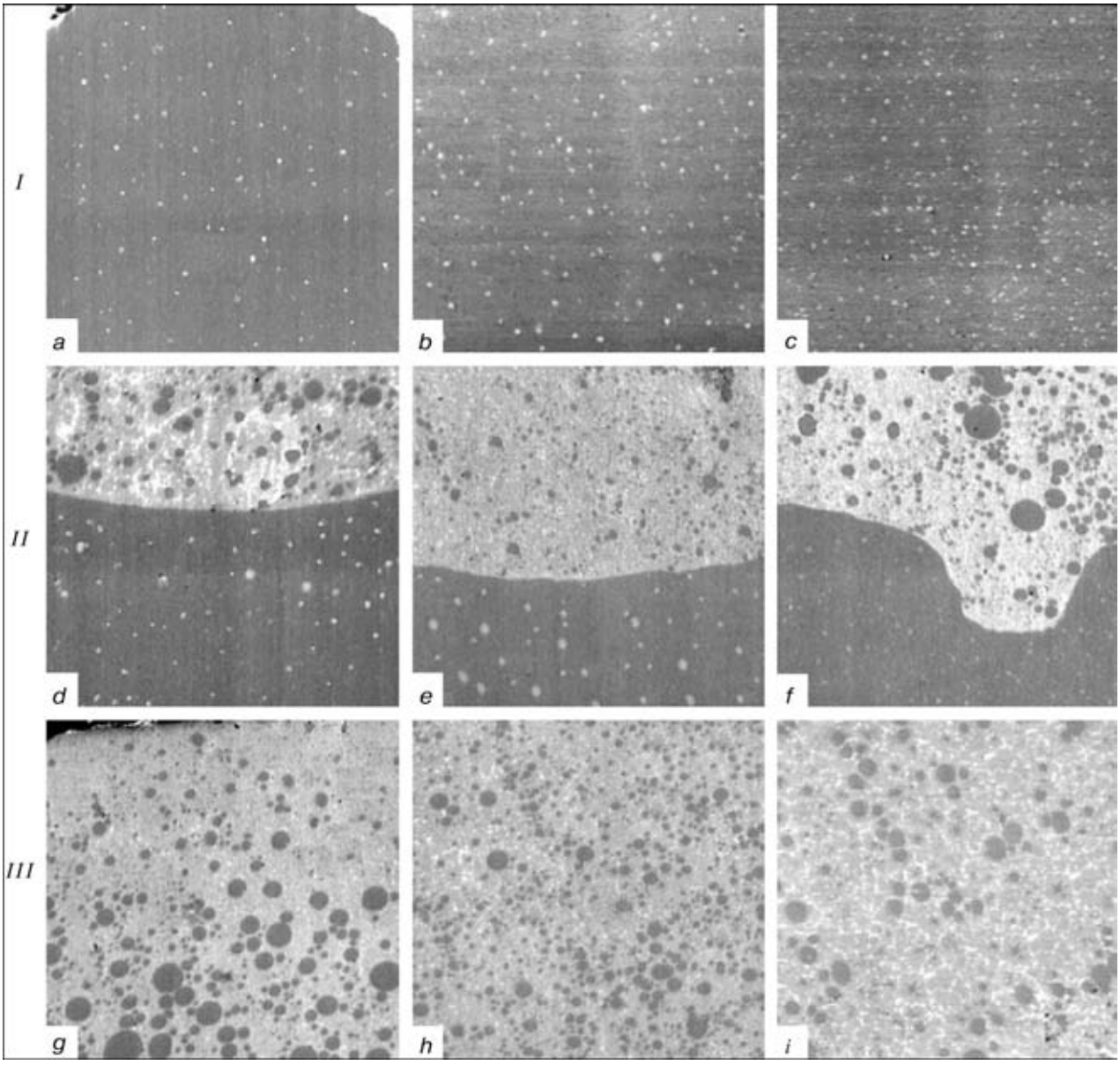

Figure 1. Microstructure of laser composite (steel–bronze) coatings with ratio of steel to bronze in them of 90:10 (*a*), 80:20 (*b*), 70:30 (*c*), 60:40 (*d*) (×300), 50:50 (*e*), 40:60 (*f*), 30:70 (*g*), 20:80 (*h*) and 10:90 (*i*) % (*I–III* — groups of coatings)

These results show that 20–30 % composition is limiting for the formation of dispersely-distributed composites for these materials both at given temperature and temporary conditions.

In this work the effect of composition and macrostructure of composite coatings on their physical-mechanical properties has been studied. It can be concluded from the data of X-ray microanalysis that a considerable redistribution of elements at the friction surface is observed under the action of loading in friction, i.e. a soft phase is escaped to the surface being a solid lubricant in friction and a solid phase undertakes load and is resistant to deformations.

Comparing results of tests for wear of composite coatings at different loads it can be concluded that at low loads the coatings with 20–30 % bronze are

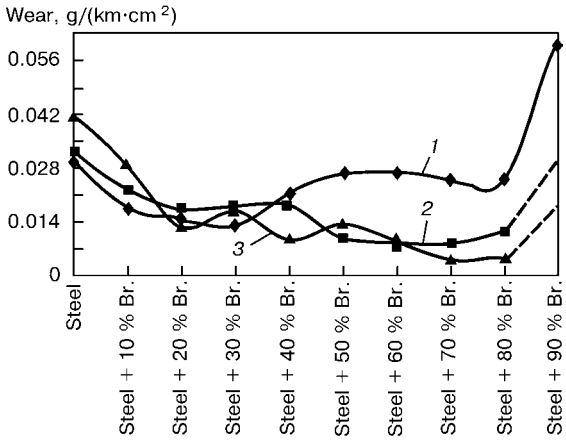

Figure 2. Wear of friction pair (composite coatings and mating body) at different loads: *1* — P = 5.1; *2* — P = 10.2; *3* — P = = 15.3 MPa

characterized by the best indices, while at high loads — the coatings with 70–80 % bronze (Figure 2).

With load increase the intensive escape of soft material to the friction surface occurs, and uniformly distributed inclusions of steel (for compositions of *III* group) play a role of a frame which, from the one side, does not hinder the soft material penetration to the surface, and, from the other side, does not allow coating to be deformed.

The use of the above compositions makes it possible to improve significantly the conditions of friction in pair due to transfer of a solid lubricant to a mating body. Significant decrease in wear (to 50 %) is most typical of friction pair as a whole, i.e. for the total decrease in wear both of investigated and mating body.

1. Kostetsky, B.I. (1970) *Friction, lubrication and wear of machines*. Kyiv: Tekhnika.
2. Kostetsky, B.I., Kolesnichenko, N.F. (1969) *Quality of surface and friction of machines*. Kyiv: Tekhnika.
3. Kovalenko, V.S., Golovko, L.F. (1990) *Strengthening and alloying of machine parts by laser beam*. Kyiv: Tekhnika.
4. Stas, O.I., Gavrilyuk, V.P. (2001) Computer methods of investigation in metallographic analysis. *Metallovedeniye i Obrab. Materialov*, **1/2**, 48–52.